TURUN
YLIOPISTO
UNIVERSITY
OF TURKU

NEXT GENERATION AQUEOUS ORGANIC FLOW BATTERIES

Gabriel Gonzalez

TURUN YLIOPISTON JULKAISUJA – ANNALES UNIVERSITATIS TURKUENSIS
SARJA – SER. F OSA – TOM. 58 | TECHNICA – INFORMATICA | TURKU 2025

TURUN
YLIOPISTO
UNIVERSITY
OF TURKU

NEXT GENERATION AQUEOUS ORGANIC FLOW BATTERIES

Gabriel Gonzalez

TURUN YLIOPISTON JULKAISUJA – ANNALES UNIVERSITATIS TURKUENSIS
SARJA – SER. F OSA – TOM. 58 | TECHNICA – INFORMATICA | TURKU 2025

University of Turku

Faculty of Technology
Department of Mechanical and Materials Engineering
Materials Engineering
Doctoral programme in Technology (DPT)

Supervised by

Professor, Pekka Peljo
University of Turku
Turku, Finland

University lecturer, Ulriika Mattinen
University of Turku
Turku, Finland

Reviewed by

University lecturer, Luis Arenas
University of Southampton
Southampton, United Kingdom

Professor, Edwin Otten
University of Groningen
Groningen, The Netherlands

Opponent

Dr, Petr Mazur
University of Chemistry and Technology
Prague, Czechia

ISBN 978-952-02-0175-3 (Print)
ISBN 978-952-02-0176-0 (PDF)
ISSN 2736-9390 (Print)
ISSN 2736-9684 (Online)
Painosalama, Turku, Finland 2025

No hace falta más que entrecerrar los ojos
Para verte gambetear

UNIVERSITY OF TURKU
Faculty of Technology
Department of Mechanical and Materials Engineering
Materials Engineering
GABRIEL GONZALEZ: Next generation aqueous organic flow batteries
Doctoral Dissertation, 173 pp.
Doctoral Programme in Technology (DPT)
February 2025

ABSTRACT

There is an urgent need to minimize the dependence on fossil fuels consumption. The use of renewable energy sources, such as wind and solar generation, requires its integration to large-scale storage systems to balance the production and consumption. The challenge arises from the development of a scalable, inexpensive and efficient storage solution. In this sense, flow batteries appear as a promising technology. Nowadays, the state-of-art is based on the use of vanadium as the redox active material, although other chemistries have been extensively developed. In this work, we focus our study on the use of organic molecules as active materials, as well as we developed a monitoring system to get an insight of the flow battery operation.

We believe that the use of organic materials obtained from natural sources can provide a sustainable, inexpensive and scalable solution. Furthermore, the new compounds need to be highly soluble and possess a suitable redox potential to produce competitive batteries with high energy and power densities. In this work, we tested new synthetized organic molecules to overcome these challenges. First, we studied pyridoxal derivatives obtained from Vitamin B6, providing an example of materials synthetized from natural sources. We next studied bisphosphonate as a new substituent for the widespread viologen core with an improved redox potential. Finally, we successfully introduced azoniafluorenone as a new organic family for energy storage. Its high solubility coupled with the ability to store two electrons at neutral pH resulted in large storage capacity.

Both the improvement of the existing systems as well as the development of new ones require methods capable to monitor the battery during operation in a reliable way. In this thesis, we present a measurement system that allows getting an insight of the battery operation by recording the half-cell state of charges and overpotentials of each side of the cell independently. We used this system to study the performance of both the vanadium and an organic flow battery during operation. Furthermore, we extended its use to analyze the improvement on the battery operation when utilizing a novel chemical treatment to activate the battery electrodes.

KEYWORDS: Vanadium flow battery, organic flow battery, half-cell measurements, state of charge, over-potentials

TURUN YLIOPISTO
Teknillinen Tiedekunta
Kone- ja materiaalitekniikan laitos
Materiaalitekniikka
GABRIEL GONZALEZ: Uuden sukupolven vesipohjaiset orgaaniset virtausakut
Väitöskirja, 173 s.
Teknologian tohtoriohjelma
Helmikuu 2025

TIIVISTELMÄ

Riippuvuutta fossiilisten polttoaineiden kulutuksesta on vähennettävä kiireellisesti. Uusiutuvien energialähteiden, kuten tuuli- ja aurinkovoiman, käyttö vaatii näiden integroimista suuriin energiavarastoihin energiantuotannon ja -kulutuksen tasaamiseksi. Haasteena on skaalattavien, edullisten sekä tehokkaiden energia-ratkaisujen kehittäminen. Tässä mielessä virtausakut nousevat esiin lupaavana teknologiana. Tällä hetkellä kaupalliset virtausakut käyttävät vanadiumia redox-aktiivisena materiaalina, vaikkakin muita materiaaleja on kehitetty laajalti. Tässä työssä keskitytään orgaanisten molekyylien käyttöön aktiivisena materiaalina sekä mittausjärjestelmän kehittämiseen saadaksemme tietoa virtausakun toiminnasta.

Me uskomme, että luonnollisista lähteistä saatujen orgaanisten materiaalien käyttö tarjoaa kestävän, edullisen ja skaalattavan ratkaisun. Lisäksi uusien yhdisteiden tulee olla hyvin liukenevia sekä omata sopiva redox-potentiaali tuottaakseen kilpailukykyisiä suuren energiatiheyden ja tehon akkuja. Tässä työssä tutkimme uusia synteettisiä orgaanisia molekyylejä ratkaistaksemme nämä haasteet. Ensin tutkimme B6-vitamiinista muokattuja pyridoksaaleja, tarjoten esimerkin luonnollisista lähteistä syntetisoiduista materiaaleista. Toisena tutkimme bifosfonaattia uutena substituenttina laajalti käytetyn viologeenin ydinrakenteelle parantaen redox-potentiaalia. Viimeisenä esittelemme azoniafluorenonin uutena orgaanisten molekyylien perheenä energiavarastoihin. Sen korkea liukoisuus yhdistettynä kykyyn varastoida kaksi elektronia neutraalissa pH:ssa johti suureen energiakapasiteettiin.

Sekä olemassa olevien energiajärjestelmien että uusien kehittäminen vaatii tapoja, joilla pystymme seuraamaan akun toimintaa käytön aikana luotettavalla tavalla. Tässä väitöskirjatyössä esittelemme mittausjärjestelmän, joka sallii akun toiminnan syvemmän ymmärtämisen mittaamalla lataustilan ja ylipotentiaalin akun molemmissa puolikennoissa itsenäisesti. Käytimme tätä järjestelmää sekä vanadium- että orgaanisen virtausakun toiminnan tutkimiseen käytön aikana. Lisäksi laajensimme mittausjärjestelmän käyttöä analysoimalla akun toiminnan paranemista, kun akun elektrodit aktivoitiin uudella kemiallisella käsittelyllä.

ASIASANAT: Vanadiini-virtausakku, orgaaninen virtausakku, puoli-kenno-mittaukset, lataustila, ylipotentiaalit.

Table of Contents

Table of Contents **6**

Abbreviations **8**

List of Original Publications **9**

1 Introduction **10**

2 Energy Storage Systems **13**

3 Flow Batteries Overview **15**
3.1 Flow Battery Technology 15
3.1.1 Main characteristics 17
3.1.2 Operational parameters 19
3.1.3 Cell components 20
3.1.3.1 End plates 21
3.1.3.2 Flow frames 21
3.1.3.3 Current collectors 22
3.1.3.4 Bipolar plates 22
3.1.3.5 Electrodes 22
3.1.3.6 Membrane 23
3.2 Vanadium Flow Batteries (VFBs) 23
3.3 Aqueous Organic Flow Batteries (AOFBs) 25
3.3.1 Posolytes 26
3.3.1.1 Organometallic complexes 27
3.3.1.2 Metalocenes 28
3.3.1.3 Aminoxyl radicals 28
3.3.1.4 Thiazines 29
3.3.2 Negolytes 30
3.3.2.1 Quinones 31
3.3.2.2 Viologens 32
3.3.2.3 Pyrazines, phenazines and alloxazines 33
3.3.2.4 Fluorenones 35
3.4 Experimental Techniques for FB Study 35
3.4.1.1 Battery cycling 36
3.4.1.2 Polarization curves 37
3.4.1.3 Impedance spectroscopy 38
3.4.1.4 Additional measurements 39

4 Materials and Methods 40
4.1 Electrochemical Techniques 40
4.1.1 Cyclic voltammetry 40
4.1.2 Bulk electrolysis in H-cell 41
4.2 Battery Tests 42
4.2.1 Battery cycling 42
4.2.2 Polarization curves 45
4.2.3 Impedance spectroscopy 45
4.3 Measurement System 45

5 Investigations of New Organic Materials 51
5.1 Pyridoxals 51
5.2 Bisphosphonate-functionalized Viologens 57
5.3 Azoniafluorenones 64

6 Experimental Measurement System 74
6.1 Validation of measurements 74
6.2 Cycling tests 76
6.3 Polarization curves 81
6.4 Study of chemically-treated carbon felts 84

7 Conclusions and Outlook 90

Acknowledgements 93

List of References 95

Original Publications 105

Abbreviations

FB	Flow battery
VFB	Vanadium flow battery
AOFB	Aqueous organic flow battery
SOC	State of charge
EESS	Electrical energy storage system
OCV	Open circuit voltage
CE	Coulombic efficiency
VE	Voltage efficiency
EE	Energy efficiency
Q	Electrical charge
I	Current
RTE	Round trip efficiency
DFT	Density functional theory
SHE	Standard hydrogen electrode
MV	Methyl viologen
NMR	Nuclear magnetic resonance
EPR	Electron paramagnetic resonance
UV-Vis	Ultraviolet-visible
CC	Constant current
CV	Constant voltage
CCCV	Constant current–constant voltage
ET	Electron transfer
PCET	Proton-coupled electron transfer
PT	Proton transfer
XPS	X-ray photoelectron spectroscopy
HT	Heat treatment
ST	Salt treatment

List of Original Publications

This dissertation is based on the following original publications, which are referred to in the text by their Roman numerals:

I Anton A. Nechaev, **Gabriel Gonzalez**, Prachi Verma, Vsevolod A. Peshkov, Anton Bannykh, Arsalan Hashemi, Jenna Hannonen, Andrea Hamza, Imre Papai, Kari Laasonen, Pekka Peljo, and Petri M. Pihko. Exploration of Vitamin B6-based redox-active pyridinium salts towards the application in aqueous organic flow batteries. *Chem. Eur. J.*, 2024; 30: e202400828.

II **Gabriel Gonzalez**, Anton A. Nechaev, Vsevolod A. Peshkov, Eduardo Martínez-González, Andrey Belyaev, Andrea Hamza, Mahsa Shahsavan, Petri M. Pihko, Pekka Peljo. Redox-active bisphosphonate-based viologens as negolytes for aqueous organic flow batteries. *Chem. Eur. J.*, 2025: e202404122.

III Maxime Artault, **Gabriel Gonzalez**, Pia Damlin, Juho Toivola, Aaron Mailman, Jenna Hannonen, Petri M Pihko, Pekka Peljo. Azoniafluorenones: a new family of two-electron storage electrolytes for sustainable near-neutral pH aqueous organic flow battery. *Adv. Energy Mater*., 2024; 14: 2401635.

IV **Gabriel Gonzalez**, Pekka Peljo. Experimental set-up for measurement of half-cell- and over-potentials of flow batteries during operation. *Batteries & Supercaps*, 2024; 8: e202400394.

V Justyna Piwek, **Gabriel Gonzalez**, Pekka Peljo, Elzbieta Frackowiak. Molten salt carbon felt oxidation for VRFB electrode performance improvement. *Carbon*, 2023; 215: 118483.

1 Introduction

There is an urgent need to reduce the greenhouse gas emissions and slow down the climate warming. This is a priority and responsibility of the whole society in order to provide a healthy world to the upcoming generations. Research done in academia should contribute to solving these issues, by researching possible solutions and technologies in the field of energy technology.

The urgent transition to a climate-neutral society requires switching to renewable and clean energy sources. Solar and wind generation appear as the leading solutions; however, they face challenges arising from their intermittent generation and the mismatch with the consumption profile. Electrical energy storage systems (EESSs) are a possible solution to solve the mismatch.

Ranging from lithium-ion batteries to hydropower storage systems, there are many different technologies available for energy storage. All these systems are characterized with strengths and weaknesses that make them suitable for different applications. Pumped hydropower is the most widespread technology for large-scale storage, but suffers from requirements of suitable locations with sufficient elevation differences. There is clearly a need for alternative technologies for such large-scale storage. Overview of energy storage technologies is presented in Chapter 2.

The main requisites for mid-term large storage systems include scalability and low cost per kWh of stored energy. On that sense, flow batteries (FBs) appear as a promising technology, also providing long-cycling life, fast response, safety and their unique capability to decouple energy and power, which makes them easy to scale. An overview of the FB technology is presented in the Chapter 3 of this dissertation.

The most developed FB, based on vanadium as the redox material, is already successfully commercialized worldwide. However, the use of the VFB for large-scale applications is still limited by the high cost and availability of vanadium. Other inorganic chemistries have also been considered, including iron-chromium and zinc-bromine, which have also reached the commercialization phase. Furthermore, aqueous organic flow batteries (AOFBs) have emerged as promising candidates for large-scale applications, considering that the organic materials could be synthetized from natural sources in a scalable and inexpensive way. An additional advantage of

organic chemistry includes the possibility of tune the molecules to achieve the desired properties to improve the battery key parameters and operation. Improvements on the stability, solubility and redox potential of the organic materials can be obtained by applying the proper molecular design, leading to longer battery lifetime and higher energy and power densities. Despite the rapid progress, further research is still required to overcome the main challenges of this technology to be competitive for large-scale applications, mainly related to cost, stability and scalability.

The research work presented on this dissertation focuses on the development of aqueous flow batteries as we believe they possess high potential for large-scale energy storage application. Chapter 4 presents the materials and methods utilized in this work, while the results are summarized in Chapters 5 and 6. In the first part of the dissertation, we focus the research work on the study of new organic molecules to be used as redox materials in AOFBs. The synthesis of the new materials was performed at the Department of Chemistry of University of Jyväskylä, while we performed the electrochemical and battery tests at University of Turku. Taking advantage of the tunability of the organic molecules, different molecular design strategies were applied aiming to overcome the current drawbacks of the FB technology. In our first work (**Publication I**), we studied pyridoxal derivatives as negolytes (electrolytes at the negative side of the cell) for AOFBs. These compounds are derivatives of Vitamin B6, presenting an example of materials obtained from natural sources that could solve the scalability and cost limitations. Despite the low performance of the pyridoxals when tested on FBs due to their poor cycling stability in aqueous electrolytes, these first investigations provided useful information for the design and study of the next molecules. In the second work (**Publication II**), we modified a widespread AOFB negolyte: the viologen core. In this case, we tuned the viologen structure by introducing a new substituent consisting of bisphosphonate group. The addition of this bulky negatively charged functional group can lead to a highly soluble and stable material, while its electron-donating effect reduces the redox potential to more negative values, resulting in higher cell voltage and power density. In our third work (**Publication III**), we introduced azoniafluorenones as a new family of negolytes for AOFBs. These novel derivatives display high solubility and the ability to store two electrons at neutral pH electrolytes; as a result, the resulting battery exhibits large storage capacity. We performed the study of the new family by introducing different functional groups and varying the position of the substituent on the pyridinium ring until finding the most promising candidate, which exhibited high performance when tested in a flow battery even at high concentration. These works clearly illustrate the broad opportunities when considering organic molecules as well as the importance of the proper molecular design for battery optimization.

In the second part of this work, we introduced an experimental set-up to monitor and get an insight of the battery operation (**Publication IV**). We understand that a reliable monitoring system during battery operation is required for both the development of new systems as well as the improvement of the existing ones. The battery set-up is based on the use of additional monitoring flow cells, before and after the battery, including reference electrodes on both the positive and negative side. This configuration allows the measurement of the half-cell open circuit potentials and overpotentials of both sides of the cell separately. These measurements enable a deeper study of the cell and the processes involved during battery operation. The measurement system was applied to perform detailed studies of the vanadium flow battery (VFB) and an organic-FB employing a viologen-ferrocene couple. Furthermore, we extended its use to investigate the performance of heat- and chemically-treated carbon felts used as electrodes in a VFB (**Publication V**). In that research work, performed in collaboration with the Poznan University of Technology from Poland, we demonstrated how a novel chemical treatment, based on molten nitrate salts, can enhance vanadium reactions with different impact on the negative and positive electrodes.

The objectives of this dissertation are centered on two main tasks:

1. First, we focused our research work on the development of new organic materials for application in Aqueous Organic Flow Batteries. Taking advantage of the tunability of the organic molecules, we studied new synthetized materials, including different structures and substituents, with the aim of overcoming the challenges of the FB technology. The studies ranged from basic electrochemical analysis to actual tests on flow cells.
2. The second task includes the development of an experimental set-up that allows an insight on the flow cell performance during operation. We believe that a reliable monitoring of the battery is crucial to understand the processes occurring during battery operation, allowing a better control and pinpointing the sources of losses of these systems. By including additional monitoring cells with reference electrodes, we were able to measure the half-cells potentials and overpotentials and, as a result, obtain a further understanding of the cell performance losses.

2 Energy Storage Systems

Our planet is facing undeniable climate change, clearly evidenced by the rising temperatures, the increased concentration of carbon dioxide in the atmosphere and the melting of polar ice and subsequent sea levels´ rise.[1] The climate change has been significantly accelerated by the human activity and its influence on the greenhouse emissions, with the main contribution arising from the consumption of fossil fuels.[1,2] The increasing concern about the irreversible damage to our planet has urged to a strong short-term reduction on the consumption of these non-renewable sources. On that sense, countries all around the world and international organizations have defined policies and commitments with the attempt of mitigating the climate change.[3] During the United Nations Climate Change Conference in 2015, 196 parties compromised, under the Paris agreement, to reduce greenhouse emissions through nationally determined contributions.[3] In the case of European Union, the target is to reduce the greenhouse gas emissions to 40% by the year 2030, compared to the levels in 1990, and by 80-95% by 2050.

In order to achieve these targets, a key solution involves the generation of electricity from renewable sources instead of fossil fuels. As a result, during the last decades, a special attention has been given to wind[4] and solar[5] energy sources because of the maturity of those technologies. However, technical and economic barriers have slowed down their deployment and commercialization.[6] A common drawback of these technologies is their intermittent generation, presenting an energy production profile that mismatches with the consumption requirement. The use of large-scale electrical energy storage systems (EESS) can balance these differences, allowing the integration of the wind and solar energy sources.[7,8]

The required energy integration has led to large and rapid improvements on the development of EESS. The available storage technologies include electrochemical (fuel cells, supercapacitors and batteries), thermal (sensible or latent heat) and mechanical (hydropower, compressed air and flywheels) systems.[9,10] Each technology presents specific drawbacks and benefits that make them suitable for different applications depending on technical and economic criteria. For example, lithium ion batteries have fulfilled the market of electronic devices and, more recently, they have been successfully incorporated into electric cars. Their

deployment for these applications is based on their high efficiency, high energy and power density, fast response and sufficient lifetime.[11] On the other hand, hydropower energy storage is a mature technology normally used for large-scale applications because of their prolonged lifetime with minimum operation and maintenance costs. However, they disadvantages include low energy density and specific topographic conditions, which limit their use for large-scale specific-located applications.[12]

When considering systems for large-scale storage applications, the main requirements include low cost and availability, besides high efficiency and sustainability.[7] Pump-hydro has been considered as one possibility as it fulfils these requirements. However, its application is strictly limited by sizing and geographical restrictions. On the other hand, lithium-ion batteries are also possible candidates for this purpose, although they present risks related with thermal runaway and fire or explosion hazards,[13,14] besides the high-production scale can be limited by lithium scarcity.[15] Li-ion batteries are required for electrification of the transportation, so their availability for large-scale stationary energy storage at the required TWh scale is questionable. On that sense, an increasing attention for large-scale application has been given to flow batteries (FBs).[16] FBs present fast response and long lifetime, while they are safe and relatively easy scalable. Furthermore, the selection of suitable redox materials can lead to reduced costs and high availability. This emerging technology seems to fulfil all the requirements needed to provide an effective solution for the integration of renewable energy sources. An overview about flow batteries is presented in Chapter 3 of this dissertation, with a focus on the state-of-art technology, based on vanadium flow battery, and aqueous organic systems, considering that our investigations were based on the study of organic compounds as redox active materials.

3 Flow Batteries Overview

Flow batteries are a type of rechargeable ESS where the electrical energy is stored as chemical energy through redox active materials that are dissolved in liquid electrolytes stored in two separate tanks. The electrolytes are pumped from the reservoirs to the electrochemical cells, where the active compounds undergo redox reactions during charge and discharge, and then pumped back to the tanks. This configuration makes FBs flexible, easily scalable and suitable for stationary large-scale applications. Since the appearance of the first FB, different aqueous and non-aqueous electrolytes and active materials have been considered, and most promising technologies are now being commercialized. In this chapter, a brief description of the flow battery technology and developed aqueous systems, including vanadium and organic chemistries, is presented.

3.1 Flow Battery Technology

The idea of a flow battery was introduced for the first time by John Doyle and patented in 1879.[17] The battery, however non-rechargeable and different from the current version of the FB technology, was a zinc-bromine *galvanic battery* (as the patent title indicated) where multiple cells were refilled by the *excitant* that flowed from a main reservoir. The denomination *flow battery* was adopted later referring to the flow of the electrolyte between the tank and the electrochemical cell. However, by that time, the demand for large energy storage was not an urgent matter and then the attention towards these systems was limited. With the increasing concern about using renewable energies to replace fossil fuels and the resulting storage necessity, the interest for these systems was renewed in the second half of the 20th century. In the 1970s, flow batteries started to be investigated by Thaller from NASA in USA and Nozaki et al in Japan.[18] An important step forward for the FB technology was the introduction of the vanadium chemistry applied to FBs by Skyllas-Kazacos in Australia by 1986.[19] In the last decades, the FB technology has evolved rapidly with the emergence of many new systems.[20]

Basically, the FB technology comprises a stack consisted of several electrochemical cells, where the reversible electrochemical reactions occur, and two reservoirs, one for the positive side (named *posolyte*) and one for the negative side

(named *negolyte*), where the active redox materials are dissolved in liquid electrolytes.[21] The electrolytes are pumped from the reservoirs to the cell stack, where the redox couples react on the electrodes surface during battery charge and discharge, and then flow back to the reservoirs. The electrical energy is stored in the solutions in the form of chemical energy after reaction: during charging by an external source, the electrical energy oxidizes the material stored on the posolyte while it reduces the one on the negolyte. In other words, through the flow of current, electrons are withdrawn from the posolyte redox couple (oxidation) while injected on the negolyte (reduction). During discharge, the opposite processes occur as spontaneous reactions and the battery provides the energy back as electricity (**Figure 1**).

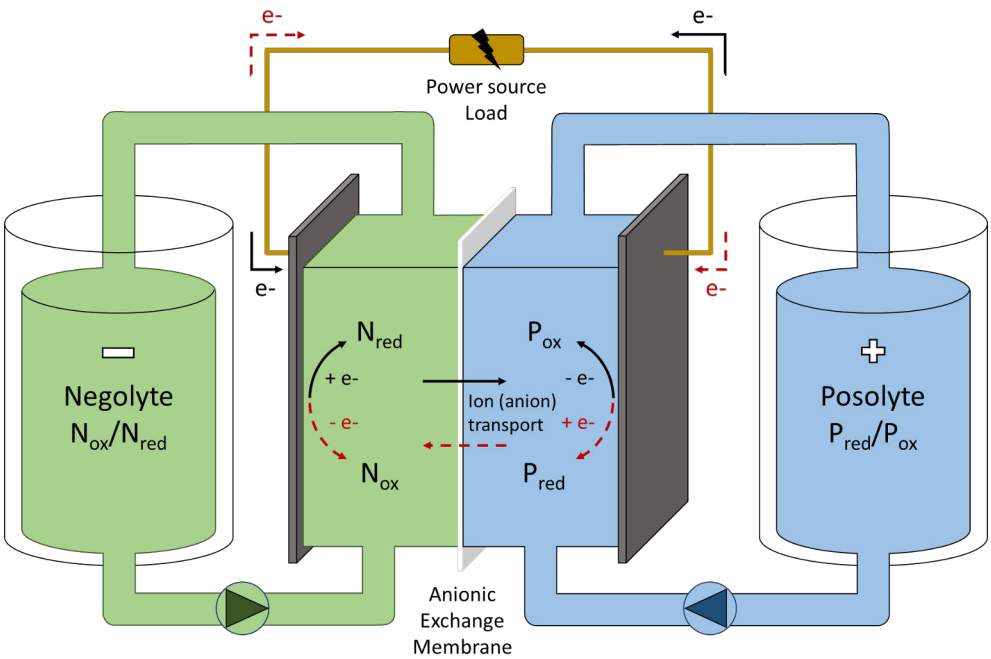

Figure 1. Flow battery scheme and redox reactions taking place on the positive and negative side. Anion exchange membrane (AEM) considered. Black arrows indicate the flow when charging, and red dashed arrows when discharging.

The electrochemical cell consists of a positive and negative electrode where the redox reactions take place.[21] These electrodes are normally porous structures, which enable the flow of the liquid electrolytes and provide high surface area for the electrochemical reactions. The electrodes are in electrical contact with current collectors that allow the flow of electrons needed for the redox reactions during the

charging and discharging processes. In the cell, the electrolytes from the positive and negative side are separated by an ionic membrane. The purpose of the membrane is not only to avoid the mixing of the electrolytes, but also to complete the electrical circuit by enabling the transport of ions and then the flow of current.[21] The membranes can be either anion or cation exchange membranes (AEM or CEM, respectively). When using AEM (**Figure 1**), anions move in the same direction as the electrons to close the electrical circuit and balance the charges on each side of the cell; when using CEM, the cations move in the opposite direction of electrons.

The FB configuration brings certain benefits for stationary applications when comparing with other conventional batteries, e.g. lithium-ion batteries.[16,21] One of the main advantages arises from storing the energy in outer reservoirs separated from the cell. This arrangement provides the possibility to size energy and power independently: while the energy is determined by the size of the tanks and the amount of dissolved material in the electrolyte, the power is defined by the single-cell voltage and the area and number of cells connected in series in the stack. This unique ability makes FBs flexible and easily scalable, reducing the costs of incremental storage capacity.[22] Furthermore, the use of liquid solutions stored apart from the power device eases the replacement and recycling of the electrolytes, as well as significantly decreases thermal runaways and fire risks, which are one of the main concerns of the lithium-ion technology.[13,14]

3.1.1 Main characteristics

The selection of the storage technologies for different applications is based on technical and economical characteristics that define the ESS.[9,10] Next, the main technical parameters of FBs are reviewed.

- *Energy storage capacity:* is the available energy stored in the ESS when it is fully charged. In a FB, it is defined by the cell voltage and the charge storage capacity, which is the amount of electrons that can be reversibly exchanged by the redox species stored in the tanks. Therefore, the energy storage capacity directly depends on the size of the tanks and the amount of dissolved electroactive material. The use of liquid electrolytes leads to lower energy density and larger systems when compared with the conventional batteries working with solid active materials: while vanadium system exhibits an energy density of 20-30 Wh L^{-1}, this value exceed 300-400 Wh L^{-1} for lithium-ion batteries.[10] For higher energy densities, many strategies have been considered, from increasing the solubility of the redox couples[23,24] to the use electroactive solid materials stored in the tanks (*solid boosters*).[25,26] Furthermore, taking advantage of molecular design and the tunability of organic materials, many redox couples have been developed

with the ability of storing multiple electrons to enhance the energy density of these systems.[27]

- *Output power:* is the rate at which the energy is transferred, e.g. the rate at which the battery is discharged (or charged). The maximum power is defined by the cell polarization response, depending on the cell voltage, resistance, polarization losses and available area.[28] The cell voltage (E_{cell}) is a function of the equilibrium redox potentials (E^0), positive and negative electrodes overpotentials (η) and ohmic losses in the cell (iR).[29]

$$E_{cell} = E^{0^+} - E^{0^-} - |\eta^+| - |\eta^-| - iR \qquad (1)$$

Higher cell voltages are obtained by using redox couples with higher redox potentials on the positive electrode and with lower values on the negative side.[30] While the open circuit voltage (OCV = $E^{0^+} - E^{0^-}$) for VFB is 1.26 V, there is a wide range for the organic chemistries, with a highest value of 4.50 V reported for a non-aqueous OFB.[31] Regarding the cell voltage losses (overpotentials), they can be minimized through proper cell design.[28,29] The use of conductive materials and electrolytes coupled with reduced gap between electrodes lead to reduction of ohmic losses (ohmic overpotentials). The utilization of flow fields and improved electrolyte flow reduce the electrodes mass-transfer limitations (concentration overpotentials), while the electrode kinetics towards the desired electrochemical reactions (charge-transfer overpotentials) can be enhanced by the use of catalysts or the activation of the carbon electrodes (thermal or chemical electrode pre-treatment).[21,32]

- *Lifetime* or *durability:* is the estimated lifespan of the ESS, which is normally reported as the maximum number of cycles or operational years. The shortening of the lifetime operation (*ageing*) is exhibited as a decrease on the usable battery capacity. While the capacity of lithium-ion batteries can drop by 20% during several years, with a lifespan of about 1.000-3.000 cycles or 5-10 years, FBs can operate in principle for more than 15.000 cycles or up to 20 years with minimal capacity decline.[33] The longer lifespan of the FB technology is attributable to the absence of solid-solid interactions and self-discharge in stand-by mode, which are common problems of the lithium technology.[34] Contrarily, the most important causes of capacity loss in FBs are related to the instability of the active materials and the crossover of the species through the membrane.[35] While these phenomena are manageable when using vanadium chemistry, they are still the main challenge for the deployment of organic systems.[36]

- *Discharge time:* is the discharge (or charge) duration at the nominal power. For most of the ESS, to select the optimal discharge time is challenging because of the link between power and energy. However, this is not a limitation for FBs where these parameters can be sized independently. Due to cost effective reasons, most of the FBs systems are designed with a discharge time of 4-6 hours.[22]
- *Round-trip efficiency (RTE):* is the ratio between the energy released during discharge and the energy required to charge the battery. This parameter is a measure of the system energy losses due to self-discharge, internal cell resistance and kinetically unfavourable reactions.[16] Normally, the losses because additional instruments or equipment (pumps, electronics, etc.) are included. The round-trip efficiency of FBs is in the range of 60-80% while it depends on the current density and operating conditions.

3.1.2 Operational parameters

The FB operation is characterized by a series of metrics that enable the analysis of the battery performance.[21,37] The assessment of these operational parameters is crucial for the development and comparison of the different FB technologies and their components. The key figures normally used to evaluate the cell performance are:

- Coulombic efficiency (CE): is the ratio between the electrical discharged capacity and the charged capacity on a cycle.

$$\mathrm{CE}\ (\%) = \frac{Q_{\mathrm{discharge}}}{Q_{\mathrm{charge}}} * 100\ \% = \int \frac{I_{\mathrm{discharge}}}{I_{\mathrm{charge}}} \mathrm{d}t * 100\ \% \qquad (2)$$

  CE is a measure of the capacity lost during a cycle, mostly attributable to active species side reactions, crossover through the membrane and parasitic reactions (hydrogen or oxygen evolution).[37] These capacity losses can be reversible or irreversible.

- Voltage efficiency (VE): is the ratio between the average voltage during discharge and the average voltage during charge.

$$\mathrm{VE}\ (\%) = \frac{\bar{V}_{\mathrm{discharge}}}{\bar{V}_{\mathrm{charge}}} * 100\ \% \qquad (3)$$

  VE is an indication of the losses due to electrode polarizations (activation and concentration overpotentials) and electrical resistance.[37] VE depends on the applied current density. The relantioship between voltage lossess and current density is normally studied using polarization curves.[38]

- Energy Efficiency (EE): is the ratio between the output energy during discharge and input energy during charge. It can be calculated as the product of the CE and the VE or by integrating the power over time.[37]

$$\mathrm{EE}\ (\%) = \mathrm{CE} * \mathrm{VE} \qquad (4)$$

  As the product of the CE and VE, EE includes all the battery losses. It is equivalent to the round trip efficiency (RTE), however it normally does not include the losses related to the additional equipment (electronics, pumps, etc).

- Capacity utilization: is the ratio between the discharge capacity and the theoretical capacity expected from the limiting side of the cell. The latter is a function of the amount of the active material (volume and concentration) and the number of electrons that it can store.[37]

$$\text{Capacity Utilization}\ (\%) = \frac{Q_{\text{discharge}}}{Q_{\text{theoretical}}} * 100 \qquad (5)$$

  The capacity utilization indicates how much material is utilized and it defines the storage capacity. It depends on the applied current density. Higher current values lead to higher overpotentials; as a result, the voltage cut-off during charging is reached at lower capacity utilization.

- Capacity decay: is the evolution of the capacity lost during cycling. It is expressed as the percentage of capacity lost per cycle or day.

$$\text{Capacity Decay}\ (\%) = \frac{\mathrm{d}Q}{Q_{\text{initial}} * \mathrm{N}_{\text{cycles}}} * 100\ \% \qquad (6)$$

  The capacity fade rate is an indication of the durability or lifetime of the battery, and it depends on the stability of the active materials and crossover of species through the membrane.[36,37] The capacity fade can be related to reversible or irreversible processes.

3.1.3 Cell components

The cell is the electrochemical device where the oxidation and reduction reactions take place through the flow of current during the charging and discharging processes.[21,29] A single-cell consists of a positive and negative electrode separated by an ionic membrane. During charging, a voltage difference is applied between the two electrodes by an external source to force the flow of electrons and drive the electrochemical reactions: oxidation on the positive electrode and reduction on the negative electrode. During discharging, the opposite spontaneous reactions take place in the cell to provide the energy back to the load. The current flow is transmited from the electrodes to the battery terminals using bipolar plates and current

collectors. To feed the active materials, the electrolytes are pumped from the reservoirs into the cell through flow frames that ideally ensure a uniform distribution over the electrodes. The outer part consists of two endplates that maintain the cell structure and provide mechanical strength. The optimization of the FB performance requires the selection and design of the suitable cell components.[21,29,39] The main cell components are depicted in **Figure 2** and briefly described below.

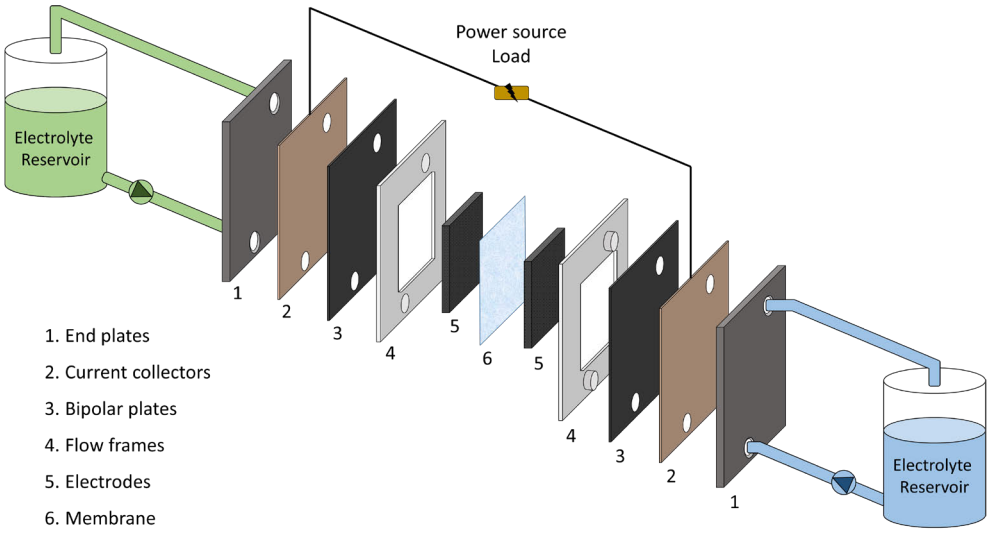

Figure 2. Single-cell main components.

3.1.3.1 End plates

The endplates on the extremes of the cell provide mechanical strength and maintain the cell structure. During the assembling, a known pressure is applied on the endplates to ensure the desired level of felt compression. High compression is required to increase the electrical contact between the felts and the bipolar plates; however, excesive values cause high pressure-drop increasing the electrical consumption of the pumps.[39] Therefore, a compromise value of felt compression is selected to optimize the battery performance.

3.1.3.2 Flow frames

The flow frames are responsible for suitable electrolyte distribution in the cell. An optimal flow distribution maximizes the use of the felt active area while maintining a low pressure-drop through the system.[29] The frame material must have high chemical stability as it is in contact with the electrolyte. The most common

configurations consist of flow-through and flow-by, and the selection depends on the different technologies.[21,39] In the flow-through configuration, the electrolyte directly flows through the porous electrodes without any specific path, while in the flow-by configuration the bipolar plates include flow channels with specific patterns that improve the electrolyte distribution and reduce the pressure-drop.

3.1.3.3 Current collectors

The current collectors conduct the flow current from the bipolar plates to the battery terminals. The current collectors are fabricated from conductive metals, with copper as the most common material.[37] Current collectors should not be in contact with the electrolytes.

3.1.3.4 Bipolar plates

The bipolar plates are in electrical contact with the carbon electrodes to conduct the current flow in the cells of the stack and finally to the current collectors.[37] The main material specifications include high conductivity, chemical and mechanical stability and low cost. Mostly, the bipolar plates are made of graphite, carbon-carbon or carbon-polymer composites.[40,41] When considering the flow-by configuration, the bipolar plates include a set of channels machined or stamped on the plate to improve the distribution of the electrolyte on the carbon electrodes and reduce the pressure-drop.[21,42]

3.1.3.5 Electrodes

In a FB cell, the role of the electrodes is to provide active sites for the redox reactions. For that purpose, inert high-surface materials are required. The electrode material also needs to be chemically and mechanically robust, electrically conductive and cost-effective.[21,43,44] Mostly, the FB electrodes consists of carbon-based materials in the form of felts or papers. Before the battery assembling, the electrodes are usually pre-treated, thermally or chemically, to activate the surface towards the electrochemical reactions.[39,45] In the case of the vanadium systems, the activation incorporates oxygen functional groups[45,46] to the carbon structure, increasing the wettability and enhancing the activity of the electrodes towards the vanadium reactions. Different activation strategies have been reported to incorporate functional groups,[47] including oxygen and nitrogen[48,49] groups, with the most common consisting of thermal treatment in air at 400-600 ºC.

3.1.3.6 Membrane

The membrane separates the two sides of the cell, preventing the mixing of the electrolytes.[21,39] At the same time, it allows the transport of ions, from one side of the cell to the other, to complete the electrical circuit and maintain the charge balance during the charging and discharging processes. The ionic membranes, which can be cation or anion exchange membranes, must have high conductivity, chemical and mechanical stability, ion-selectivity and low cost.[21,50] The classification depends on the functional groups that are responsible for the pass of ions: while the cation exchange membranes (CEM) are based on negatively charged groups to allow the movement of cations, the anion exchange membranes (AEM) have positively charged groups enabling the pass of anions.[21] The most common groups considered for CEMs are sulfonate, caboxylated and phosphate groups, while AEM include ammonium, guanidinium, and pyridinium groups.[51] The selection of the membrane depends on the charge of the active materials and the supporting electrolyte.

3.2 Vanadium Flow Batteries (VFBs)

Currently, vanadium flow batteries are the most developed and commercialized FB technology[16,52]. They were presented for the first time in the mid-1980s by Skyllas-Kazacos at the University of New South Wales, Australia.[19] Since the first large scale implementation in 1995 (800 kWh energy storage and 200 kW power), installed to perform load-levelling at a power station in Japan, the technology has spread worlwide with the largest battery constructed in 2023 in Dalian (China) with energy capacity of 400 MWh and power of 100 MW.[53]

The advantages of VFB systems arise from the vanadium chemistry. Besides its high solubility and stability, vanadium offers four oxidation states with enough potential difference between the redox couples that allows using the same electrolyte on both sides of the cell.[52] While the negative side contains the redox couple V^{+2}/V^{+3}, the positive side uses V^{+4}/V^{+5} (**Figure 3**). This configuration significantly reduces issues because of crossover of vanadium species and, at the same time, permits the regeneration of the electrolyte by simple mixing of the liquids of both tanks.[54] As a result, commercial vanadium systems can provide a stable operation for over 15.000 cycles or 20 years.[33]

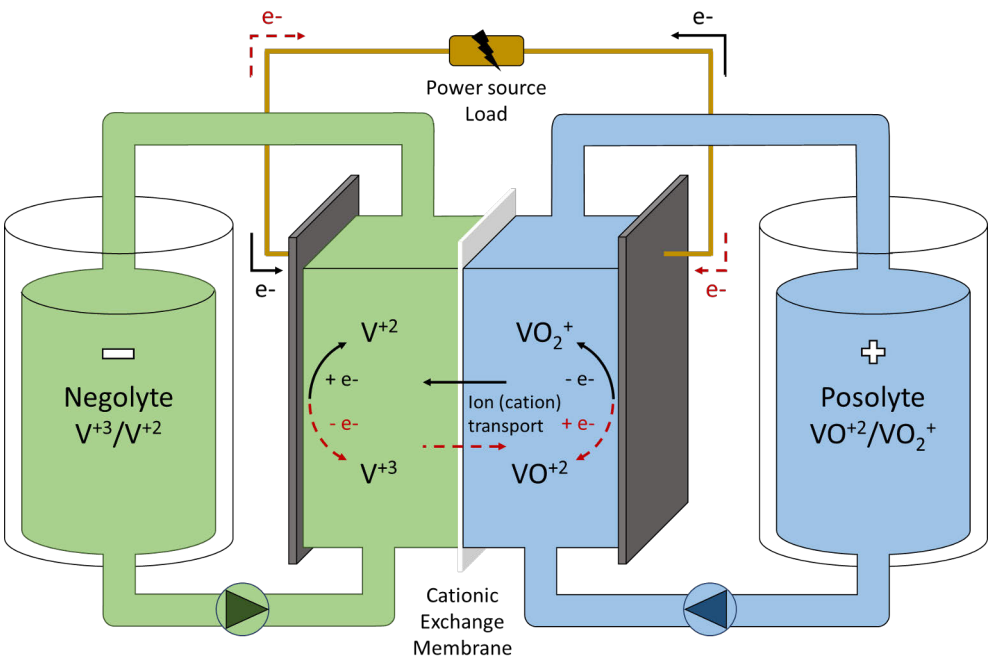

Figure 3. Vanadium flow battery scheme and redox reactions taking place on the positive and negative electrode. Cation exchange membrane (CEM) considered. Black arrows indicate the flow when charging, and red dashed arrows when discharging.

Vanadium electrochemical reactions consists of one-electron redox processes, with redox potentials of 1.00 and –0.26 V vs standard hydrogen electrode (SHE) for the positive and negative side, respectively, producing a open circuit potential of 1.26 V (equations 7-9).[52] Despite the low kinetics of these reactions on carbon electrodes, (rate constants of $1.4 \cdot 10^{-4}$ and $2.5 \cdot 10^{-5}$ cm s^{-1}, for the positive and negative side, respectively)[55] large improvements have been attained to increase the electrochemical reaction rates. On that sense, instead of using expensive catalytic materials, different activation methods have been applied to the carbon electrodes to improve their activity towards vanadium reactions and produce competitive systems.[32,56,57] During operation, side reactions on the electrode surface, including carbon corrosion and hydrogen and oxygen production on the negative and positive electrodes, respectively, can lead to a reduction on the battery lifetime.[58]

Positive side $\quad VO_2^+ + 2H^+ + e^- \leftrightarrow VO^{+2} + H_2O \quad E^o = +1.00\ V$ *(7)*

Negative side $\quad V^{+3} + e^- \leftrightarrow V^{+2} \quad E^o = -0.26\ V$ *(8)*

Full cell $\quad VO_2^+ + 2H^+ + V^{+2} \leftrightarrow VO^{+2} + H_2O + V^{+3} \quad E^o = +1.26\ V$ *(9)*

Furthermore, there are additional side reactions of the vanadium electrolyte that lead to capacity fade on the vanadium systems.[59,60] On the negative side, V^{+2} can be easily oxidized to V^{+3} in the presence of oxygen, which generates a self-discharge of the negolyte leading to cell-imbalance.[59,61] At the same time, the movement of vanadium cations through the membrane generates self-discharge because of the reaction of the V^{+5} and V^{+4} species of one side with the V^{+2} and V^{+3} species of the other side of the cell to produce the discharged species.[60] Regarding the membrane, cationic perfluorinated polymeric exchange membranes (Nafion technology) have been extensively used since the beginning of the vanadium flow batteries because of their high proton conductivity and stability in the strongly acidic and oxidative media.[62] The self-discharge generated by the movement of vanadium cations through the membrane increases the frequency of the regeneration process. Furthermore, an additional drawback on the use of these membranes arises from their high cost. As a result, anion exchange membranes have been further developed and they are currently being considered for commercialized vanadium flow batteries.[62,63] Despite their lower ionic conductivy, they strongly reduce the crossover of vanadium ions and battery self-discharge.

Vanadium electrolyte is based on acidic aqueous solutions, which enable high solubility of all vanadium oxidation states and provide the required protons for the electrochemical reactions.[64] Although some acid mixtures and addivitives have been investigated to increase solubility and stability at wide temperature ranges, the most common electrolyte consists of vanadium ions at 1.5-2 M concentration dissolved in 2-3 M sulphuric acid, leading to specific energy capacities of 20-35 kWh/kg.[64,65] The ideal electrolyte acid concentration arises as a compromise from the solubility and stability of the different vanadium species: while V^{+2} becomes less soluble at increase sulphuric acid concentration, V^{+5} suffers of precipitation issues at temperatures above 40 ºC that can be minimized by using higher acid concentration.[64] The strong acidic media demands the use of highly resistant cell materials, increasing the initial investment. Furthermore, the electrolyte has a major contribution to the cost of these systems, mainly because of vanadium, which amounts among 30-45% of the total cost.[66,67] The high cost and limited availability of vanadium are the main the main challenges limiting the deployment of the VFB technology for stationary large-scale storage applications.[68]

3.3 Aqueous Organic Flow Batteries (AOFBs)

The integration of FBs for stationary ESS has given special attention to organic materials due to the possitility of large-scale production from natural sources in a sustainable and inexpensive way.[69] Furthermore, with the proper molecular design, the organic molecules can be tuned to modulate the desired chemical and

electrochemical properties and make them stronger candidates for FB anolytes. In that sense, the redox potential, solubility, stability, number of electrons, kinetics, etc, can be improved to boost the cell performance and parameters, opening an unlimited scope for investigations.[70,71] Computational tools, such as density functional theory (DFT) calculations and machine learning, have been implemented to accelerate the screening of the organic molecules and the deployment of AOFBs.[72,73] These were main tasks of CompBat Project (European Union's Horizon2020 Research and Innovation programme under grant agreement No 875565), in which part of this research work was conducted.

One of the main challenges that has delayed the deployment of AOFBs arises from the reduced lifetime of the organic systems compared with the state-of-art technology consisting of vanadium chemistry.[36] The shorter lifespan is a result of the the lower stability of organic materials and the crossover of the species through the membrane, which appeared among the main challenges to overcome.[36] Despite being on developing phase, the AOFB systems have evolved at outstanding rate since the emerging of the first full-organic cell in 2009.[74] As a result, AOFB demonstrators of 100 kW and 400 kWh have already been successfully tested with a focus on the next scales in the order of MW.[75]

Despite the extensive bibliography and the fast development of organic molecules intended for aqueous flow batteries, the following sections provide a review about the candidates that, for the best of our knowledge, are representive materials. The main properties and technical characteristics of the materials are summarized. This overview is by no means comprehensive. Furthermore, some of the most interesting molecules developed are briefly presented, because of either their promising results or the improvement of a particular property of interest.

3.3.1 Posolytes

This section presents the main organic and organometallic materials that have been considered as posolytes for application in AOFBs. The molecular structure of the posolytes discussed in this section are presented in **Figure 4**.

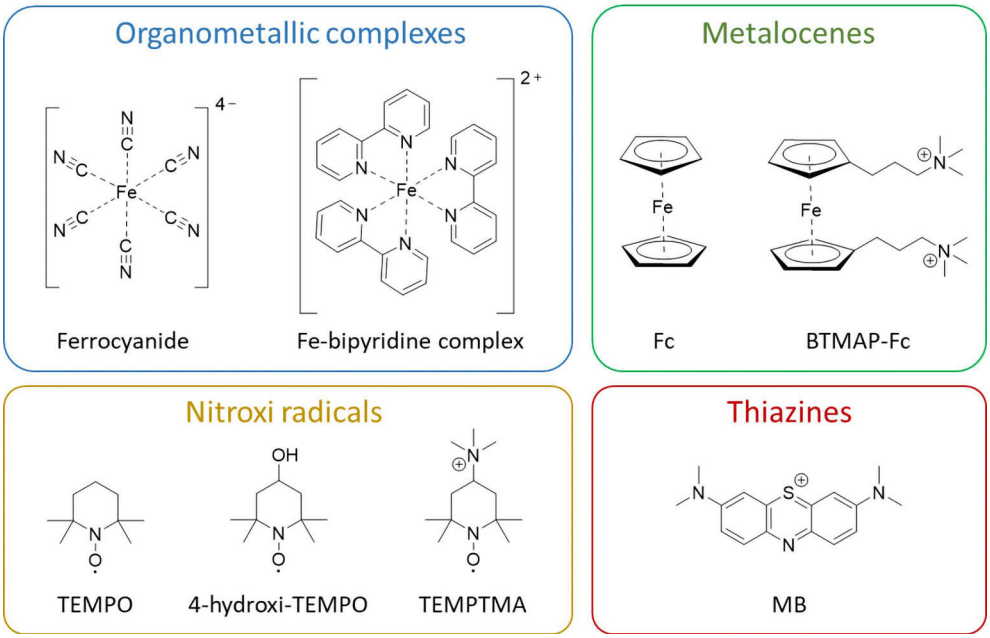

Figure 4. Molecular structure of the organic and organometallic posolyte materials discussed in this work.

3.3.1.1 Organometallic complexes

A metal complex is the union of a central metal ion with surrounding molecules, called *ligands*, through coordinated covalent bonds.[76] The amount of bounded ligands depends on the coordination number of the metal, the amount of electrons pairs that the ligand can offer (monodentate ligands offer one pair of electrons while polydentate offer multiple electrons), and the array. In the case of organometallic complexes, the metal atom is linked to the organic ligand via a metal-carbon bond or through a heteroatom such as nitrogen or oxygen.

Organometallic complexes consisting of earth-abundant transition metals (Fe, Ni, Cu, etc) have been extensively investigated as posolytes for flow batteries because they can provide a scalable, cost-effective and sustainable energy storage solution.[76] Metal complexes offer broad possibilities as different ligands can be considered to tune the desired characteristics for flow battery application. In a coordinated complex, the redox couple belongs to the metal center M^{+2}/M^{+3}, consisting of one-electron redox reaction with broad redox potential range that can be easily shifted by the selection of the ligand. For example, the redox potential of Fe^{+3}/Fe^{+2} as aqua complex is 0.77 V vs. SHE, while it shifted to 0.40 V when complexed with cyanide and to 1.10 V when complexed with bipyridine.[77,78] On the

same way, solubility and stability of the metal complex can be modified with the proper complex design.[79,80]

Several organometallic complexes have been reported as AOFB posolytes,[76,80] with ferrocyanide as the most popular candidate. Despite its relatively low redox potential (0.40 V vs SHE), ferrocyanide presents high availability, low cost and high stability at neutral and basic pH that make it a suitable candidate.[81] Furthermore, although ferrocyanide´s water solubility is moderate, 0.56 and 0.76 M when including Na^+ or K^+ as counter ions, respectively, it has been successfully increased by using counter ion mixtures (up to 1.5 M) or NH_4^+ (up to 1.6 M).[82,83]

3.3.1.2 Metalocenes

Metalocenes are a type of organometallic complexes formed by a metal atom bonded to two planar and parallel aromatic ligands.[84] Similar to metal complexes, they undergo one-electron redox reaction corresponding to the metal center. The most famous metalocene is ferrocene (Fc), consisting of iron ion sandwitched between two cyclopentadienyl ligands.[85] Ferrocene displays a highly reversible one-electron redox process and sufficient stability, which has led to use it as an internal standard to calibrate redox potentials (Fc^+/Fc) in non-aqueous solutions.[86]

Despite ferrocene´s high solubility in most organic electrolytes, it is nearly insoluble in water. In order to incorporate it to AOFBs, polar groups have been introduced to the ferrocene structure to give solubility in aqueous electrolytes.[76,87] For example, in a successful research work, quaternary ammonium groups were added to form a highly stable ferrocene (BTMAP-Fc) with increased solubility (up to 1.9 M in water) and a redox potential of 0.39 V vs SHE.[88] By coupling BTMAP-Fc with BTMAP-viologen, a highly stable battery was assembled at neutral pH using 1.3 M concentration of the active species and exhibiting a capacity decay of 0.10% per day. Due to the high stability and reversibility, several metalocenes have been considered for both aqueous and non-aquous OFBs.[76,80]

3.3.1.3 Aminoxyl radicals

An aminoxyl radical is a functional group with general structure $R_2N\text{-}O^{\bullet}$, characterized by a high stability because of the delocalization of the free electrons among the nitrogen and oxygen atoms.[89] Among aminoxyl radicals, 2,2,6,6-tetramethylpiperidine-1-oxyl (TEMPO) has been considered one of the best candidates for AOFBs posolytes because of its highly reversible one-electron reaction at high redox potential (0.76 V vs SHE),[90] high stability, low cost and easy accesibility. However, TEMPO derivatives exhibit poor stability in strong acid (disproportionation reaction)[91,92] and alkaline electrolytes (self-discharge reaction),[93]

which limits their use to neutral-pH media. Additionally, ring-opening reactions have been also proposed as decomposition pathways for TEMPO derivatives in both acidic and alkaline media.[94] Furthermore, because of its low solubility in water (70 mM), TEMPO needs to be functionalized with hydrophilic groups at the para position for aqueous flow battery application.[95,96]

The first TEMPO applied for AOFBs was introduced by Liu (4-hydroxi-TEMPO), exhibiting a redox potential of 0.80 V vs SHE and a maximum solubility of 2.1 M in water.[97] However, it demonstrated lower capacity retentions at increased concentration (above 0.5 M), which are mainly attributed to crossover of the oxidized species through the membrane.[94] Several TEMPO derivatives were further developed and different functional groups were introduced to optimize their performance as AOFB posolytes.[74,95] One well-known example was the development of TEMPTMA,[98] 4-trimethylammonium-TEMPO, which exhibited an increase on solubility (up to 3.2 M in 0.3 M NaCl), redox potential (1.0 V vs SHE), and stability, attaining a capacity loss of 0.27% per day even at 2 M concentration. Because of their high stability and very positive redox potential, TEMPO derivatives are considered the most popular posolyte materials for all-organic FBs when considering neutral-pH electrolytes.

3.3.1.4 Thiazines

Thiazines are aza-aromatic compounds in which one of the carbons has been replaced by a sulphur atom.[70] Different thiazine derivatives have been proposed as organic posolytes,[99,100] but their low solubility in aqueous electrolytes has limited their utilization for non-aqueous FBs. Methylene blue (MB), ammonium-functionalized phenothiazine, is one of the most representative materials within this family.[101] MB presents high stability coupled with positive enough redox potential in very acidic electrolytes (0.57 V vs SHE in 3 M H_2SO_4). However, it presents low solubility in water (0.2 M), which has been highly increased by using a mixture of acetic and sulphuric acid (up to 1.8 M).[101] When tested in a flow cell at 1.5 M, MB exhibited a capacity fade rate of 0.76% per day. Although this value is not low enough for FB consideration, the cause of the capacity decay was not attributed to the stability of MB as there was no evidence of decomposition after cycling. Indeed, the capacity loss was attributed to the unstability and crossover of the negolyte that became the limiting side of the cell.[101] These results encourage further investigations of this derivative.

3.3.2 Negolytes

This section presents the main organic materials that have been considered as negolytes for application in AOFBs. The molecular structure of the negolytes discussed in this section are presented in **Figure 5**.

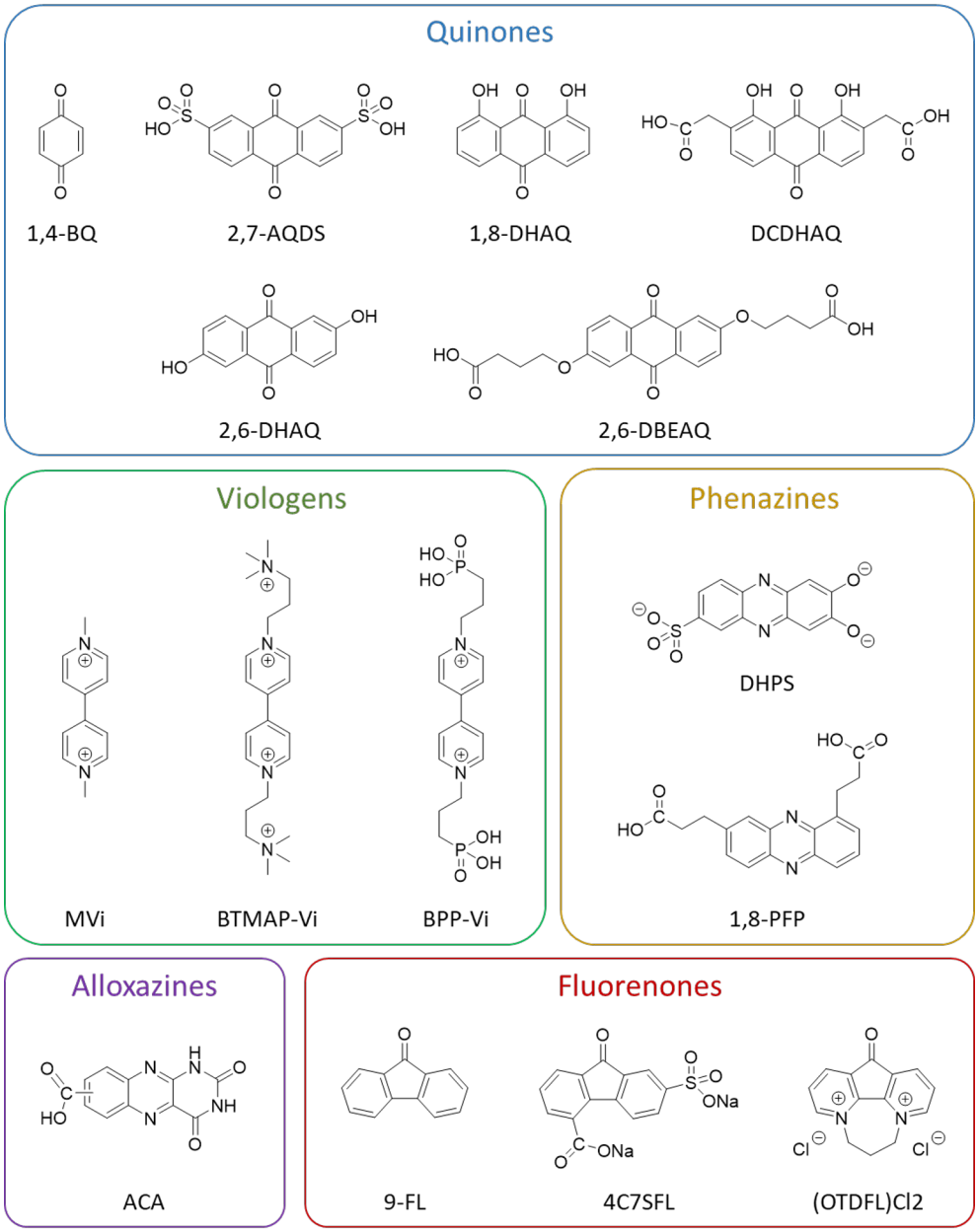

Figure 5. Molecular structure of the organic negolyte materials discussed in this work.

3.3.2.1 Quinones

Quinones are carbonyl (C=O) based compounds derived from aromatic structures. While 1,4-benzoquinone (1,4-BQ), the simplest member of the family, is formed by one aromatic structure, anthraquinone presents three aromatic rings. They are electrochemically active with the ability of exchange two electrons in acid, neutral and basic pH electrolytes. Their low cost, high solubility and stability after functionalization, make them promising candidates for flow battery applications, which have led to extensive investigations to optimize their performance in these systems.[102] Some of the current pilot-scale AOFBs technologies are built using quinones on the negative side of the cell, while one of these derivatives (DCDHAQ[103]) is already being produced in industrial scale (ton-scale) for FB application.[104]

Quinones can exhibit suitable solubilities once functionalized with aprotic groups. For example, functional groups as $–SO^{3–}$, $–CO^{2–}$, and $–PO_3^{2–}$ result on high solubilities when incorporated for antraquinones, while $–CO_2H$ and $–PO_3H_2$ leads to more soluble antraquinones in alkaline electrolytes.[102] It is worth to mention that the position of these substituents also plays an important role on the design of the quinone molecules.[105] Furthermore, quinone´s ability to exchange two electrons boost the storage capacity of quinone-based batteries. The mechanism of the redox process as well as the redox potential are strongly dependent on the pH of the solution and the pKa of the reduced forms.[69,105] The mechanisms, consisting of proton-coupled electron transfer (PCET) reactions have been studied in detail.[106] In acidic media, quinones undergo two-protons two-electrons process. At neutral pH, the process involves one proton and two electrons, while no protons are involved in the two-electron process at basic pH. Regarding the redox potential, it varies with the pH of the media at a rate of –59 mV and –30 mV per unit of pH, at acidic and neutral pH, respectively, while it is constant at basic pH. The pH values at which the electrochemical behaviour shifts is defined by the pK_a values of the reduced species. For example, anthraquinone-2,7-disulfonic acid (2,7-AQDS), with a solubility in pH-neutral electrolytes up to 1.9 M, has been further studied because of the availability and good performance in flow cells.[107,108] 2,7-AQDS exhibits pK_a values of 7.6 and 10.6 for the single and double reduced species, respectively, while clearly presenting PCET processes at pH values below 7.6, two-electron one-proton transfer reactions in the pH range 7.6-10.6, and finally electron transfer (ET) reactions with no protons involved at pH values above 10.6.[109] Regarding the redox potentials, 2,7-AQDS shows values of 0.17, –0.16 and –0.28 V vs SHE at pH 0, 7 and 13, respectively. Because of the positive redox potentials exhibited at acidic electrolytes, some quinone derivatives have been proposed as posolytes in the literature, in some cases leading to all-quinone FBs.[110]

Despite the versatility of quinones to be used in various electrolytes, the decomposition rates have been reported to be accelerated in acidic and neutral conditions, with the highest stabilities demonstrated in basic electrolytes.[36] The decomposition pathways include various mechanisms (disproportionation, dimerization, tautomerization),[34] as well as the self-discharge process occurring in presence of oxygen.[111] The reactivity of the reduced forms of negolyte materials with oxygen is a common issue for organic compounds, which leads to conduct the flow battery investigations in nitrogen-filled environments.[70,74] In the case of dimerization, however it can be reversible under specific conditions, the mechanism limits the use of the full capacity at increased quinone concentration. This has been previously demonstrated for 2,7-AQDS: when tested at 50 mM in 1 M H_2SO_4, only 1.5 electrons per molecule of quinone could be reversibly accessed.[108] Numerous quinones derivatives have been developed in order to minimize the rates of the decomposition reactions at the same time that improving redox potentials and solubilities, leading to extensive bibliography on quinones applied to AOFBs.[102] One example is the improvement attained with the derivative 2,6-dihydroxylanthraquinone (2,6-DHAQ). Despite its good stability for two-electron cycling and low redox potential when tested in alkaline electrolyte, its use in AOFBs has been limited because of its low solubility. [112] In a recent work, [113] 2,6-DHAQ was further functionalized with highly alkali-soluble carboxylate groups, increasing its solubility six fold in basic electrolytes (0.6 and 1.1 M at pH 12 and 14, respectively) while also improving its stability. The resulting 4-4′((anthraquinone-2,6-diyl)dioxy)dibutyrate (2,6-DBEAQ) exhibited a capacity decay of 0.05 % per day (3% per year) when tested at a concentratrion of 0.5 M at pH 12, acchieving one of the lowest values reported for quinone derivatives. A similar approach was performed for the development of DCDHAQ,[103] after functionalization of the precursor 1,8-DHAQ with carboxymethyl groups. The strong improvements on solubility and stability, together with the easy obtention and potential low-cost, resulted on an organic material that seems to fulfil the technical requirements requested for an AOFB negolyte for commercialization.

3.3.2.2 Viologens

Viologens are N,N′-disubstituted-4,4′-bipyridinium salts, exhibiting two consecutive reversible one-electron redox reactions on the nitrogen atoms. Viologens also have good solubility in aqueous media and can be easily synthetized and tuned, which make them suitable candidates for AOFBs.[114] The simplest form studied is 4,4-dimethyl bipyridinium, known as Methyl Viologen (MVi) or paraquat, widely used as a herbicide. MVi exhibits a solubility of 2.5 M in water, with redox potentials of –0.42 and –0.73 V vs SHE for its first and second reduction reactions, respectively.[115]

The second process of viologens is typically not considered for AOFB application because of the low stability of the double reduced form in aqueous electrolytes.[116,117] In the case of MVi^0 (double reduced species of MVi), it also presents very low solubility in water. Furthermore, MVi has demostrated poor stability when tested in aqueous batteries, even when cycling the first electron process. The low stability of the single reduced species has been attributed to a dimerization-disproportionation mechanism[118,119] that forms the oxidized species and MVi^0, which is unstable in aqueous electrolytes. Further decomposition side reactions at extreme pH values have limited the use of viologens derivatives to near-neutral pH electrolytes. While they suffer from dealkylation after deprotonation of the alkyl groups at high OH^- concentration,[120,121] acidic conditions lead to irreversible redox process because disproportionation-protonation side reactions that form electrochemical inactive species.[122] Finally, it is worth to mention that the single reduced form is easily oxidized back by oxygen.[123]

Bulky charged functional groups have been introduced to the viologen structure to minimize the bimolecular reactions and degradation rate through steric and electrostatic hindering.[74] Two of these substituted viologen derivatives were suggested by Aziz´s group with outstanding performance in neutral and slightly basic AOFBs. The first one includes positively charged ammonium groups, called BTMAP-Vi, presenting a solubility up to 2 M in water and high stability (capacity fade rate of 0.1% per day, against 3.5% of MVi).[88] However, the electron-withdrawing effect of the ammonium groups moves the redox potential to more positive values compared to MVi, resulting on –0.36 V vs SHE, which is not desired for molecules intended for negolytes. In a later work, they introduced negatively charged phosponate groups, obtaining a negative shift on the redox potential (–0.46 V vs SHE) at the same time that further improving the stability. The resulting viologen derivative, BBP-Vi exhibited unprecedent capacity fade rates of 0.016% per day.[124]

Regarding the second electron process of viologens, separated ca. 300-400 mV from the first one, there have been some attempts to increase its stability in aqueous electrolytes and boost the storage capacity of viologen-FBs.[125–127] One of the strategies was based on the use of a stabilizer to form a host-guest complex in order to avoid the protonation of the double reduced form of viologen that leads to inactive redox species.[127] However, the current results are still not competitive with other organic materials, excluding them for AOFB application.

3.3.2.3 Pyrazines, phenazines and alloxazines

Aza-aromatic compounds, containing two redox-active nitrogen atoms on the aryl rings, have also been considered as negolytes for AOFBs. The most studied families

includes two nitrogen atoms in the aromatic structure and, similar to viologens, they are able to exchange two electrons. The aromatic structures are characterized by spin and charge delocalization that provides chemical stability and make them suitable for AOFB application.[74] Pyrazines, consisting of one aromatic ring with 1,4-diaza groups, offer interesting properties such as low molecular weight, high solubility (up to 6 M in water) and multiple reversible redox processes at relatively high potentials.[128] While they present two separated redox reactions in acid electrolytes, these processes coalesce in one two-electron redox reaction in alkaline media. However, the low stability in aqueous electrolytes has limited their utilization in AOFBs.[70,129]

Phenazine consists of a pyrazine ring between two benzene rings. Phenazines were first considered for AOFB application in a work performed by Schubert in 2016 using TEMPO/Phenazine combi-molecule.[130] Since then, different phenazine derivatives have been developed after incorporation of different functional groups in order to either increase solubility or reduce chemical decomposition mostly attributed to tautomerization.[131–134] The phenazine-based AOFBs, assembled in highly alkaline conditions, have demonstrated high energy density and cell voltage when coupled with ferrocyanide with good capacity retentions. In particular, dihydroxyphenazine sulfonic acid (DHPS)[132] exhibited one of the most negative redox potential among organic negolytes (–0.81 V vs SHE), with a maximum solubility of 1.8 M and a capacity fade rate of 0.68% per day when tested in a cell at 1.4 M concentration. After the FB cycling, the material did not exhibit signal of decomposition, but the decay was attributed to crossover through the membrane. In a later work, a propionic-acid-functionalized phenazine (1,8-PFP), with a redox potential of –0.59 V vs SHE, was tested at 2 M concentration in alkaline media with no visible capacity fade rate for more than 50 days.[133] Although the synthesis of this derivative was not straightforward as other proposed candidates, those results remark the high performance of phenazine derivatives in alkaline AOFBs and the necessity to develop new synthetic routes.

Similar to phenazines, alloxazines offer suitable electrochemical and chemical properties for AOFB application. Furthermore, alloxazines derivatives are interesting because they are derived from the vitamin B2 backbone, which could solve cost and scalability limitations.[135] Among alloxazines derivatives, alloxazine 7,8-carbolyxic acid (ACA) with a solubility up to 2 M in alkaline electrolytes (pH 14) and a redox potential of –0.68 V vs SHE, was tested at 0.5 M in an alkaline flow cell exhibiting a capacity decay of 1.2% per day.[135] In this case, the fade rate was attributed to ACA unstability in the alkaline media due to hydrolysis of the amidic carbonyls generated by OH^- to finally form redox-inactive species. The low stability of this organic family has limited their further development and deployment in AOFBs.[36]

3.3.2.4 Fluorenones

Fluorenones, polycyclic aromatic ketones, have been recently proposed for AOFBs considering their ability to store two electrons and their relavitely high solubility and stability when including appropriate functional groups. When considering aqueous electrolytes, functionaliztion of fluorenones is crucial in order to avoid the protonation of the reduced species. After protonation, the corresponding alcohol is formed and much higher potentials are required to oxidize it back.[136] On that way, the simplest fluorenone derivative, 9-fluorenone (9-FL), has been functionalized to stabilize the ketyl dianion (double reduced form) and allow the reversible conversion between the ketone and alcohol form.[136,137]

Because of the low solubility of fluorenone, there are limited works that include them in aqueous FBs. First, an asymmetric fluorenone derivative including carboxylate and sulfonate groups (4C7SFL) was presented as negolyte for an alkaline AOFB.[136] This derivative exhibited relatively good solubility in highly basic electrolytes (up to 1.5 M in 2 M NaOH) coupled with very stable behaviour when tested in a flow battery at 1.36 M concentration (capacity decay of 0.021% per day). Despite the demonstrated high stability, complex disproportionation-comproportionation chemical reactions competing with the redox process prevented the use of the full material, leading to capacity utilizations lower than 80%. In a later work, a pyridinium-functionalized fluorenone named (OTDFL)Cl_2 was proposed for AOFB negolyte in neutral-pH electrolyte.[138] (OTDFL)Cl_2 exhibits high solubility in water (3.35 M) and reversible two one-electron redox processes when working at neutral pH. However, the redox potentials are considerably high for materials intended for negolytes (0.17 and –0.08 V vs SHE for the first and second electron at neutral pH, respectively). Furthermore, this compound exhibited low stability in a flow cell even when tested at a low concentration of 0.25 M (capacity decay of 6% per day). Despite the mentioned drawbacks, the recently presented fluorenones for AOFB application show promising starting results to continue the development of the fluorenone family materials.

3.4 Experimental Techniques for FB Study

The study of flow battery operation is extensive, ranging from investigations about the battery lifetime, linked to the stability and crossover of the redox species as well as degradation of the cell materials, to the measurement of the battery energy efficiency and optimal power operation, related to the reaction kinetics and voltage losses on the cell.[21,37,139] Although preliminary studies are required to characterize the redox activity of the active materials (cyclic voltammetry or rotating disc electrode measurements, among others) and the mechanical and chemical stability

of the cell components, this section focus on presenting the most common techniques applied to investigate the actual flow cell operation.

3.4.1.1 Battery cycling

Battery cycling at constant current (CC) density is the most common technique to study the performance of the cell. Long-term cycling tests allow estimating the battery lifetime by the measurement of the capacity fade rate and the analysis of the cause.[37,139] The use of different cell configurations and cycling protocols can provide broad information about the processes occurring in the cell.[140] For example, by utilizing a capacity non-limiting electrolyte (use of an excess amount of stable electrolyte on one side of the cell), the capacity fade of the battery can be exclusively attributed to phenomena occurring on the other side of the battery (limiting side). Furthermore, crossover issues can be minimized by assembling symmetric batteries, prepared using the same electrolyte on both sides of the cell.[141] Regarding the cycling protocols, the use of constant voltage (CV) steps permits to conduct tests disregarding the effects due to cell resistance changes or temperature fluctuations, as well as allows the attainment of higher capacity utilization.[140] The use of different cycling protocols, including CC, CV or a combination of both, CCCV, depends on the studied system and the purpose of the experiment.

Furthermore, cycling experiments at different current densities can provide useful information about voltage losses by the analysis of the energy and voltage efficiencies. In that way, the performance of different electrolytes and electrode materials in a flow cell can be investigated, compared and optimized.[142]

Despite being a powerful approach, battery cycling needs to be coupled with other techniques to get a better understanding of the processes occurring in the cell. On its own, this technique only provides cell voltage and current measurements, while the rest of key figures (as energy efficiency) are derived from these recorded parameters. For example, a common approach for validation of the proposed redox mechanisms and decomposition reactions is the utilization of ex situ analytical techniques. On that way, the structure of charged species as well as side products can be identify by using spectroscopy techniques as nuclear magnetic resonance (NMR), electron paramagnetic resonance (EPR) and ultraviolet-visible (UV-Vis).[37,139] Furthermore, computational studies have been recently applied to provide additional validation of the mechanisms involved.[143] The combination of these techniques has demonstrated to provide insightful information about the processes occurring in the battery during operation.

3.4.1.2 Polarization curves

Polarization curves have been extensively used for the study of fuel cells.[144,145] By running a current scan, the relationship between the developed cell voltage and the applied current density can be easily obtained. The plot of these two measurements allows studying the potential losses developed at different current densities.[38] In that way, three regions in the polarization curve have been clearly differentiated (**Figure 6**). The low current density region is mostly dominated by electrode kinetic losses (activation overpotentials), while at higher current densities mass transfer limitations (concentration overpotentials) start to have significant effect. The middle region is characterized by a constant slope that is attributed to the ohmic resistance of the cell components (ohmic overpotentials). Polarization curves can clearly show the dominant overpotential that is affecting the cell performance. Furthermore, by plotting the cell power against the current density, the maximum power that the cell can delivered can be easily determined. Normally, the polarization curves are performed for both the charge and discharge processes at different conditions, including different flow rates and state of charges.

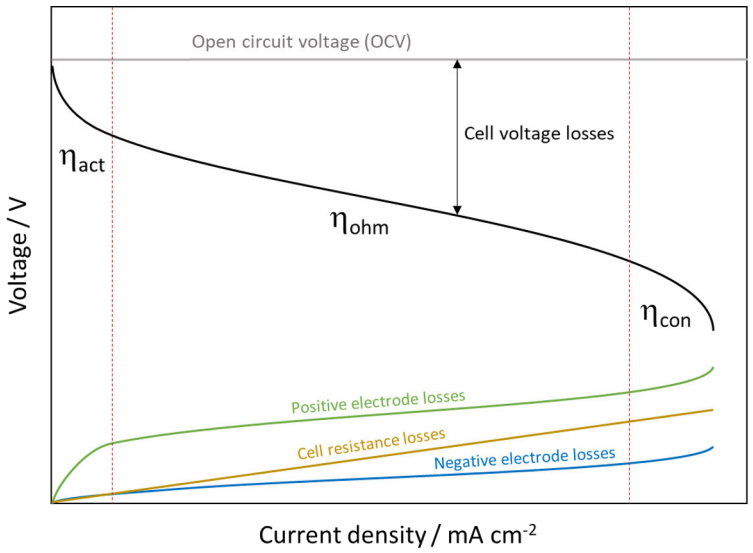

Figure 6. Example of polarization curve including the different regions: η_{act} (activation overpotentials), η_{ohm} (ohmic overpotentials) and η_{con} (concentration overpotentials).

Even though the polarization curves provide useful information, the simplest form of the technique presents the same limitation than the battery cycling. As the voltage measurements belong to the whole cell, the polarization curves provide

information about the full cell losses but they cannot distinguish the contribution from each electrode.[147] Furthermore, in a flow battery the reactants are recirculated, which leads to the risk that the state of charge of the electrolytes fed to the battery is changing during the measurement.[146] Different solutions have been considered to avoid this problem, including the use of large electrolyte reservoirs or the discharge of the electrolyte in a separate reservoir.[148] A different approach is based on alternating charge and discharge current steps while measuring the cell voltage.[142] On that way, each step corresponds to a point in the polarization curve while the state of charge of the battery remains constant.

3.4.1.3 Impedance spectroscopy

Electrochemical impedance spectroscopy (EIS) is one of the most utilized electrochemical techniques to characterize batteries as it can provide useful information about proceeses occurring inside the cell, ranging from reaction kinetics and mechanisms to battery performance and state of charge.[149,150] EIS technique presents the advantages of being non-destructive, fast, and well established for electrochemical processes. The approach is based on applying an AC signal at constant voltage or current and measuring the response. The impedance Z can be determined by the frequency-dependent voltage/potential and the frequency dependent current. The resulting data is analysed at each frequency considering that the different voltage loss contributions evolve at different time scales. The analysis is based on the use of equivalent circuit models composed of different elements such as resistors, inductors and capacitors, constant phase elements, Warburg elements describing mass transfer, etc.[150,151] These elements represent the different physical, chemical or electrochemical processes. Then, the match of the mathematical model with the experimental data allow their quantification. Applied for FBs,[152,153] EIS allows measuring the potential losses of the battery while identifying and quantifying the contribution of the different rate limiting processes (charge, ohmic and concentration overpotentials) to the total cell overvoltage. By applying impedance spectroscopy theory and the corresponding equivalent circuits, the charge transfer, ohmic and diffusion resistances can be estimated in a simple and fast way.

Although the EIS measurements are conducted for the full cell, the contribution from each side can be estimated considering equivalent circuits.[150] In order to measure the actual individual electrode contributions of positive and negative vanadium electrolytes, further studies have been conducted working with symmetric batteries assembled with the same redox couple on both sides of the cell.[152]

3.4.1.4 Additional measurements

As previously commented, there are some limitations on the analysis of the standard measurements recorded during battery operation. While the cell measurements (current and voltage) corresponds to the whole battery, they do not provide information about each electrode separately. As a result, the measured capacity fades or voltage losses are attributed to the whole system, but they cannot be separated among the electrodes. Aiming to obtain further information about the processes occurring on each side of the cell during operation, different approaches have been developed to study each electrode individually.[37,142]

In that sense, different methods have been proposed to record the individual half-cell potentials and, as a result, the corresponding states of charge of each electrolyte. Mostly, these recordings have been performed using reference electrodes on both sides of the cell. In some research works, the reference electrodes were integrated into the main cell[154–156] while others suggested the use external measurements by introducing the reference electrodes in the reservoirs[157] or using additional flow cells with integrated reference electrodes after the battery.[158] Additionally, the half-cell state of charge monitoring has been also performed by measuring physical properties of the electrolytes.[37,142,157] On the same way, similar approaches have been utilized to differentiate the potential losses occurring on each electrode.[147,156] By distinguish the origin of capacity fades and the distribution of the voltage losses on the cell, a further understanding of the processes occurring in the cell can be obtained, boosting the development and operational control of FB systems.

4 Materials and Methods

In this chapter, we present the techniques used for the study of the new synthetized organic materials proposed as redox active materials for AOFBs. First, the new materials were investigated using cyclic voltammetry to analyze their reversibility and redox potentials in different supporting electrolytes and pH conditions. The most interesting candidates were then studied in a flow cell at low concentration of the redox material (5-10 mM). The tests involved long term cycling to evaluate their stability and optimize the battery conditions and operational parameters. Finally, the most promising and stable materials were tested at high concentration. The electrochemical investigations were coupled with analytical techniques (NMR, UV-Vis, Raman and EPR) to get an insight on the reaction and decomposition mechanisms.

Additionally, we introduce and explain the experimental set-up developed to monitor the battery operation. The measurement system, consisting of additional monitoring cells, includes eight potential measurements to obtain further information about the cell performance. The tests performed to validate the measurement system involved short cycling and polarization curves at different conditions.

4.1 Electrochemical Techniques

4.1.1 Cyclic voltammetry

Cyclic voltammetry was used to study the new organic candidates synthetized within CompBat Project at University of Jyväskylä for **Publications I, II and III**. The initial investigations were based on the study of the redox behaviour of the new materials, including reduction potential and reversibility. The tests were conducted using different supporting electrolytes, from acidic to alkaline pHs. In a later stage, cyclic voltammetry was also used to characterize the redox species by calculating the diffusion coefficient D, using Randles-Ševčík equation,[159] and standard reaction rate constant k^0, using Nicholson´s method[160] or Marcus-Hush approximation.[161] Finally, cyclic voltammetry measurements were performed to analyse the electrolytes after battery cycling.

We performed the cyclic voltammetry tests using different potentiostats: Biologic SP-240 or SP-150, Gamry Reference 600+ or PalmSens4. All the voltammograms were performed with a three electrode set-up using glassy carbon (3.0 mm diameter), Ag/AgCl (3 M KCl solution), and platinum wire as the working electrode, reference electrode, and counter electrode, respectively (**Figure 7**). Before each test, the glassy carbon was polished with 1 μm alumina and rinsed with deionised water. Once the cell was assembled, the electrolyte was degassed by bubbling nitrogen for 10 minutes before starting the experiment. For the initial studies of the new compounds, the concentration of the studied material was always 1 mM in 10 ml of the studied supporting electrolyte. All the potentials are reported against standard hydrogen electrode (SHE).

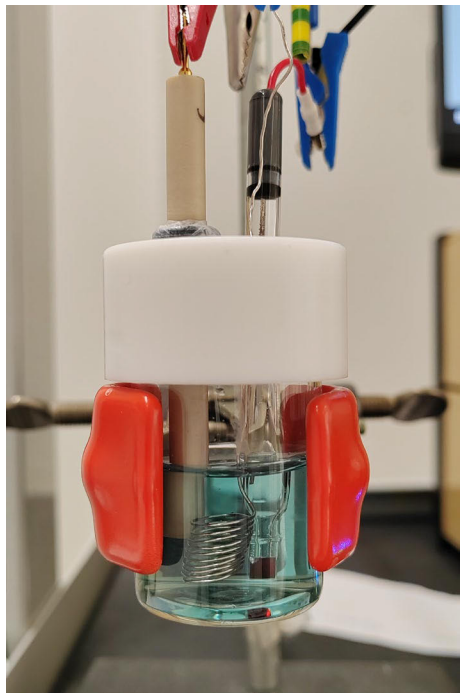

Figure 7. Cyclic voltammetry cell with a three-electrode set-up.

4.1.2 Bulk electrolysis in H-cell

In order to identify and characterize the redox species in their charged state, the charged species were electrogenerated via electrolysis in an H-cell. The electrolytes of the two compartments, consisting of 10 mL, were separated using an ionic membrane (**Figure 8**). Carbon foam or titanium mesh with RuO_2 and IrO_2 coating were used as working electrodes, depending on the experiment. An Ag/AgCl (3 M

KCl) electrode was used as reference electrode and the potential of the side of the cell where the species were generated was controlled against it. The electrolytes were purged with nitrogen for 10 minutes before and during the experiments. The electrolysis were conducted either in galvanostatic or potentiostatic mode. After completion of the electrolysis, the samples were taken to NMR analysis.

The bulk electrolysis in H-cell was chosen for electrogeneration of the charged species in the investigations conducted for **Publication I**, while the species were electrogenerated in a flow battery in the studies performed for **Publication II** and **III**.

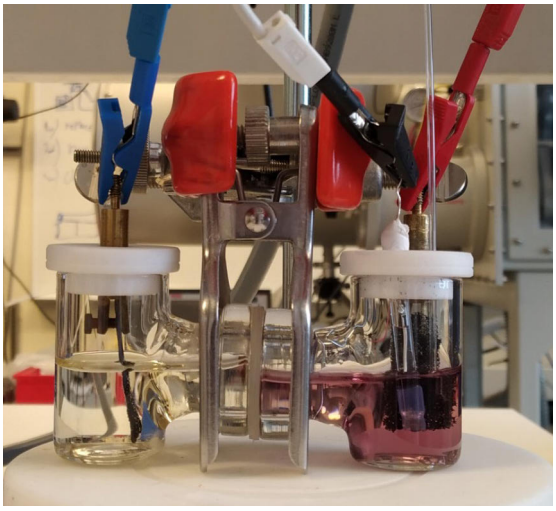

Figure 8. H-cell for electrogeneration of charged species.

4.2 Battery Tests

4.2.1 Battery cycling

The performance and stability of the new organic materials for **Publications I**, **II** and **III** were studied in lab-scale flow batteries (**Figure 9**). The new candidates were first tested using low concentration at different conditions, including different supporting electrolytes, pHs, concentrations of the active material (5-10 mM), etc. The investigations involved the use of different cell configurations (full cell or symmetric cell) and protocols (CC or CCCV). The most promising materials were tested later at increasing concentrations to confirm their stability at those conditions.

All the experiments including organic materials were conducted inside a nitrogen-filled Glovebox (MBRAUN) at 25-30 ^{o}C in order to avoid the presence of oxygen that could increase the decomposition rate or self-discharge of the active

materials. In some cases, the tests were performed outside the glovebox, resulting in very low stability. In the case of full cells, the non-limiting side of the cell consisted of an excess amount of active material to guarantee the correct study of the side of interest. Normally, if not specify on the text, the flow rate was kept constant at 100 ml min^{-1} using a peristaltic pump Baoding Chuangrui and the tubing was Masterflex C-Flex (MFLX06434). The cycling was performed using a cycler LANHE Battery Testing System G340A.

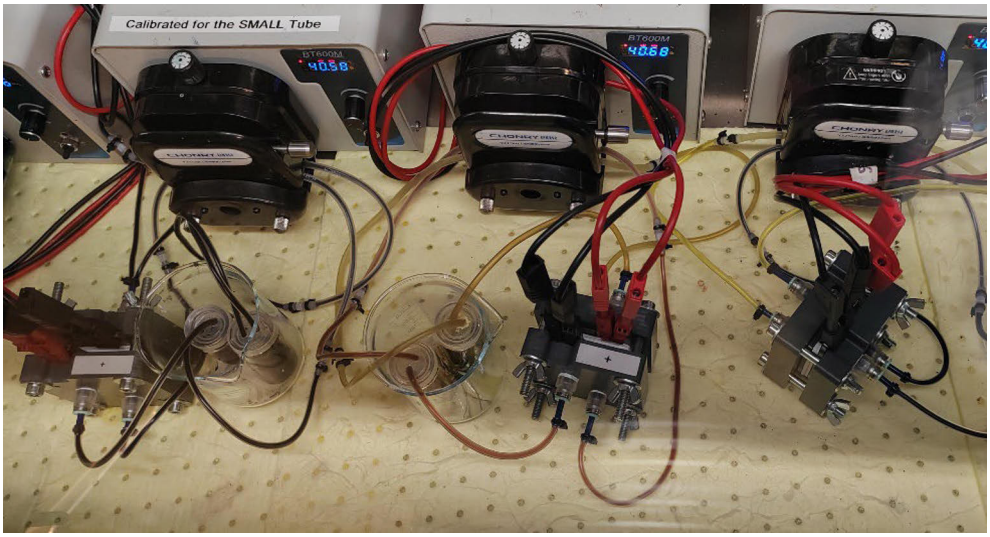

Figure 9. Lab-scale flow batteries used in this research work.

The batteries used for investigations of the new materials were flow cells of 5 cm^2 (electrode dimensions: 2x2.5 cm^2 area, 3 mm thickness after compression) fabricated at the mechanical workshop of University of Turku. The cells consisted of endplates (made from PVC), bipolar plates (fabricated from carbon composite plates from Pinflow) and 3 mm thick expanded-PTFE gaskets (cut from 24SH-ePTFE gasket sheets from TEADIT, Switzerland). The electrodes were thermally activated SGL carbon felts 4.6 mm from SIGRACELL (GFD 4.65 EA), which were sonicated in deionised water for 10 minutes before assembling the battery. The ionic membranes used on each battery test depended on the studied system. The used membranes during these investigations were Nafion 212 (or Nafion 117) from IonPower in the case of cation exchange membranes, and Selemion DSVN (or AMVN) from AGC, in the case of anion exchange membranes. **Figure 10** presents a sequential workflow of the flow cell assembling indicating the battery elements.

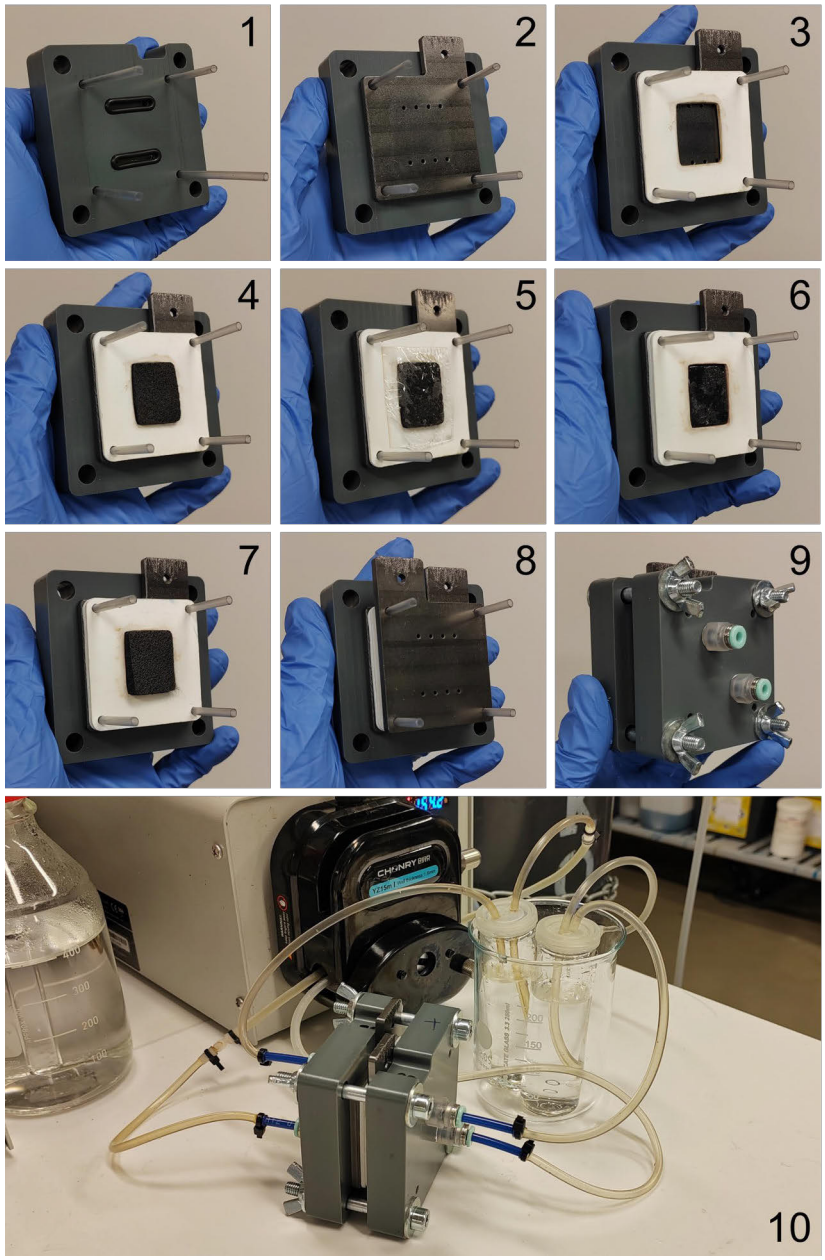

Figure 10. Workflow step-by-step of the flow battery assembling. 1- First endplate with plastic pipes for alignment of all elements. 2- First bipolar plate. 3- First PTFE gasket. 4- First carbon felt electrode. 5- Ionic exchange membrane. 6- Second PTFE gasket. 7- Second carbon felt electrode. 8- Second bipolar plate. 9- Second endplate and screws tightened up to the desired torque. 10. Assembled flow cell connected to reservoirs and peristaltic pump.

4.2.2 Polarization curves

Polarization curves were performed to study vanadium and an organic FB during the tests conducted with the new measurement system developed in **Publication IV**. The polarization curves were measured at three different states of charge (20, 50 and 80%) and three different flow rates (20, 50 and 100 ml min^{-1}).

First, the polarization curves were measured using the standard slope approach using an increasing rate of the current of 5 A in 60 seconds. Additionally, the experiments were conducted in galvanostatic mode using discharge current steps of 30 seconds and measuring the cell voltage at the steady state. Each discharging step was alternated with a charging step applying the same current with the aim of keeping the state of charge of the electrolytes constant. The current values were gradually increased on each step until the cell voltage reached 0 V for discharge and the upper cut-off voltage of the studied system for charge. The voltage measured in the steady state of each step corresponds to a point in the polarization curve. This method allows the measurement of the polarization curves without changing the state of charge of the electrolytes during the experiment. In this case, we used it to compare and validate the results obtained with the standard slope approach.

4.2.3 Impedance spectroscopy

Potentiostatic electrochemical impedance spectroscopy (PEIS) measurements were performed to determine the resistance of the flow cells. During this research work, we did not conducted a detailed study of the resulting PEIS spectrum, limiting our analysis to the intersection of the curve (in the Nyquist-plot) with the real axis in order to obtain the internal ohmic resistance of the battery. In all the cases, the PEIS was conducted using Biologic SP-240 potentiostat.

During the investigations of the new materials (**Publications I, II and III**), the battery resistance was measured before and after cycling for most of the analysed systems. In the case of the measurement system studies (**Publications IV** and **V**), the impedance was measured before and after each polarization curve and cycling test for both vanadium and the organic system.

4.3 Measurement System

The experimental measurement set-up developed within this work to obtain an insight on the battery operation (**Publication IV**) consists of two additional monitoring flow cells located before and after the main battery. The electrolyte was recirculated from the reservoirs through the first monitoring cell, the main battery and the second monitoring cell to finally come back to the reservoirs. **Figure 11** presents a scheme of the system configuration, while **Figure 12** shows a picture of

the experimental set-up. The monitoring cells were assembled using the same membrane and electrode carbon material as the main cell. Considering that no current flows through the monitoring cells, the OCV can be measured before and after the battery during operation. Additionally, this configuration also allows measuring the overpotentials of both positive and negative electrodes by recording the potential difference between the end plates of the battery (polarized during operation) against the end plates of the monitoring cell (non-polarized) during operation. Furthermore, reference electrodes were incorporated on both sides of the cell located after the main battery, which allows recording the half-cell potentials by measuring the potential of the carbon plates against the reference electrodes. The reference electrodes were leakless Ag/AgCl reference electrodes (ET072 electrode from eDAQ) provided by Pinflow. Knowing the relationship between the states of charge of the electrolytes and the corresponding redox potentials, this configuration permits recording the state of charge of each half-cell individually during operation. Finally, we included the measurement of the potential drop through the membrane by measuring the potential difference between the reference electrodes located on each side of the OCV-cell.

The scheme presented in **Figure 12** includes all these measurements recorded during battery operation, which are also listed below:

1. Main cell voltage and current density
2. Open circuit voltage (OCV) before the main cell
3. Open circuit voltage (OCV) after the main cell
4. Positive electrode half-cell state of charge (potential difference between positive electrode on OCV-cell against reference electrode)
5. Negative electrode half-cell state of charge (potential difference between negative electrode on OCV-cell against reference electrode)
6. Positive Electrode Overpotential (potential difference between positive electrode on the main cell against the positive electrode on the OCV-cell)
7. Negative Electrode Overpotential (potential difference between negative electrode on the main cell against the negative electrode on the OCV-cell)
8. Membrane potential drop (potential difference between the reference electrodes located on each side of the OCV-cell)

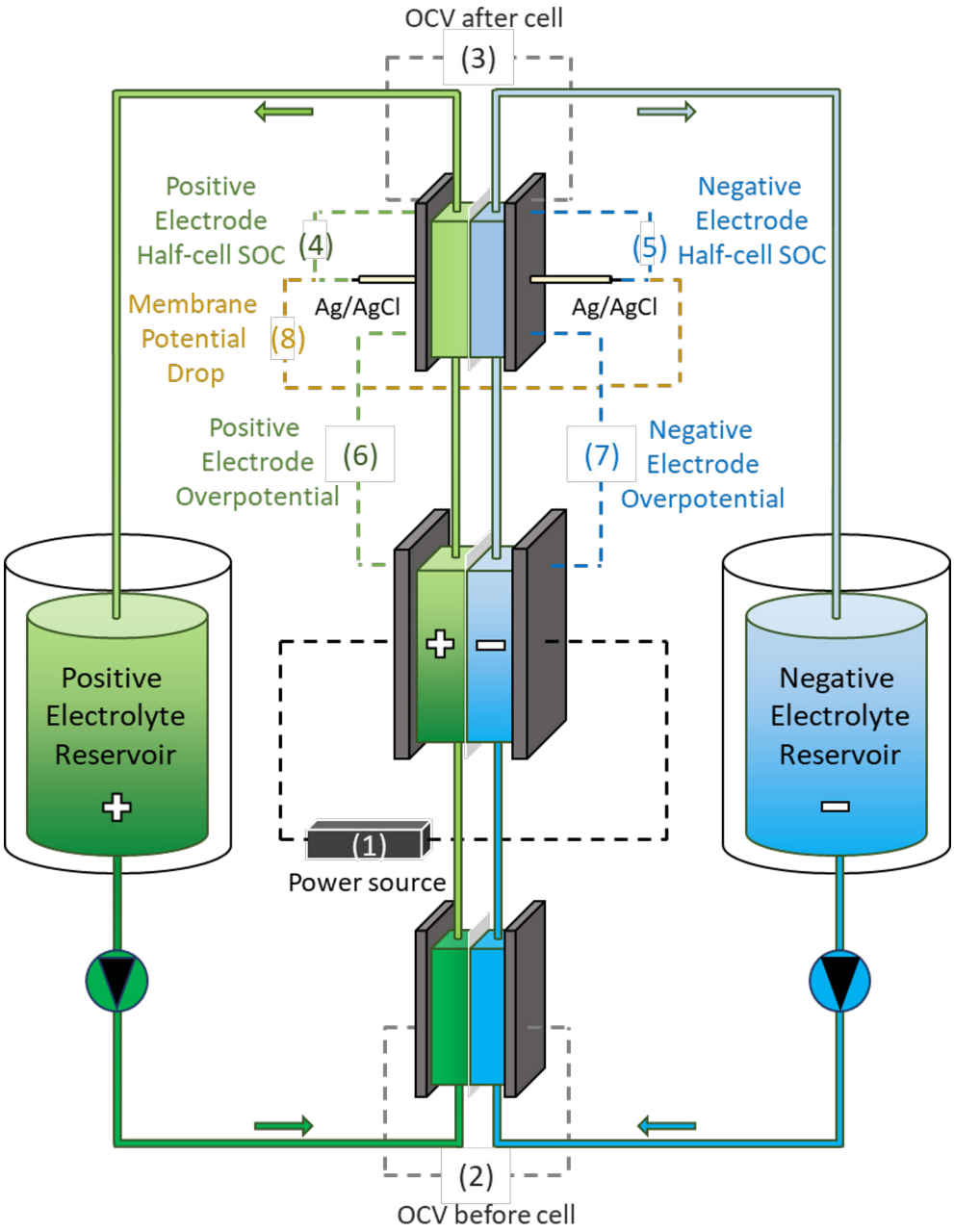

Figure 11. Scheme of the battery set-up including the additional measurements recorded during the experiments.[IV]

The main battery and monitoring flow cells were obtained from Pinflow. The main battery was a standard single cell with flow-through geometry and an area of

20 cm^2. The bipolar plates of the main battery and the monitoring cells were made of carbon-polymer composite. The flow rate of the electrolyte was kept constant with a peristaltic pump Baoding Chuangrui, using Masterflex C-Flex tubing. All the measurements were recorded using a LANHE Battery Testing System G340A (one channel for each measurement). During the polarization curve measurements for the VFBs, additional channels were needed in the main cell to apply the high currents required (maximum current per channel: 5 A).

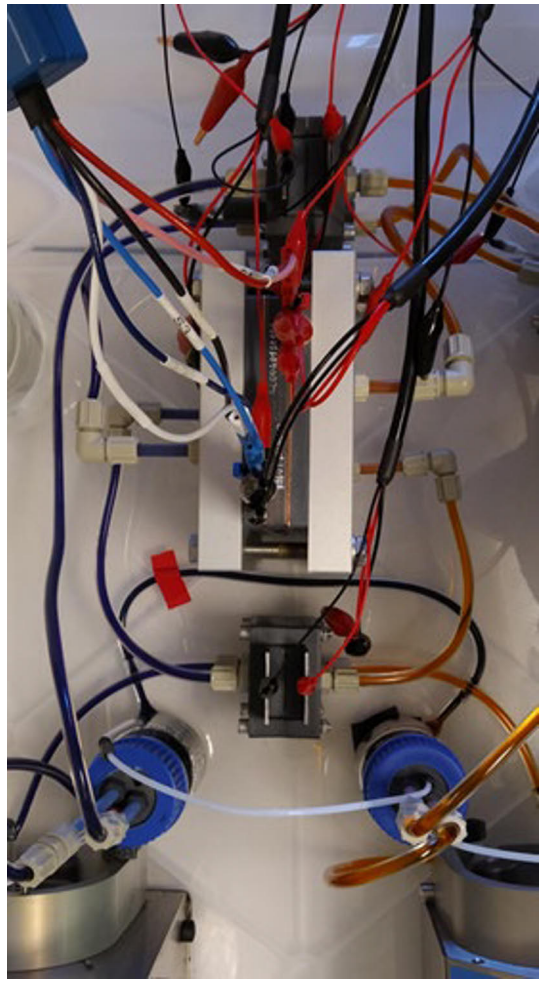

Figure 12. Experimental battery set-up used for the measurements.

In **Publication IV**, the experimental set-up was used to study the vanadium system and an organic system consisting of bis((3-trimethylammonio)propyl)-ferrocene dichloride (BTMAP-Fc) as positive electrolyte and bis(3-

trimethylammonio)propyl viologen tetrachloride (BTMAP-Vi) as negative electrolyte. In the case of the VFB, two systems using different treated carbon felts electrodes were studied to analyse their influence on the cell performance and electrode overpotentials. **Table 1** summarizes the main characteristics of the studied systems. The investigations performed in this work consisted of short cycling operation at different current densities and polarization curves at different flow rates and states of charge.

Table 1. Main characteristics of the flow batteries studied using the measurement system.[IV]

	Vanadium FBs		**Organic FB**
Initial electrolyte composition	Positive and negative electrolytes: commercial vanadium electrolyte (1.6 M $V^{+3.5}$ in 2 M H_2SO_4) from GfE		Positive electrolyte: 0.4 M BTMAP-Fc in 1 M KCl Negative electrolyte: 0.4 M BTMAP-Vi in 1 M KCl Commercial chemicals from TCI
Electrolyte volume	50 ml		40 ml
Electrodes	**VFB1** Rayon Graphite Felt BGF5 (6-7 mm thickness) from CGT Carbon GmbH (heat-treated at 400 ºC for 24 hours)	**VFB2** Thermally activated PAN carbon felts GFD 4.65 (4,6 mm thickness) from SIGRACELL	Thermally activated PAN carbon felts GFD 4.65 (4,6 mm thickness) from SIGRACELL
Exchange membrane	Nafion™ NR212 from IonPower	Selemion AMVN from AGC	Selemion AMVN from AGC
Electrolyte degassing	Nitrogen gas was bubbled to the reservoirs during the experiments		Experiment conducted inside nitrogen-filled GloveBox

In **Publication V**, a simplified version of the measurement system was used to analyse the VFB performance assembled with carbon felts activated via a novel heat- and chemical-treatment. In this case, the samples were activated exposing the carbon felt to a molten salt of potassium nitrate as a mild oxidizing agent at high temperature. Different temperatures, in the range of 380-500 ºC, and treatment times, from 3 to 12 hours, were investigated in order to find the most appropriate oxidation conditions. The felts preparation and initial characterization, conducted at Poznan University of Technology (Poland), are presented in detail in **Publication V**, while this dissertation is focused on the flow battery investigations. During the initial characterization studies, X-ray photoelectron spectroscopy (XPS) was conducted to analyse the surface composition of the samples, and cyclic voltammetry was used to study the reversibility towards vanadium reactions. Additionally, conductivity, water

uptake and burn-off measurements were performed. The initial studies included different PAN (polyacrylonitrile) carbon felts: carbonized material KFD 2.5 and graphitized GFD 4.6 from SIGRACELL. Considering that GFD is more stable, conductive and prone to oxidation, this material was selected for further exploration. Selected GFD treated samples were tested working as positive and negative electrodes in a vanadium flow battery. In this case, the experimental set-up included only the OCV-cell after the main battery in order to measure the individual electrodes overpotentials and analyse the effect of the new chemical treatment on each side of the cell. The performance of the chemically treated felts was then compared against the standard heat-treatment. The experiments consisted of short cycling tests at different current densities. Additionally, impedance spectroscopy measurements were performed to determine the ohmic cell resistance. Commercial vanadium electrolyte (1.6 M $V^{+3.5}$ in 2 M H_2SO_4) from GfE was used, and the battery was assembled with Nafion 117 membrane. Further information about the tests is presented in **Publication V**.

5 Investigations of New Organic Materials

In this chapter, the results obtained during the investigations of the new organic molecules proposed for AOFBs, included in **Publications I, II and III,** are presented. The discussion is focused on the electrochemical behavior and battery performance of the new materials, while their synthetic routes are depicted in the corresponding articles.

5.1 Pyridoxals

The selection of the pyridoxal family (**Publication I**) was based on the use of an organic material that can be obtained from natural sources, leading to a scalable and renewable solution. Pyridoxals are Vitamin B6 derivatives,[162] which are highly biodegradable and available via fermentation,[163,164] making them ideal candidates for sustainable large-scale applications. Furthermore, they are water soluble and contain pre-installed functional groups that allow wide synthetic exploration.[165]

Benzoyl-pyridinium salts have already been proposed for aqueous systems by Sandford et al.[166] In their research work, they analysed the electrochemical behaviour of a pyridinium derivative, which exhibits two separated one-electron redox processes at close redox potentials (–0.62 V and –0.72 V vs SHE). Even though the first process showed reasonable reversibility, the second one was irreversible in aqueous conditions because of protonation of the double reduced species. These observations limited the subsequent battery studies to the first electron reaction as well as demanded the utilization of strongly alkaline conditions to minimize the protonation reaction. By using a conservative cell voltage to avoid the second process, the battery was shortly cycled using 2 M KOH as supporting electrolyte.

During a research work performed within CompBat project, combining DFT calculations and machine learning, a computational protocol was developed to predict the redox potentials and stability of the reduced species of N-alkylated pyridoxal derivatives.[167] The protocol, that enables a fast screening of possible candidates, includes the calculation of the reduction potentials of more than 6700 molecules. Based on the computational results and synthetic availability, selected

pyridoxals were synthetized at University of Jyväskylä using pyridoxal hydrochloride, a vitamin B6 vitamer, as the starting material. The structures of the starting material and the pyridoxal-based scaffold are presented in **Figure 13**, while the structures of all the studied pyridoxal derivatives are shown in **Publication I**. We next studied the electrochemical behaviour of these new molecules at University of Turku.

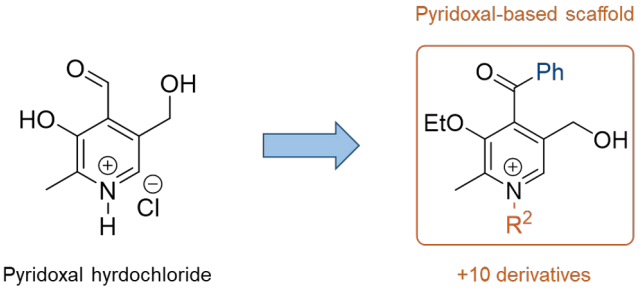

Figure 13. Obtention of pyridoxal derivatives from pyridoxal hydrochloride.[I]

We performed cyclic voltammetry measurements to determine the redox potential and reversibility of the synthetized molecules. The tests were performed in neutral and alkaline aqueous electrolytes (1 M KCl and 0.1 M NaOH). All the materials presented higher reversibility when tested at higher pH, presenting one redox event at suitable negative potentials for materials intended for FB negolyte (reduction potentials ranging from –0.65 V to –1.04 V vs SHE). The redox potential values of the different derivatives are consistent with the functional groups incorporated to the pyridoxal core, showing positive shifts when including electron-withdrawing substituents, and negative shifts for electron-donating groups.[168] These values are discussed and compared in **Publication I**. Additionally, the experimental values obtained at neutral pH are in high agreement when compared with the computational redox potentials determined by the developed protocol, which validates the reliability of the calculations (**Figure 14**). Furthermore, the cyclic voltammograms show a shift to more negative potentials at higher alkalinity, suggesting an electrochemical reaction involving protons. This proton-coupled electron transfer mechanism has been extensively studied for quinones using square diagrams, which allow analysing the sequential steps involved in the electrochemical process.[106]

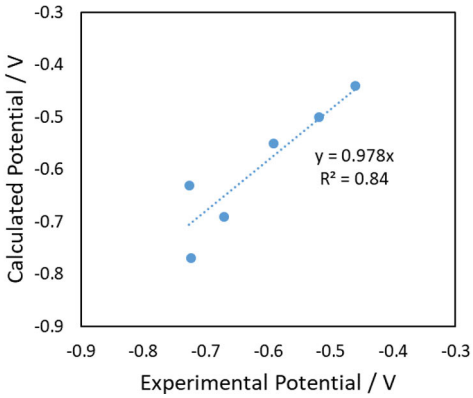

Figure 14. Comparison of experimental and calculated reduction peak potentials of pyridoxal derivatives using 1 M KCl as supporting electrolyte. Values reported against SHE.[I]

Based on the voltammetry studies, we selected the two most promising molecules, in terms of reversibility, for further studies in lab-scale flow batteries using 0.1 M NaOH as supporting electrolyte. The reversibility of the studied materials is presented and discussed in **Publication I**, considering the ratio between the oxidation and reduction peak currents as an indication of the process reversibility. The flow battery tests were performed inside a nitrogen-filled glovebox using low concentration of the pyridoxal derivative. The batteries were assembled using anion exchange membrane Selemion DSVN (from AGC) and an excess amount of ferrocyanide on the positive side. Both pyridoxals demonstrated the same behaviour in the battery: they were charged for a capacity corresponding to two electrons but just a small fraction was discharged back in the first cycle (less than 1%), suggesting a low stability of the reduced species in the studied conditions. The cycling profile of the pyridoxal derivative **11a** is presented in **Figure 15**.

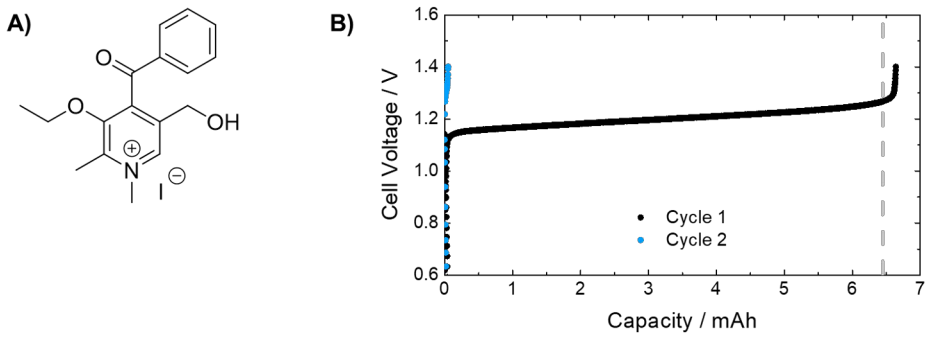

Figure 15. Pyridoxal derivative **11a** tested in lab-scale flow battery. **A)** Structure of the pyridoxal **11a**. **B)** Results using 10 mM of the pyridoxal **11a** in 0.1 M NaOH as supporting electrolyte. CC protocol using 1 mA cm^{-2}. The dash line shows the capacity expected for two-electron reduction.[I]

With the attempt of elucidate the cause of the instability, we performed further investigations of pyridoxal **11a** considering its high solubility and reversibility during voltammetry tests. First, the cyclic voltammograms at different scan rates suggest a two-electron process after analysis of the peak separation and Randles-Ševčík equation, discussed in **Publication I**. This was also confirmed via electrochemical simulations performed using a model developed by a collaborator from University of Turku using COMSOL Multiphysics software. The cyclic voltammograms were simulated considering 1, 2 and 3 electrons, and compared with the experimental curve. As shown in **Figure 16**, the voltammogram considering two electrons correlates the best with the experimental curve. These calculations and model are presented in detail in the Supporting Information of **Publication I**.

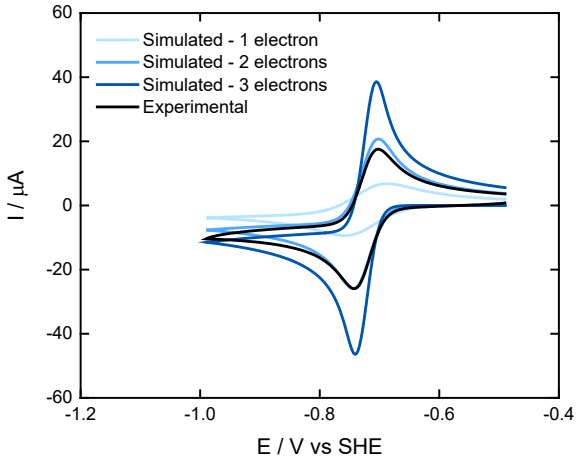

Figure 16. Experimental and simulated cyclic voltammograms of 1 mM of pyridoxal derivative **11a** in 0.1 M NaOH. Scan rate: 100 mV s^{-1}. The simulated curves correspond to 1, 2 and 3 electrons redox process. Potentials reported against SHE.[I]

Secondly, we electrogenerated the reduced species of selected pyridoxal derivatives in an H-cell and analyzed the product via NMR. The resulting spectra showed the structures of the corresponding alcohols, which are the double-reduced forms of the analyzed pyridoxals, confirming the transfer of two electrons. From the previous work conducted by Sandford for benzoyl-pyridinium salts,[166] it was demonstrated that the double reduced species were protonated in aqueous electrolytes to form the corresponding alcohol, which could not be oxidized back. In that work, as the two redox processes were separated by 100 mV, the negolyte could be discharged back and shortly cycled if avoiding the second reduction. However, in the case of the pyridoxal derivatives studied during this work, the two electron

transfers occur at the same potential. As a result, the second reduction and subsequently protonation leading to alcohol formation cannot be avoided.

To gain insight into the reaction mechanism of the pyridoxal derivatives, computational studies were performed at Aalto University to access the thermodynamic parameters of the electrochemical reduction. The square representation for the reduction of the pyridoxal **11a** (**Figure 17**) was built after calculation of the redox potentials and acid dissociation constants (pK_a values) using DFT calculations. The computational study is further presented in the Supporting Information of **Publication I**. From these calculations, we concluded that the reduction of pyridoxals occurs through three consecutive steps: first, electron transfer (ET) to form the intermediate **A**, followed by a proton-coupled electron transfer (PCET) reaction to obtain intermediate **C**, and finally proton transfer (PT) to form the corresponding alcohol **21a**. The calculated redox potentials of the consecutive reductions (ET and PCET) at pH 7 are similar, which agrees with the experimental voltammograms that suggest that both process occurs simultaneously. However, the experimental results at pH 13 indicates that both reductions should occur together at more negative potential, which does not agree with the first ET step presented in the computational study.

The last PT step to form the alcohol is either irreversible or much higher potential is required for the oxidation, which agrees with the previous studies about the difficulty to oxidize back the alcohol.[136,169] Regarding the reversible behavior observed in the cyclic voltammograms in basic pH, we understand that the protonation is slow enough that it is not observed at the timescale of the cyclic voltammetry measurement in alkaline condition. As a result, the double reduced not protonated form can be oxidized back during the cyclic voltammetry tests at high pH. This also explains the less reversible voltammogram obtained when using neutral pH electrolyte, where the concentration of protons is higher, leading to increased protonation rate. On the other hand, during the flow battery tests, considering the much longer timescale, the protonation reaction cannot be avoided and, as a result, the cell cannot be discharged back. Finally, to confirm these results, we assembled a last battery using the same pyridoxal **11a** in more alkaline conditions, in this case 2 M NaOH. The higher alkalinity and lower concentration of protons would reduce the protonation rate and increase the reversibility of the process. In this experiment, a much higher fraction was oxidized back during the discharge in the first cycle (8%) and the battery was shortly cycled (**Figure 18**), which validates our conclusions.

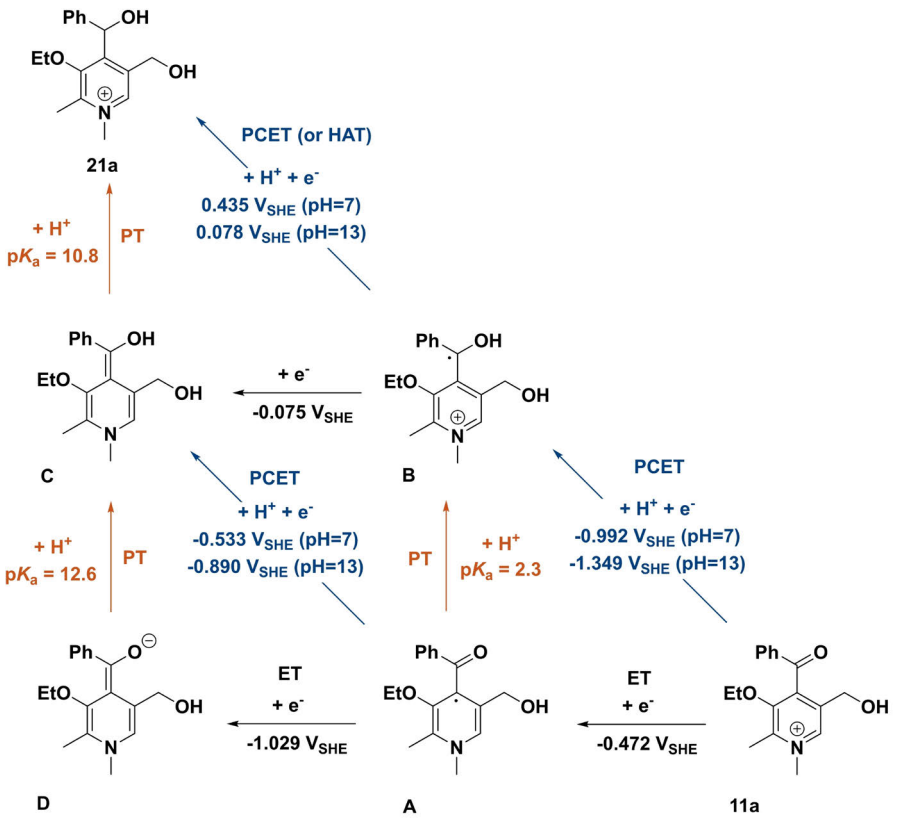

Figure 17. Computational square diagram for the reduction of pyridoxal 11a. The horizontal direction indicates a reduction reaction through ET, the vertical direction indicates protonation via PT reaction and the diagonal indicates a reduction via PCET.[I]

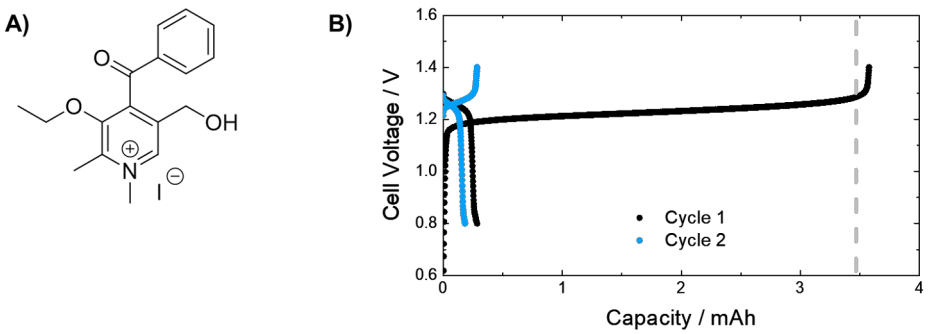

Figure 18. Pyridoxal derivative **11a** tested in lab-scale flow battery. **A)** Structure of pyridoxal **11a**. **B)** Results using 5 mM of pyridoxal **11a** in 2 M NaOH as supporting electrolyte. CC protocol using 1 mA cm^{-2}. The dash line shows the capacity expected for 2-electron reduction.[I]

In summary, this research work involved the study of different pyridoxal derivatives selected on the base of a computational screening. Despite the reversible voltammograms of some derivatives obtained in alkaline conditions, the pyridoxal compounds show poor cycling stability when tested in a battery. After a multidisciplinary integrated research work, including electrochemical techniques, analytical characterization and computational works, we were able to rationalize the reaction mechanism and the source of instability. Although the final battery results still show a low performance of pyridoxal derivatives as negolytes for FB applications, they illustrated how the understanding of the process can help to design the new conditions to slow down the degradation mechanism and improve performance in flow cells. Furthermore, the results obtained during these investigations are useful for the design of the next generation of pyridinium compounds for FB application. The efforts should focus on molecular changes to slow down the protonation reaction and/or separate the two consecutive reduction processes in order to avoid the assessment of the double reduced species.

5.2 Bisphosphonate-functionalized Viologens

In the research work presented in **Publication II**, we studied the inclusion of bisphosphonate group as a new substituent for the viologen core. As we previously discussed, different functional groups have been considered for organic materials in order to tune their chemical and electrochemical properties and make them suitable for their use in flow batteries.

Viologens exhibit two highly reversible one-electron redox reactions with a well-established ET mechanism. Furthermore, their high solubility and easy functionalization make them suitable for broad investigations. The simplest form, methyl viologen (**MVi**), was used to assemble one of the first fully organic aqueous FBs.[115] However, it presented low stability mainly attributed to dimerization reactions[118,119] and crossover of species that resulted in fast capacity loss (3.5 % per day). Different molecular design strategies have been considered to increase viologen performance in aqueous systems, leading from conventional to polymeric structures.[170] The so-called conventional viologens can be easily obtained from 4,4´-bipyridine in a general way by N-alkylation reaction with the desired functional groups, forming the functionalized viologen core substituted at the nitrogen positions.[170] On that way, Aziz´s research group presented two viologen derivatives functionalized with positively charged ammonium groups (BTMAP-Vi)[88] and negatively charged phosphonate groups (BPP-Vi).[124]. The incorporation of bulky charged functional groups increased steric and electrostatic repulsion and, as a result, minimized bimolecular side reactions and crossover through the ionic membranes, leading to a significant increase of the capacity retention.

In this work, following a similar strategy, we studied two viologen derivatives featuring a bisphosphonate group on the N-alkyl chain of just one or the two pyridinium rings, named **MBPE-Vi** and **BBPE-Vi** for the mono- and bi-substituted forms, respectively. **Figure 19** presents the molecular structure of the two investigated derivatives. The bulky branched structure and high stability of the P–C–P bonds against chemical reagents[171] make the bisphosphonate fragment an interesting functional group for inclusion in molecules intended for FB electrolytes.

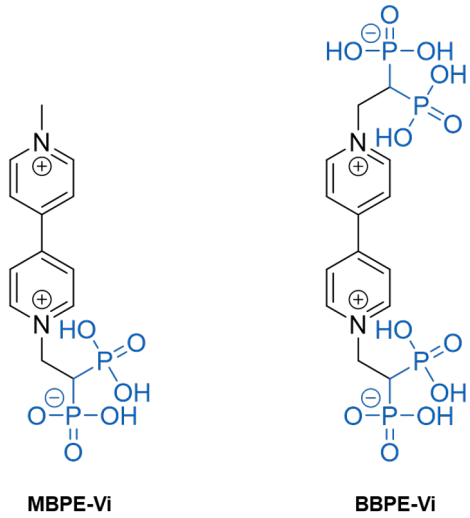

Figure 19. Molecular structure of the studied bisphosphonate-functionalized viologens, MBPE-Vi and BBPE-Vi.

The initial cyclic voltammetry measurements showed the two one-electron processes of viologens, in this case exhibiting a more reversible behavior when increasing the basicity of the electrolyte. In the case of **BBPE-Vi**, 1 M NaOH was required to obtain a reversible process, while less basic condition using 0.1 M NaOH was enough for **MBPE-Vi**. Considering the lower stability of the double-reduced species in aqueous electrolytes,[116,117] we focus our investigations in the first electrochemical reaction. **Figure 20** shows the cyclic voltammograms of the first redox process of both derivatives, while compares them with the pristine viologen, **MVi**. Both compounds present an important improvement on the redox potentials compared with **MVi**, obtaining –0.503 V for **MBPE-Vi** and –0.550 V for **BBPE-Vi** (against SHE). This shift to more negative redox potentials is promoted by the strong electron-donating effect of the negatively charged oxygen atoms of the bisphosphonate group, which is advantageous to develop higher cell voltage and power. In the case of **BBPE-Vi**, it exhibits the most negative redox potential among

the reported viologen derivatives, developing an OCV of 1.03 V when coupled with ferrocyanide in a cell (**Figure 20**).

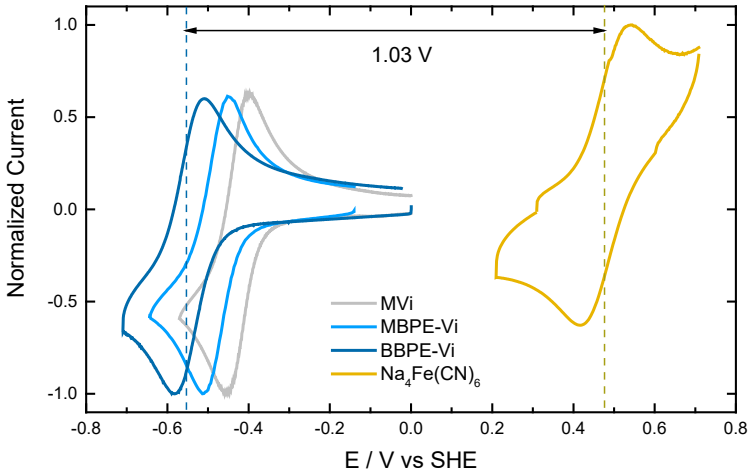

Figure 20. Cyclic voltammograms of the bisphosphonate-viologen derivatives, MBPE-Vi and BBPE-Vi, compared with MVi. The OCV of a battery assembled with BBPE-Vi coupled with ferrocyanide on the positive side is indicated. CV conditions: 1 mM BBPE-Vi in 1 M NaOH; 5 mM MBPE-Vi in 0.1 M NaOH; 1.2 mM MVi in acetate buffer 0.5 M; 1 mM $Na_4Fe(CN)_6$ in 0.1 M NaOH. Scan rate: 100 mV s^{-1}.[II]

We continued the investigations by testing the stability of the bisphosphonate-functionalized viologens at low concentration in lab-scale flow cells. The full cells were assembled pairing the viologen derivatives with an excess amount ferrocyanide and, considering the instability of the reduced form in presence of oxygen,[123] all the experiments were performed in a nitrogen-filled glovebox. Further information about the battery studies is presented in the Supporting Information of **Publication II**.

The flow cell of **BBPE-Vi** was assembled with 5 mM of the viologen dissolved in 1 M NaOH. The battery was cycled using a current density of 1 mA cm^{-2} and a cut-off voltage of 1.02 V, accessing 70% of the total capacity. In that condition, the cell demonstrated a significant capacity decay (0.166% per cycle) over 200 cycles. We attributed the low stability to the high basicity of the electrolyte. As it has been previously reported,[120,121] the degradation of viologens is accelerated in strongly alkaline electrolytes because of dealkylation generated by nucleophilic attack of hydroxide anions. To support our assumption, we compared the cell performance of the mono-bisphosphonate derivative, **MBPE-Vi**, using different concentrations of NaOH as supporting electrolyte, 0.1 and 1 M. When tested at similar cycling conditions (70% of capacity utilization), the battery with 1 M NaOH as supporting

electrolyte exhibited four times higher capacity decay than the one using 0.1 M NaOH (0.137% against 0.034% per cycle), confirming our hypothesis. The low stability of viologens at high-pH electrolytes and the requirement of that highly basic condition to achieve a reversible electrochemical behavior, make **BBPE-Vi** an inadequate candidate for AOFB negolyte.

We next focus our research on the battery studies of **MBPE-Vi**, in this case using 0.1 M NaOH as supporting electrolyte. During the low-concentration battery test (10 mM), this derivative exhibited much higher stability than the bi-substituted viologen, possibly due to the lower OH^- concentration. The initial cycling conditions, using a cut-off voltage of 0.90 V and 50% of the total capacity, did not exhibit visible capacity loss. However, as the cut-off voltage was increased, accessing higher capacity utilization, a faster capacity fade was observed (**Figure 21**). While a capacity fade of 0.034% per cycle was observed using a cut-off voltage of 0.925 V (68% of total capacity), the capacity loss increased to 0.092% per cycle for a cut-off voltage of 1.00 V (95% of capacity utilization). We believe that the increased fade rates when setting higher cut-off voltage are related to the accessing of the second electron process and generation of the less stable double-reduced species. This assumption was supported by a battery test at higher cut-off voltage (1.30 V) to cycle the two electrons. In that condition, the battery exhibited a capacity fade rate of 2.03% per cycle, in agreement with our hypothesis.

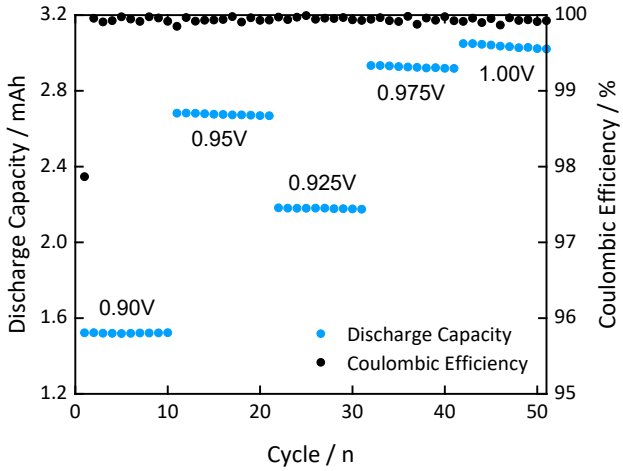

Figure 21. Performance of 10 mM MBPE-Vi battery in 0.1 M NaOH using different cut-off voltages for one-electron cycling. CC protocol using 2 mA cm^{-2}. Theoretical capacity expected: 3.2 mAh.[II,SI]

Our previous observations were further supported by UV-Vis measurements conducted to characterize the reduced species of **MBPE-Vi** (**Figure 22**),

electrogenerated in a flow cell. In this case, by setting different cut-off voltages, we generated the single-reduced species working with two different cut-off values (0.90 and 1.00 V) and then the double-reduced form using a higher cut-off (1.35 V). We conducted a qualitative analysis of each sample via UV-Vis measurements. The spectra of the single reduced species shows the characteristics peaks of viologen radical at 400 and 604 nm (with secondary bands).[117,172] In the case of the double reduced form, the spectra also agrees with previously reported results, however it exhibits an extra peak at 310 nm. This same band, that we attributed to the second reduced species or a decomposition product arising from them, is also visible in the spectra of the single-reduced form when using a higher cut-off (1.00 V), suggesting that those conditions are enough to access the second electron process.

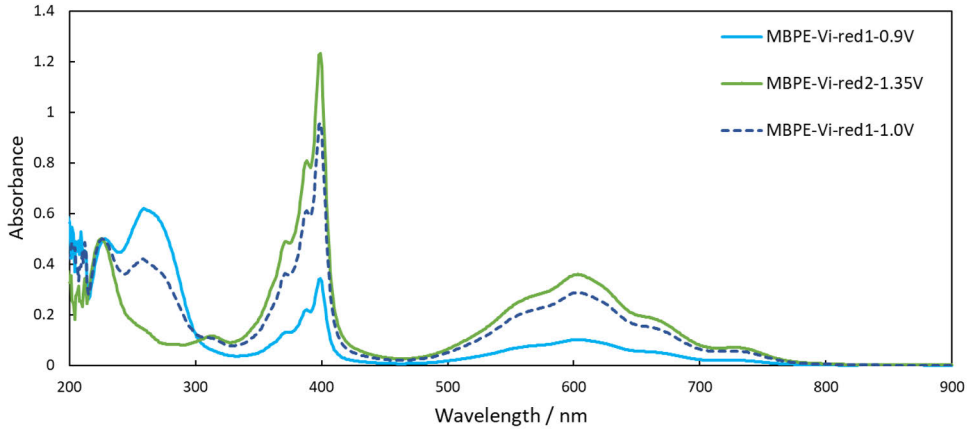

Figure 22. UV-Vis spectra of the reduced species of MBPE-Vi electrogenerated in a flow cell using different cut-off voltages during charge. MBPE-Vi-red1-0.9V and MBPE-Vi-red1-1.0V corresponds to the spectra of the single reduced species generated using cut-off voltages of 0.9 and 1.0 V, respectively. MBPE-Vi-red2-1.35V corresponds to the spectra of the double reduced form generated with a cut-off voltage of 1.35 V.[II,SI]

These results suggest that the stability of viologen derivatives may be influenced by the assessment of the second electron during the cycling conditions and, as a result, by the separation of the two redox processes characteristic of viologens. A comparison of viologen derivatives from this work and other previosly reported, analyzing the separation between the redox processes together with the reported stabilities in flow batteries, supports our hypothesis. This comparison is presented in **Table 2**, showing that viologen derivatives with larger separations between the redox processes exhibit more stable behavior when tested in a cell. Despite the visible trend, we understand that these tests were performed at different conditions (different concentrations, electrolytes, cycling protocols) and the different functional groups

play an important role on the stability. Further studies are needed to confirm the impact that the redox processes separation has on the viologen cycling stability.

Table 2. Comparison of viologen derivatives in terms of redox processes separation and cycling stability.[II]

Column 1	Separation between redox processes / V	Cycling conditions	Reported stability
MVi[115]	0.31	0.5 M in 1.5 M NaCl	0.12% per cycle 3.5% per day
BBPE-Vi (our work)	0.32	0.005 M in NaOH 1 M	0.166% per cycle 6.7% per day
BTMAP-Vi[88]	0.37	1.3 M in water	0.0057% per cycle 0.1% per day
BPP-Vi[124]	0.39	1 M in water (titrated with NH_4OH to pH 9)	0.00069% per cycle 0.016% per day

Finally, we assembled a battery with 0.5 M concentration of **MBPE-Vi** in 1.6 M NaOH as supporting electrolyte. The higher concentration of NaOH was selected considering the deprotonation of the bisphosphonate group, based on the previously determined pK_a values of biphosphonic acids.[173] The pH of the resulting electrolyte was adjusted to 13.5. More detailed information about the battery test is exhibited in **Publication II**. The cycling test was performed with a CC protocol (40 mA cm^{-2}) and a cut-off voltage of 1.02 V for over 200 cycles, accessing a capacity utilization of 64%. The cycling profiles are presented in **Figure 23**. The battery exhibited high stability with a capacity decay of 0.009% per cycle (0.229% per day) and high coulombic efficiency (99.98%). We attribute a small contribution of the decay to the positive side, which was ferrocyanide on the limits of the solubility. This assumption was confirmed after recovering a fraction of the capacity lost when adding a small amount of supporting electrolyte to the posolyte reservoir (cycle 171). Furthermore, a short cycling conducted at 20 and 40 mA cm^{-2} demonstrated high energy efficiencies of 87.5 and 80%, respectively, which agrees with the high rate constant of **MBPE-Vi** determined via Marcus-Hush approximation (0.13 cm s^{-1}). Cyclic voltammetry measurements of the electrolytes after cycling did not show crossover of species, confirming the low permeability of **MBPE-Vi** obtained with the inclusion of the bisphosphonate groups to the viologen core. This observation was further validated by permeability measurements performed in an H-cell, which are shown in the Supporting Information of **Publication II**.

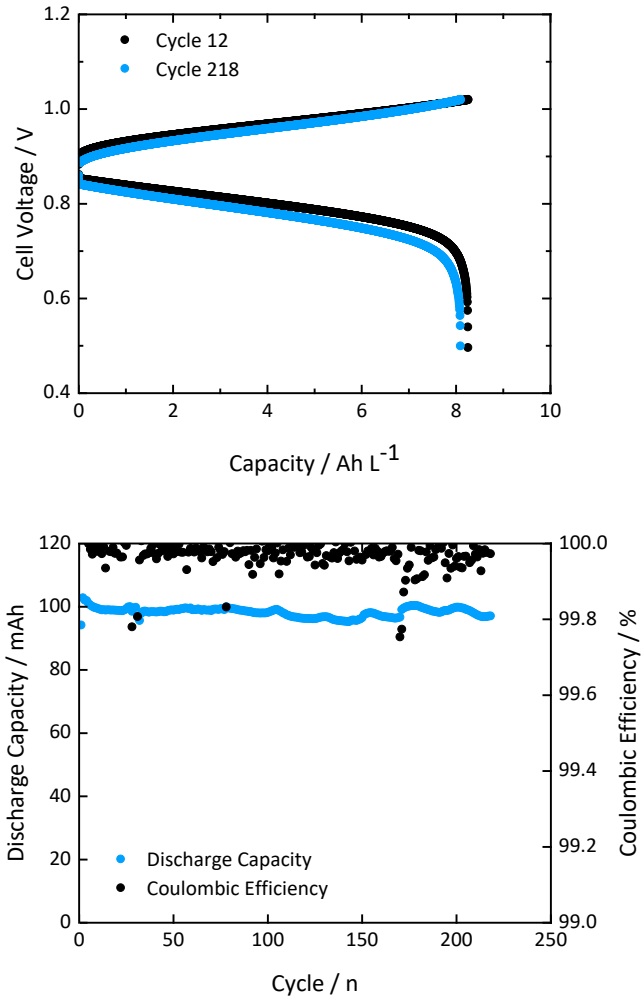

Figure 23. Performance of 0.5 M MBPE-Vi battery in 1.6 M NaOH. CC protocol using 40 mA cm^{-2} and cut-off voltage of 1.02 V.[II]

Despite the increased capacity fade rates exhibited at higher capacity utilization, the high solubility of these viologen derivatives allows high storage capacity even when limiting the capacity usage. The maximum solubility of **MBPE-Vi** was determined experimentally as 1.45 M, leading to a storage capacity 27.0 Ah L^{-1} when operating at 70% of the total capacity. These results demonstrate the high capability of bisphosphonate as a side group for inclusion in molecules intended for AOFB negolytes, enabling very negative redox potentials as well as highly soluble materials. When applied to the viologen core, high battery performance was

obtained, however it is still not competitive with other previously reported derivatives. In this case, we believe that the lower performance arises from the reduced stability of the viologen core in alkaline electrolytes. However, we believe that the bisphosphonate group is still a strong candidate to functionalize other organic molecules that present higher performance in basic conditions.

5.3 Azoniafluorenones

In our last work exploring organic molecules intended for negolytes for AOFBs, **Publication III**, we introduced azoniafluorenones as a new family of organic materials. The investigations include the analysis of different functional groups and positions on the pyridinium and secondary rings, aiming to optimize their performance in flow cells.

In previous works, fluorenone derivatives have been proposed for aqueous systems exhibiting certain drawbacks that limit their actual application in flow cells. In the case of 4C7SFL,[136] fluorenone including carboxylate and sulfonate groups, the reaction mechanism involves complex disproportionation-comproportionation chemical reactions that limit the full capacity utilization. Furthermore, it requires high-pH electrolyte (2 M KOH) that we prefer to avoid in this work in order to mitigate the possible instability issues related with highly alkaline conditions considering our previous results with the biphosphonate-functionalized viologens. The second derivative, a pyridinium-functionalized fluorenone (OTDFL)Cl_2,[174] was tested at neutral pH but exhibiting considerable positive redox potentials (0.17 and –0.08 V vs SHE) and poor stability even at low concentrations (capacity decay of 6% per day at 0.25 M). We believed that including a pyridinium ring, to form the azoniafluorenone structure, could bring about improvements on solubility and redox potential.[71] Furthermore, the variation of the nitrogen position on the ring, besides its easy functionalization, enabled a broad scope for investigations, leading to a wide range of molecules with different chemical and electrochemical properties.

During this research work, a synthetic pathway to access a broad set of azoniafluorenone derivatives was developed at University of Jyväskylä, however the synthetic procedure is out of the scope of this dissertation. The structures of the new synthesized molecules analysed within this research work, including different positions of the nitrogen atom as well as different functional groups on either the nitrogen or the second benzene ring, are presented in **Figure 24**. We started the investigations including an ammonium group to analyse the position of the nitrogen atom on the pyridinium ring.

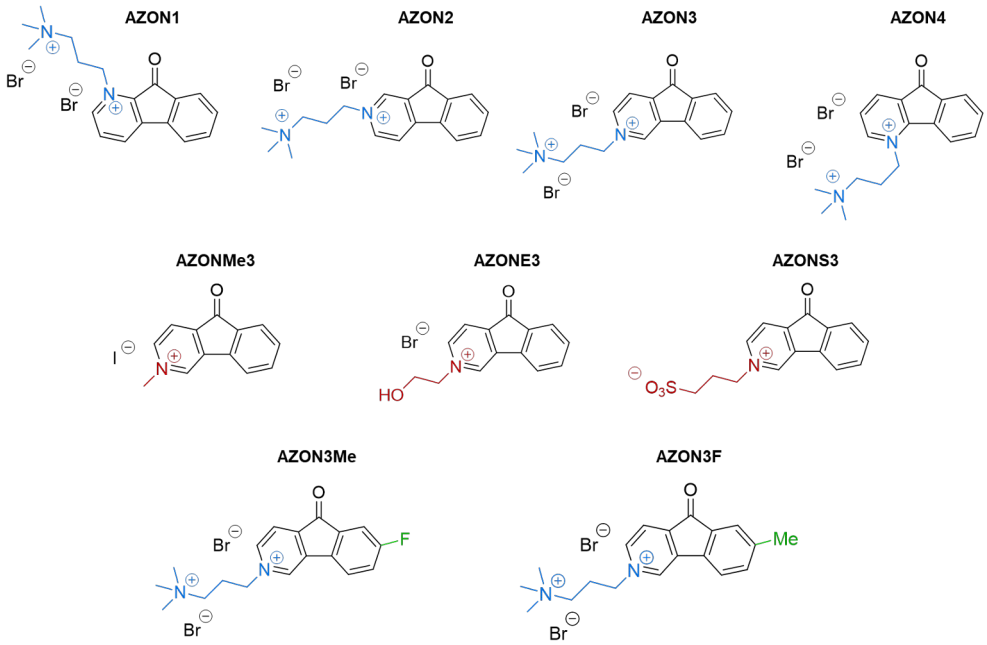

Figure 24. Azoniafluorenone derivatives investigated during this research work.

The electrochemical investigations started with cyclic voltammetry measurements at neutral and alkaline conditions, using 1 M KCl and 0.1 M NaOH as supporting electrolytes. In most of the cases, the voltammograms exhibited two one-electron electrochemical reactions, with varying reversibility when considering different positions of the nitrogen atom. **AZON3**, with the nitrogen in the γ position, presented the most promising results, showing two highly reversible redox processes both in neutral and basic pH. While the redox potentials were –0.10 V and –0.37 V vs. SHE in neutral pH, the first process shifts to more negative values in alkaline conditions, which suggested an electron transfer involving protons. The electrochemical mechanism was further analysed in this work and it is presented below. **AZON1** demonstrated quite reversible voltammogram at neutral pH, but it did not exhibit any peak in alkaline conditions. In the case of **AZON2** and **AZON4**, they showed poor reversibility in both studied electrolytes. The cyclic voltammograms considering different N-positions are summarized in **Figure 25**. We believe that the higher reversibility of **AZON1** and **AZON3** arises from the delocalization of the charge on the double reduced form, as the ketyl anion and the pyridinium cation are in consonant relationship, forming a stable zwitterion. Contrarily, because of the different N-position, these functionalities are in dissonant relationship for the double reduced forms of **AZON2** and **AZON4**, leading to unstable species that cannot be oxidized back.

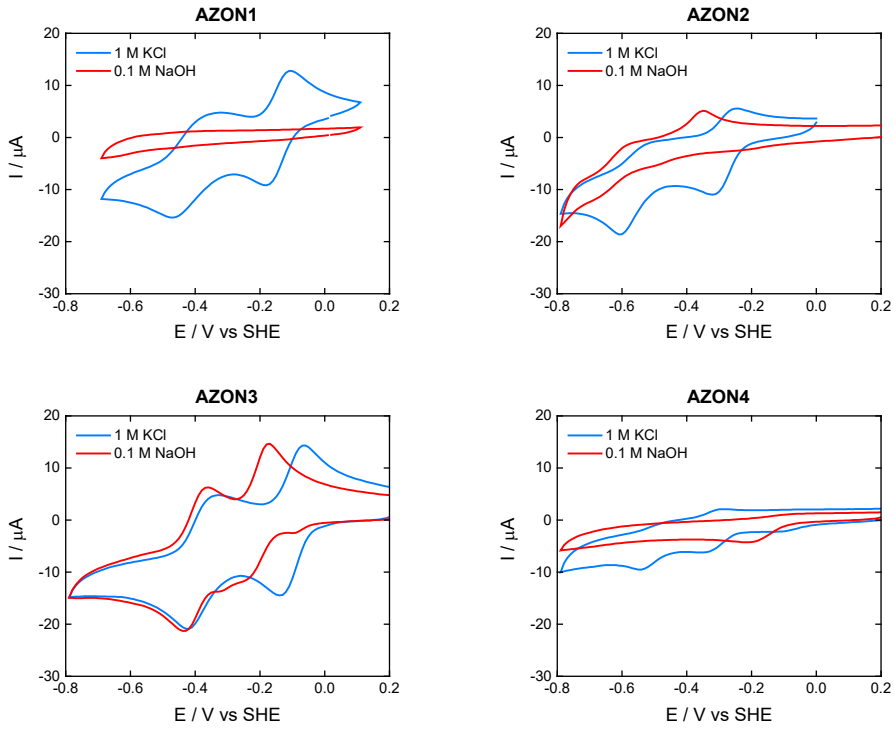

Figure 25. Cyclic voltammograms of the quaternary-ammonium-substituted azoniafluorenone derivatives in 1 M KCl and 0.1 M NaOH. Concentration of azoniafluorenone: 1 mM. Scan rate: 100 mV s^{-1}.[III,SI]

Considering the cyclic voltammetry results, we selected **AZON1** and **AZON3** for further stability studies in flow batteries. The initial tests were performed using low concentration of the azoniafluorenone derivative (5-10 mM) and an excess amount of BTMAP-Fc on the positive side. Further information about the battery tests conditions and results are shown in **Publication III.** At pH-neutral conditions, **AZON3** presented high stability, with no visible capacity decay when cycling the first electron, and a fade rate of 0.179% per cycle (3.5% per day) when cycling the second process. In alkaline conditions, using 0.1 M NaOH as supporting electrolyte, the cell assembled with **AZON3** was able to discharge back just a small fraction of the capacity in the first cycle, indicating a very low stability at high pH. Then, we continued our investigations focusing on neutral pH electrolytes. Regarding **AZON1**, it exhibited poor performance when tested in a cell in 1 M KCl, with a fade rate of 0.138% per cycle (5.70% per day) for the first electron cycling. We think that the lower stability of **AZON1** arises from the proximity of the nitrogen of the pyridinium ring to the ketone group, which can destabilize the reduced species. However, we did not perform further investigations to validate this assumption.

The studies considering different functional groups was conducted with the nitrogen atom in the position 3 of the pyridinium ring because of the higher performance demonstrated by **AZON3**. Three additional substituents were studied, including methyl, ethanol and sulfonate groups, leading to **AZONMe3**, **AZONE3** and **AZONS3**, respectively. The cyclic voltammograms of these derivatives exhibited high reversibility without altering the redox potential values compared with **AZON3**. All the voltammograms, as well as flow cell cycling profiles, are reported in the Supporting Information of **Publication III**. The methyl-substituted azoniafluorenone, **AZONMe3**, was tested in a cell in 1 M KCl exhibiting high stability but using a small fraction of the total capacity, which we attribute to the low solubility of this derivative. The low solubility of both **AZONMe3** and **AZONS3** excluded them for further investigations, and suggested the inclusion of polar groups to obtain more soluble molecules. In the case of **AZONE3**, the hydroxyl group allows a highly soluble but poorly stable material at neutral pH conditions (capacity decay of 0.518% per cycle when tested in a flow cell in 1 M KCl). In this case, we attribute the low stability to the nucleophilic attack of the OH group to the N-substituted carbon, similar to the effect reported for viologens,[120,121] generating a pyridine ring that cannot be oxidized back in the studied conditions.

With **AZON3**, including the quaternary ammonium group on position 3, as the most promising candidate, we continued the investigations by analysing the effect of substituents on the benzene ring. On that sense, the addition of methyl and fluorine side groups on position 7 of the fluorenone was analysed. The resulting **AZON3Me** and **AZON3F**, respectively, exhibited similar reversibility and stability than **AZON3** during the voltammetry and battery tests (shown in the supporting information of **Publication III**). While the addition of the methyl group did not show any change on the redox potential value, **AZON3F** exhibited slight positive shifts of 40 and 15 mV on the first and second electron processes, respectively, in agreement with the electron-withdrawing effect expected for the fluorine group. Despite the similar performance compared with **AZON3**, these results emphasise the broad possibilities for investigations for the azoniafluorenone core.

We next focused our research on understanding the electrochemical mechanism of our best candidate, **AZON3**. First, we investigated the relation between the redox potential and pH using buffered and unbuffered electrolytes (**Figure 26**). The cyclic voltammograms conducted using Robinson-Britton buffer electrolyte showed that within the pH range from 7 to 10, the first process corresponds to ET while the second to PCET, shifting to more negative redox potentials with a slope of 57 mV per unit of pH. These results are in agreement with the mechanism reported for the fluorenone (OFTDL)Cl_2.[138] Above pH 11, the mechanism behaves the opposite way: while the first process is PCET, the second is ET. Furthermore, the yellow colour of the solution vanished at pH higher than 11, to finally become red. We believe that at

alkaline conditions the azoniafluorenone structure is deprotonated at the N-CH_2 group leading to species with radical character that decomposed in contact with oxygen.[175] This observation further strengthened our decision to avoid alkaline conditions. We next conducted a similar study using unbuffered 1 M KCl as supporting electrolyte. In this case, within the pH range of 7-10, we observed that both processes behave as ET, with the second event happening at a redox potential of –0.37 V vs. SHE. Considering that this is the same value observed for the second redox process when using Britton-Robinson buffer at pH above 10, we believe that, in unbuffered solutions, the pH around the electrode increases because of the PCET reaction that consumes protons. As a result, in unbuffered solutions, we observed the second wave at a more negative redox potential, which corresponds to the higher pH value. This behaviour has been previously reported for quinones: while they show two sequential PCET reactions in buffered solutions, the mechanism shifts to ET in unbuffered conditions because of the local pH increase.[176] To summarize it, we present the proposed mechanism in **Figure 27**. We believe that **AZON3** reacts first via ET to form the radical **A**. The second step depends on the local pH of the electrolyte, occurring as either PCET or ET to form the double reduced species **BH** or **B**, respectively. Finally, the single and double reduced species of **AZON3** were electrogenerated in a flow cell and characterized via NMR, Raman, EPR and UV-Vis. The spectra, presented in the main article of **Publication III**, confirmed the structure of the radical and the double reduced specie of the studied azoniafluorenone derivative.

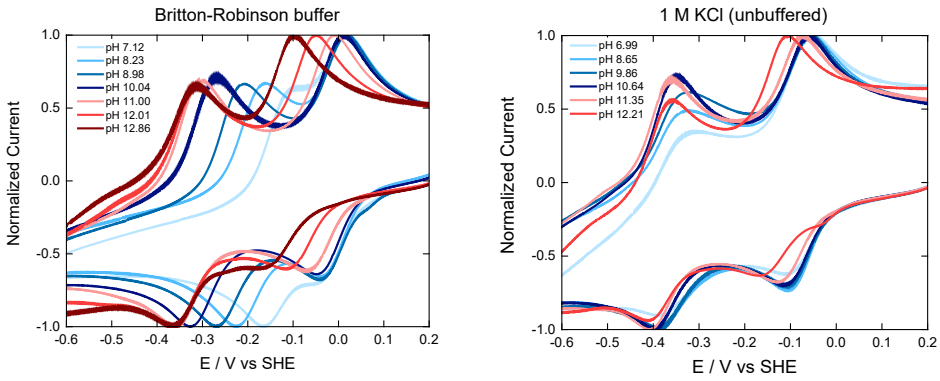

Figure 26. Cyclic voltammograms of AZON3 at different pH, using Britton-Robinson buffer and 1 M KCl (unbuffered) as supporting electrolytes. Concentration of AZON3: 1 mM. Scan rate: 100 mV s^{-1}.[III]

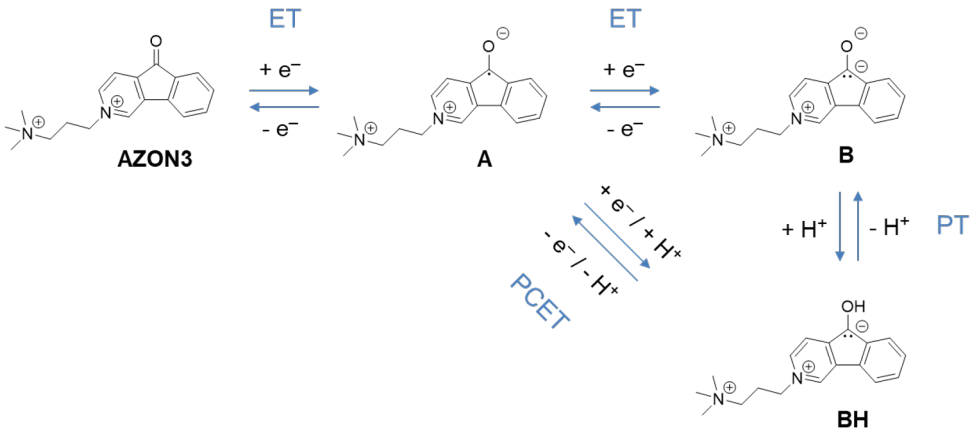

Figure 27. Proposed reduction mechanism of azoniafluorenone AZON3 after one- and two-electron reduction.[III]

During battery charging in unbuffered conditions, with higher concentration of **AZON3**, the pH of the electrolyte increases fast because of the PCET step until it reaches the pK_a of **BH** (around 10.5-11). Then, most of the reaction occurs via ET mechanism, while the pH of the electrolyte remains constant at that level. During discharge, the reaction begins as ET followed by PCET, releasing protons and reducing the pH. As a result, we expect a fluctuation of the pH during battery cycling. This behaviour was reported by Aziz in a previous work with a phosphonate-functionalized quinone by recording the pH during cycling.[177] In our work, we confirmed it by measuring the pH at different stages during cycling of **AZON3** (reported in the main article and Supporting Information of **Publication III**). Finally, the following battery investigations were performed using unbuffered KCl as supporting electrolyte. Despite the slightly higher pH developed during battery cycling, close to 11, the redox potential of the second process of **AZON3** in this conditions is around 200 mV more negative than in buffered electrolyte, which enables higher cell voltage and power density. **Figure 28** presents the cycling figures of **AZON3** flow cells using buffered and unbuffered solutions, clearly showing the improvement on the cell voltage when using unbuffered electrolyte.

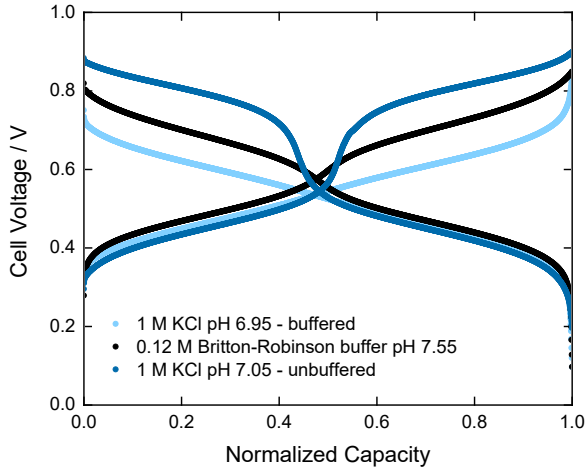

Figure 28. Cycling figures of 5 mM AZON3 flow cells using different buffered and unbuffered electrolytes. CC protocol using 1 mA cm^{-2}.[III]

Finally, we tested the performance of **AZON3** in flow cells when using high concentrations of the active material (presented in detail in **Publication III**). The battery experiments were conducted inside the glovebox with KCl (unbuffered) as supporting electrolyte. A symmetric cell with 0.46 M of **AZON3** exhibited high stability for two-electron cycling, with a capacity decay of 0.010% per cycle (0.27% per day) and coulombic efficiency of 99.98% over more than 1000 cycles. During this long cycling, we noticed a reduction on the electrolyte volume due to evaporation. To keep the same electrolyte concentration, we periodically added a corresponding amount of water to the reservoirs. After these additions, a small fraction of the lost capacity was recovered, which suggests that the electrolyte was on the limit of the solubility after water evaporation. We associate the resulting capacity decay with azoniafluorenone decomposition, considering that the loss because of crossover is eliminated because of using the symmetric cell configuration and the solubility issue is already contemplated.

The last battery consisted of a full cell, assembled with 1 M concentration of **AZON3** and an excess amount of BTMAP-Fc on the positive side. When cycling the two electrons, the battery exhibited relatively high stability with a capacity fade rate of 0.097% per cycle (0.79% per day) and coulombic efficiency of 99.94% (**Figure 29**). At that condition, the battery developed a cell voltage of 0.63 V and large volumetric capacity, reaching 46.4 Ah L^{-1} when using 87% of the full theoretical capacity. During the cycling at 60 mA cm^{-2}, the battery exhibited an energy density of 23.8 Wh L^{-1} and a round trip efficiency of 65%. This value is comparable with previous results obtained for organic molecules tested in AOFBs studies[178], while it is in accordance with the relatively fast kinetics of **AZON3**

determined within this research work via Nicholson approach[179] (9.52×10^{-2} and 6.07×10^{-2} cm s^{-1}, for the first and second electron, respectively), presented in the Supporting Information of **Publication III**. We did not perform further investigations to analyse the energy density and power, as these parameters are also influenced by the selected posolyte and the cell architecture. In our case, we used a non-optimized cell as well as a posolyte with relatively low redox potential (0.39 V). However, the tests conducted within this work validated the high performance of **AZON3** to develop high storage capability and stable operation under near-neutral pH conditions. Finally, after 170 cycles, the battery was disassembled to perform port-mortem analysis. The cyclic voltammetry measurements of the electrolytes did not show visible crossover of species through the membrane, suggesting a low permeability of **AZON3**.

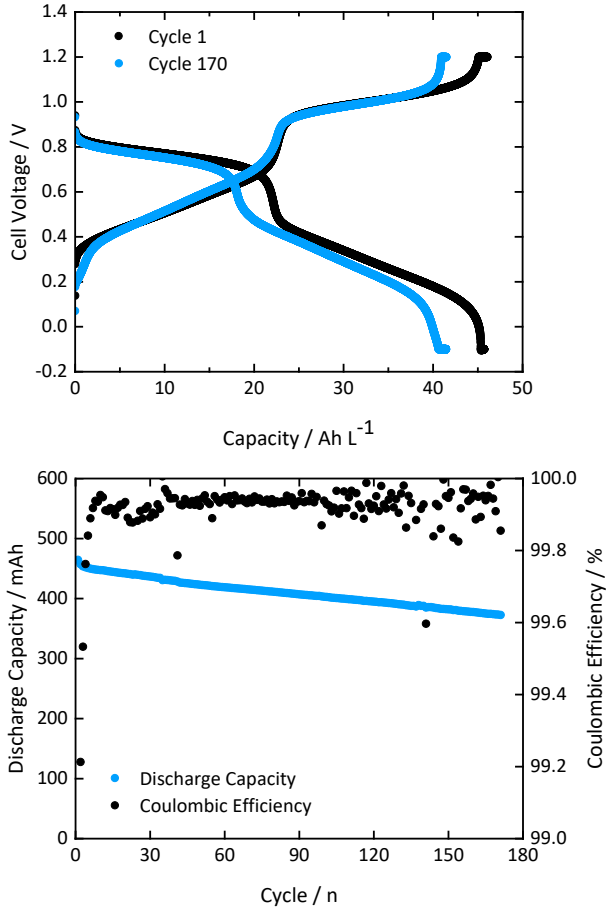

Figure 29. Cell performance of 1 M AZON3 flow cell using 3 M KCl (pH 7.75) as supporting electrolyte. CCCV protocol using 60 mA cm^{-2} (cut-off current during CV step: 2 mA cm^{-2}).[III]

The results presented in this work successfully introduced the azoniafluorenone structure as a promising negolyte candidate for near-neutral pH AOFBs. Azoniafluorenones exhibit two reversible redox reactions in neutral pH electrolytes as well as high solubility when incorporating the appropriate functional groups. **AZON3**, the most promising derivative that includes a quaternary ammonium group with the nitrogen atom in the γ position of the pyridinium ring, demonstrated high performance for two-electron cycling even when tested in a flow cell at 1 M concentration. The relatively high stability was coupled with large storage capability, reaching 46.4 Ah L^{-1}, which is one of the highest values reported for neutral-pH AOFBs.[180,181] Considering the maximum solubility of **AZON3**, determined as 1.64 M, and its ability to effectively store two electrons, it could enable an outstanding

storage capacity up to 88 Ah L^{-1}. Finally, a synthetic route developed within this work allows the obtention of multiple azoniafluorenone derivatives, opening a broad scope for investigations that boosts our enthusiasm to continue our investigations with this new organic family.

6 Experimental Measurement System

This chapter presents the discussion about the measurement system developed within this work to monitor the battery operation. During the investigations conducted in **Publication IV**, the experimental set-up was used to analyse two vanadium flow cells assembled with different carbon felts (VFB1 and VFB2), as well as an organic flow battery (OFB). By confirming previous results reported for vanadium systems, we validated the reliability of this experimental set-up, extending its use to further systems. The experiments were based on short cycling tests at different current densities and polarization curves at different flow rates and states of charge. This study provides a discussion about the half-cells states of charges and overpotentials developed on each electrode during the experiments. Finally, in **Publication V** we studied the performance of carbon felts activated with a novel chemical treatment, presented in section 6.4 of this dissertation. In that case, a simpler set-up was used to study the overpotentials developed on the individual half-cells and evaluate the impact of the nitrate molten salt treatment on the performance of VFB.

6.1 Validation of measurements

All the measurements recorded during battery operation are listed in Page 44 of this dissertation, while **Figure 11** shows a scheme of the full measurement set-up. The reliability of the measurements recorded during battery operation was validated by comparing the measured cell voltage against the calculated value using the half-cells and membrane measurements recorded with this set-up. The cell voltage can be calculated with the half-cells open circuit potentials, and electrodes and membrane potential losses using equation 10.[29]

$$E_{Main\ Cell} = E_{OCP}^{+} + E_{OCP}^{-} + \eta^{+} + \eta^{-} + E_{memb} \qquad (10)$$

where

- E_{OCP}^{+} is the positive electrode half-cell open circuit potential, recorded with measurement 4.

- E_{OCP}^{-} is the negative electrode half-cell open circuit potential, recorded with measurement 5.
- η^{+} is the positive electrode overpotential, recorded with measurement 6.
- η^{-} is the negative electrode overpotential, recorded with measurement 7.
- E_{memb} is the potential drop through the membrane, recorded with measurement 8.

All these values were recorded with the measurement system. Then, by comparing the main cell voltage (measurement 1) against the calculated value, we can validate the reliability of the experimental set-up. **Figure 30** shows the excellent agreement between the measured and calculated cell voltage during the cycling test of the system VFB1. The curves of VFB2 and OFB are exhibited in the Supporting Information of the **Publication IV**. In all the cases, the difference between the measured and calculated values does not exceed 10 mV for most of the cycling, with the exception of the end of some cycles where the overpotential values exhibit a sudden increase.

Despite this excellent agreement, which suggests a high reliability of the recorded measurements, we assumed the possibility of shunt currents flowing through the OCV-cells, which could affect the measurement of the overpotentials. This was deduced after noticing the variation of the membrane potential (measurement 8), recorded on the OCV-cell, when applying current on the main battery. To confirm this, we performed an additional experiment assembling the OCV-cell after the main battery with a Teflon sheet instead of the ionic membrane in order to block possible shunt currents passing through this cell. Using this new set-up for the VFB1 system, we performed polarization curves obtaining an important reduction of the measured half-cells overpotentials compared with the normal system using an ionic membrane in the OCV-cell. This experiment confirmed the presence of shunt currents flowing through the OCV-cell, and its effect on the recorded half-cells overpotentials. We next measured the ohmic resistances of the whole hydraulic circuit in order to determine the magnitude of this effect. Despite we estimated a small value flowing as shunt current through the additional cell (0.006% of the total current), the large ohmic drop between the two cells (around 1300 Ω) leads to a high contribution to the recorded half-cell overpotentials. All these experiments and results are further explained in the Supporting Information of **Publication IV**.

After these experiments, and considering the high agreement between the recorded cell voltage values and the ones obtained with equation 10, we concluded that main cell ohmic losses are incorporated in the measurements of overpotentials and potential drop across the membrane (measurements 6, 7 and 8). Furthermore, we understand that the original system is not measuring real overpotentials, which could

be done by blocking the shunt currents on the OCV-cells, as described above. Finally, we decided to refer to measurements 4 and 5 as *apparent overpotentials* of the positive and negative electrodes, respectively. Despite the deviation against the real values, the apparent overpotentials offer comparable information to make an analysis of the potential losses distribution and the contribution of each electrode to the overall electrode overpotential.

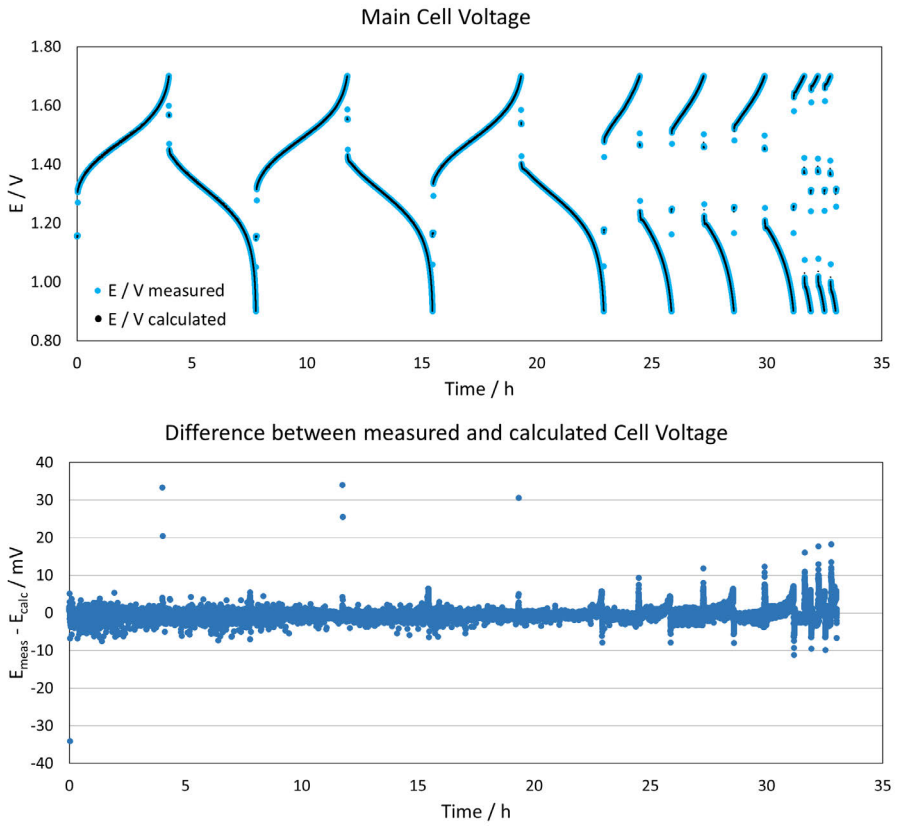

Figure 30. Comparison of measured and calculated cell voltage during the cycling experiments performed for the VFB1 system.[IV]

6.2 Cycling tests

The charge-discharge curves recorded on the main cell during the cycling experiments showed, as expected, that higher current densities lead to increase potential losses (overpotentials) and, as a result, lower cell energy efficiency and capacity utilization. These results were in agreement with the half-cells measurements, demonstrating the ability of this set-up to provide further information

about the studied systems. In the case of the half-cells apparent overpotentials, they exhibited an increase at higher current densities, in accordance with the main cell measurements, while also showing the distribution of the potential losses on each side of the cell. Furthermore, the half-cell open circuit potentials clearly showed the assessment of lower states of charge when increasing the current density, confirming the lower capacity utilization and providing useful information for the analysis of the half-cells evolution during the cycling process. All the measurements for the three studied systems are shown in the Supporting Information of **Publication IV**.

In order to analyse the half-cell states of charge, the corresponding *E* vs SOC curves were built up for the vanadium and the organic systems. The experimental curves are in agreement with previous results obtained for vanadium,[156] and they show a high correlation with the theoretical curves obtained from Nernst equation.[182] **Figure 31** exhibits the half-cells curves for both systems, evidencing the high agreement between the theoretical and experimental curves. The obtention of these curves is further explained in the main draft and Supporting Information of **Publication IV**. The high correlation suggests that these curves are suitable enough to predict the half-cells SOCs during battery operation, although their reliability decreases at the extreme SOC values.

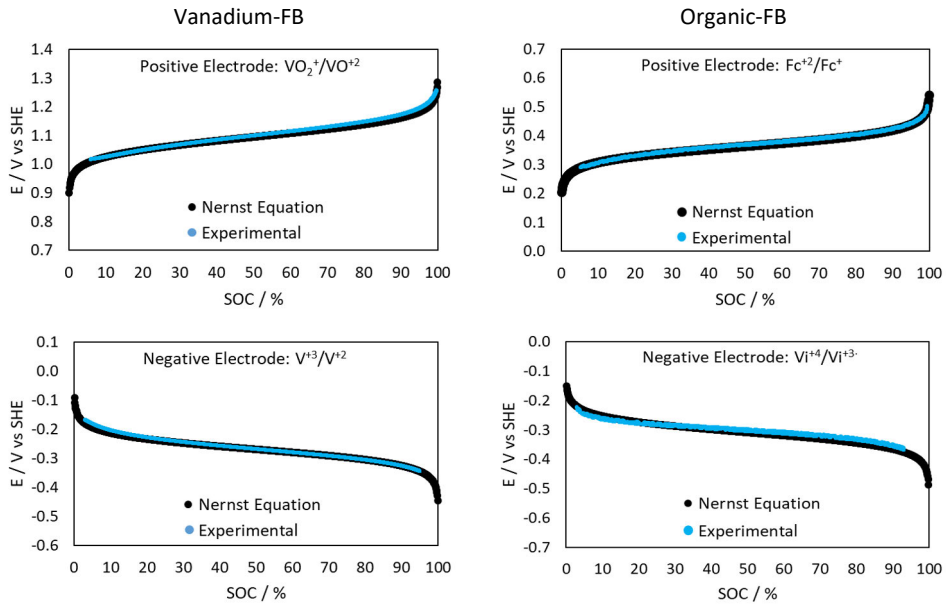

Figure 31. Comparison of experimental and theoretical half-cells state of charge curves (*E* vs SOC) obtained for vanadium-FB and organic-FB. [IV,SI]

The analysis of the half-cell SOCs during the cycling test of VFB1 system, presented in **Figure 32**, clearly shows the lower capacity utilization when increasing the current density, with the SOCs moving further away from the extreme values. Furthermore, the SOCs achieved in every cycle evidenced the battery capacity lost during the cycling test, in agreement with the main cell measurements. We attribute this capacity decay to the self-discharge of V^{+2} ion in contact with oxygen, as it can be easily oxidized back to V^{+3} leading to cell imbalance.[61] This assumption is confirmed by the half-cell SOC measurements, with the negative side working at lower SOCs as a result of the self-discharge. In addition, **Figure 32** provides a comparison between the capacity utilization per cycle measured in the main cell against the value calculated as a difference between the half-cell SOCs achieved at the end of the charge and discharge steps in each cycle. The high agreement between these values confirms the reliability of the half-cell SOC measurements.

Regarding the SOCs analysis during the cycling of the organic-FB, a similar discussion is presented in **Publication IV**. In this case, the lower current densities together with the faster kinetics of these organic molecules,[88] lead to higher capacity utilization, working close to the extreme SOCs even at the highest current values. Furthermore, we noticed a small imbalance with the posolyte moving at higher SOC values as well as high capacity retention that is in agreement with the high stability of this organic redox couple when operating in the studied conditions.[88] These half-cell SOC measurements show high reliability to perform a deeper study of the flow battery operation, allowing the prediction of the possible causes of imbalance and capacity loss. It is important to mention that the analysis becomes more useful for long cycling processes when working with stable redox couples while it fully relies on the quality of the half-cell state of charge curves built beforehand.

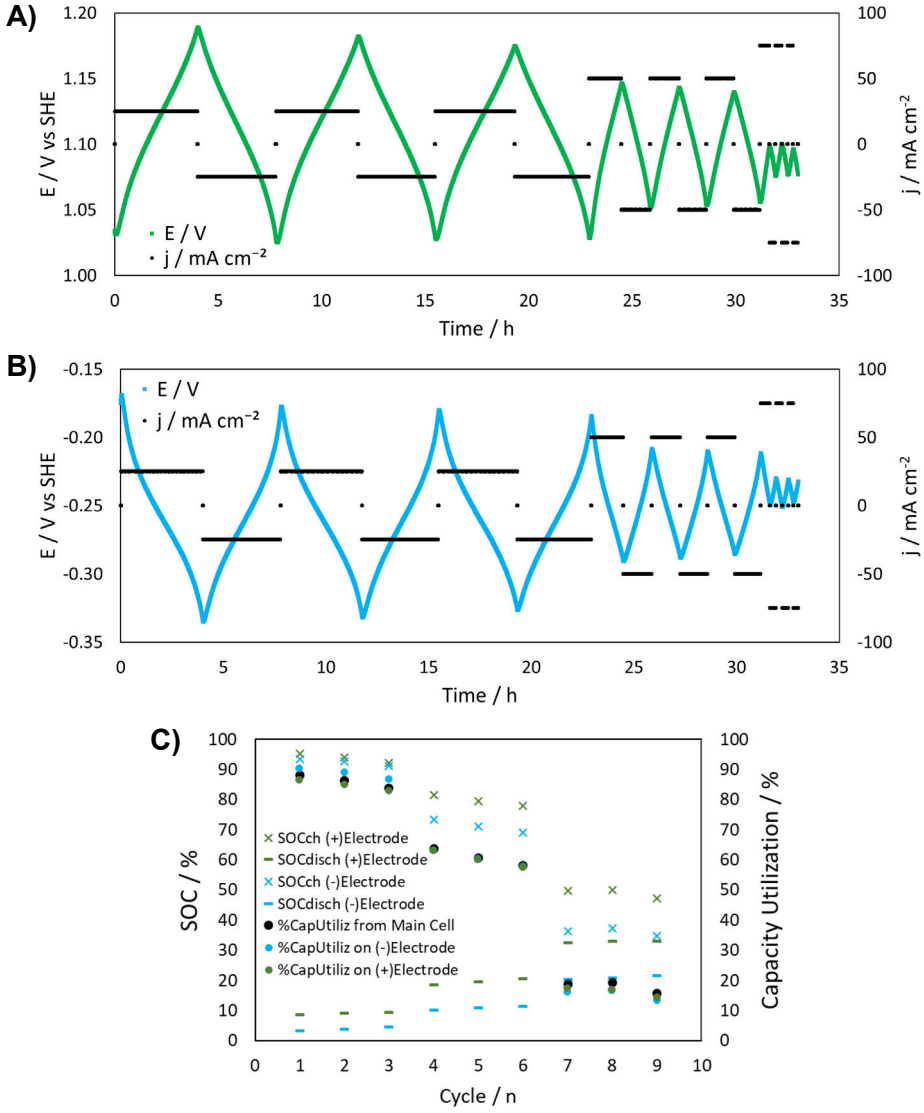

Figure 32. Half-cell redox potentials recorded during cycling tests of VFB1. **A)** Posolyte cycling curves (measurement 4). **B)** Negolyte cycling curves (measurement 5). **C)** SOCs achieved at the end of each charge (SOCch) and discharge (SOCdisch) step on each electrode. Capacity utilization measured at the main cell and calculated as the difference between SOCch and SOCch on each electrode.[IV]

The analysis of the half-cell apparent overpotentials during cycling was focused on the values on the steady state, at 50% SOC, in order to make a proper comparison of the systems at different current densities at similar conditions. Furthermore, the

evolution of the apparent overpotentials during cycling can be used to obtain additional information. For example, the recordings show which electrode is the limiting side on each step, exhibited as a sudden increase of the electrode apparent overpotential at the end of the step for the limiting side, which we attribute to increased mass transfer limitations. While the cycling curves are presented in the Supporting Information of the **Publication IV**, **Table 3** summarizes the apparent overpotentials of each electrode at the steady state during discharge for the three studied systems.

Table 3. Apparent overpotentials of the positive and negative electrodes (measurements 6 and 7, respectively) measured at 50% SOC during the cycling tests. The values presented in the table are calculated as an average of the three cycles for each current density and considering the background potential before starting the discharge step.[IV]

	VFB1		VFB2		OFB		
j / mA cm^{-2}	η+ / mV	η– / mV	η+ / mV	η– / mV	j / mA cm^{-2}	η+ / mV	η– / mV
25	–41	91	–49	79	12.5	**	13
50	–84	175	–72	146	25	–32	26
75	–118	263	–102	197	37.5	–42	34
100	*	*	–126	241	50	–54	42

* VFB1 was not cycled at 100 mA cm^{-2} because the cell voltage exceeds the cut-off due to the high overpotentials required at that current density.
** Not reported because of noise on the measurement and short resting time that did not allow obtaining a clear value.

The developed apparent overpotentials shown in **Table 3** are consistent with the higher electrode polarization expected because of the increased current density and the lower kinetics. First, the vanadium systems (VFB1 and VFB2) exhibited considerable higher electrode potential losses than the OFB, which is in agreement with the much faster kinetics of the organic materials. While the rate constants of vanadium electrochemical reactions for the negative and positive electrode have been estimated as $2.5 \cdot 10^{-5}$ and $1.4 \cdot 10^{-4}$ cm s^{-1}, respectively,[55] the reported corresponding values for the studied organic couples are $2.2 \cdot 10^{-2}$ and $1.4 \cdot 10^{-2}$ cm s^{-1}.[88] Furthermore, in the case of the vanadium systems, the measured apparent overpotentials clearly demonstrated that most of the electrode potential losses (66-69%) belongs to the negative electrode, which fully agrees with the slower kinetics of the redox couple V^{+3}/V^{+2} compared with V^{+5}/V^{+4}.[55,183,184] On the other hand, the electrode potential losses on the organic system are equally distributed, with a slightly higher contribution of the positive side (52-56%), in accordance with the

lower rate constant of BTMAP-Fc. Finally, a comparison between the studied vanadium systems shows the higher apparent overpotentials developed at increased current densities for VFB1, which confirms the lower performance of this system and the limitation to operate at the highest current densities. We attributed this to the lower activity of the carbon felts used in the VFB1 towards vanadium reactions, emphasizing the importance of the electrode activation to improve the performance of these systems.[32,56] A more detailed analysis of the electrode pre-treatments is presented in the section 6.4 of this dissertation.

Finally, the comparison of the OCV measurements before and after the main cell (measurements 2 and 3) exhibited the conversion occurring in the battery. However, evaluation of the achieved conversion is poorly accurate because of the high flow rate and low conversion per pass. We believe that this analysis would be more useful for larger systems or stacks with higher conversion level per pass. After this consideration, and the limitation of the system to measure real overpotentials, we conclude that the system can be simplified to one additional cell assembled with Teflon sheet as separator and including a reference electrode on each side. That configuration would allow the measurement of the real half-cells overpotentials and states of charge, while the OCV can be easily calculated with the half-cells OCP.

6.3 Polarization curves

The study of the polarization curves was focused on the analysis of the half-cells apparent overpotentials, presenting the strength of the experimental set-up to obtain an insight on the distribution of the potential losses. The polarization curves were performed using the step and slope approaches, showing a high correlation with the exception of the high current region of the test at 20% SOC and 20 ml min^{-1}. We attribute that deviation to the poor accuracy of the step approach at that condition, where it becomes challenging to define a steady voltage value because of exhaustion of the electrolyte. All the cell measurements and comparison of the approaches are presented in the Supporting Information of **Publication IV**. We conducted the discussion based on the results obtained with the slope approach because of simplicity.

The half-cell apparent overpotentials recorded during the polarization curves for the VFB1 are presented in **Figure 33**. The first observation, which agrees with the lower kinetics of the V^{+2}/V^{+3} couple and our previous results during the cycling tests, is that the apparent overpotentials on the negative electrode are higher than on the positive side for all the studied conditions. Secondly, the curves present a linear trend on the whole range, suggesting that most of the contribution arises from cell ohmic losses, as it has been previously reported for VFBs.[75] We believe that this ohmic component is also increased by the shunt currents flowing through the OCV-cell, as

we previously explained, leading to the apparent overpotentials. Regarding the charge transfer overpotentials, they are not visible in the low current region. Possible explanations are that they are hindered by the increased ohmic component or minimized because of the high surface area and activity of the carbon felts.[75] Finally, despite the lack of a clear mass transfer region at high current density values due to starvation effects, we can notice slightly higher slopes when working at lower SOCs that we attribute to mass transfer limitations. This observation contradicts the results presented by Roth,[147] claiming that the slope of the polarization curves remains constant at different SOCs in absence of starvation effects. However, we believe that the slight change on the slope arises from the higher potential losses due to the lower concentration of reacting species. Additionally, we believe that mass transfer limitations are responsible for the higher overpotentials developed on the positive electrode at higher current densities when reducing the flow rate, presumably because of the higher viscosity of the positive electrolyte.[185]

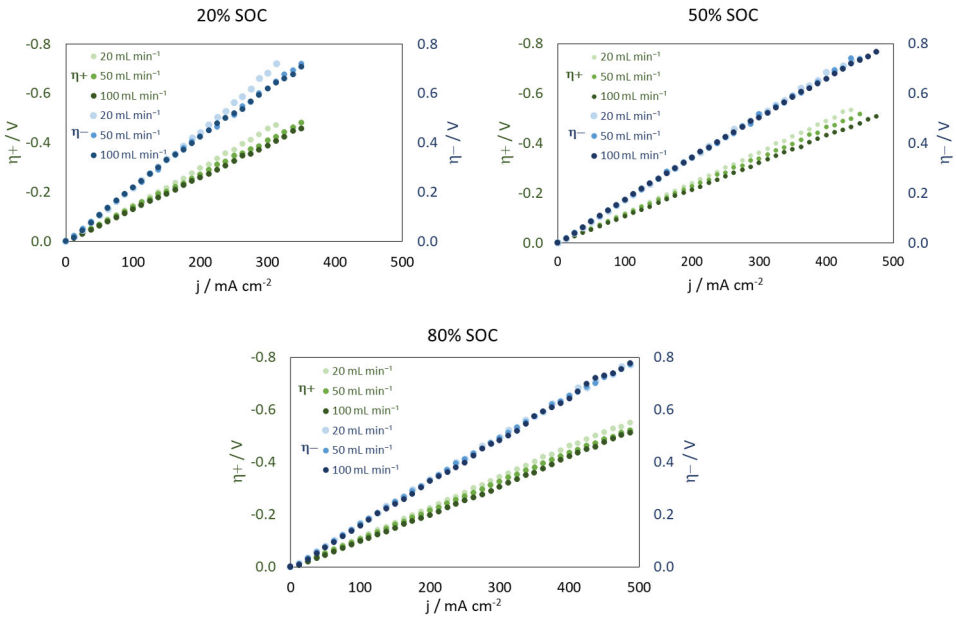

Figure 33. Half-cell apparent overpotentials recorded during polarization curves of VFB1 at different SOCs and flow rates (measurements 6 and 7).[IV]

The measurements of half-cell apparent overpotentials during the polarization curves of the OFB also agree with the results obtained during the cycling tests, showing an equal distribution with a slightly higher contribution of the positive electrode (**Figure 34**). In this case, the curves clearly show high mass transfer limitations in the high current density region because of starvation effects. These

effects are exhibited as a loss of the linear trend at higher current densities and, as expected, they become more significant when working at lower SOCs. We believe that the higher mass-transfer limitations are related with the lower concentration of the active materials of the studied OFB (0.4 M). This assumption is supported by the linear trend presented when working at 80% SOC, where the concentration of the reacting species is higher.

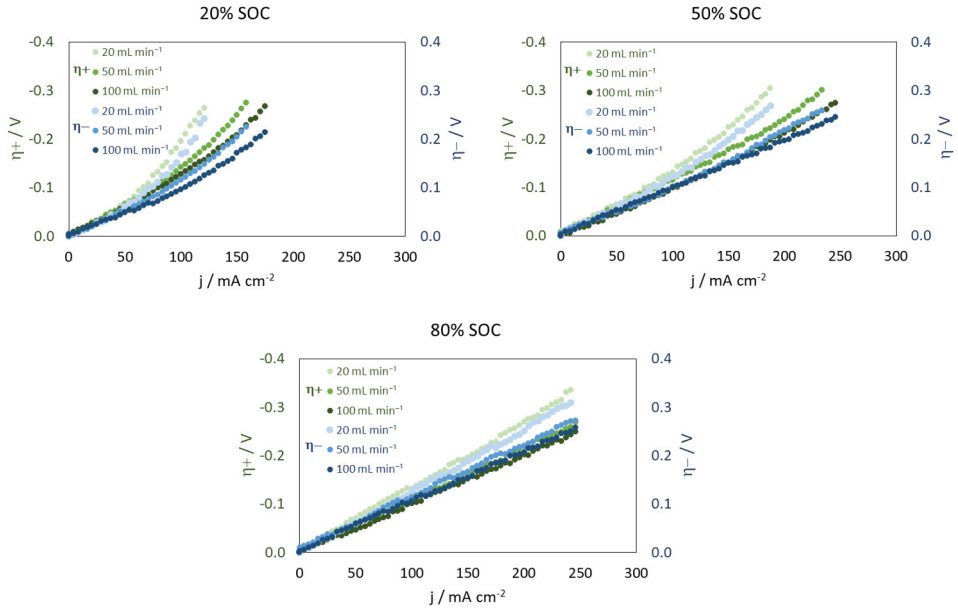

Figure 34. Half-cell apparent overpotentials recorded during polarization curves of OFB at different SOCs and flow rates (measurements 6 and 7).[IV]

Finally, we performed an analysis of the apparent kinetic parameters of the studied systems using Tafel plots.[184,186] The study and calculated apparent kinetic parameters are presented in the Supporting Information of the **Publication IV**, showing a coherent trend considering the kinetic rates of the studied systems. Unfortunately, the use of apparent overpotentials lead to an underestimation of the calculated exchange current density. However, we believe that this analysis can be performed using the set-up that blocked the shunt currents to calculate the real values, providing strong information about the in-situ electrode kinetics in an actual flow cell.

6.4 Study of chemically-treated carbon felts

During the investigations conducted in **Publication V**, a simplified version of the measurement system was used to evaluate the performance of VFB assembled with carbon felt electrodes activated with a novel chemical treatment. The treatment, developed by our collaborators from Poznan University of Technology (Poland), was based on oxidation at high temperatures in presence of nitrate molten salt. In this case, the measurement system only includes the OCV-cell after the main battery (without reference electrodes) in order to measure the half-cell apparent overpotentials and studying the effect of the nitrate molten salt treatment on the felts activity towards vanadium reactions. The discussion presented in this dissertation focuses on the results obtained during the flow battery tests using chemically treated GFD felts. In order to study the impact of the new chemical treatment, the performance of the chemically treated felts was compared with heat-treated samples.

The initial characterization studies, performed at Poznan University of Technology (Poland), demonstrated that GFD pristine carbon felts are inactive for vanadium reactions, while that could be improved by the incorporation of oxygen[45,46] and nitrogen[48,49] functional groups to the carbon structure. After carbon felt treatment at high temperature in presence of nitrate salt, the voltammograms of the samples exhibited reversible redox reactions, except for the couple V^{+4}/V^{+3} that is kinetically unfavorable.[187] The voltammograms of the pristine and treated GFD sample are presented in **Figure 35**. As the temperature was increased (from 380 to 440 ºC), more reversible behaviour was obtained, with larger improvement on the negative electrode reaction, corresponding to the V^{+3}/V^{+2} redox couple. This trend correlated with the results obtained during XPS measurements, which showed higher oxygen content at increased treatment temperatures. However, these temperatures were not high enough to incorporate nitrogen to the felt surface.

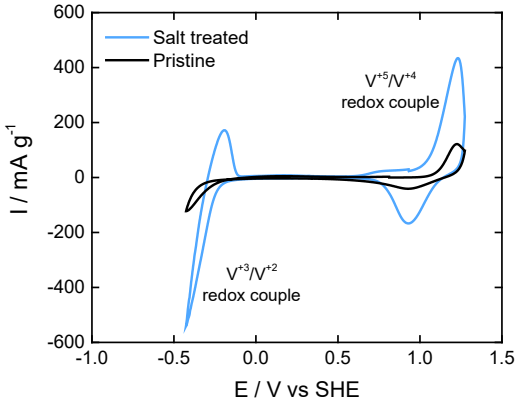

Figure 35. Voltammograms of vanadium reactions using pristine and treated GFD carbon felt. Treatment: heat treatment in presence of nitrate salt at 420 ºC for 10 minutes. Scan rate: 2 mV s^{-1}.[V]

For the next tests, a treatment temperature of 500 ºC was selected as a recommendation from SIGRACELL, enabling the addition of nitrogen functional groups as well as an optimal oxygen content. The resulting samples were analysed with the same procedures and further tested in a flow battery including the half-cell overpotential measurements. The tested samples were treated in the presence of nitrate salt at 500 ºC, heat and salt treatment (HT+ST), during different treating times of 3, 6 and 12 hours, named 3h HT+ST, 6h HT+ST and 12h ST+HT, respectively. Furthermore, felts treated without salt at 500 ºC, only heat-treatment (HT), for the same treatment times were also analysed for comparison (named 3h HT, 6h HT and 12h HT). In the case of the sample 12h ST+HT, the long oxidative treatment was too destructive for the carbon felt, leading to a fragile sample and a significant loss of the total mass (68%). As a result, this sample was excluded for the battery experiments.

Table 4 summarizes the results obtained with the HT+ST samples treated at 500 ºC during the initial physico-chemical investigations, together with the pristine and the 12 HT sample for comparison. The XPS measurements clearly showed that the salt presence and temperature rise to 500 ºC enabled the incorporation of nitrogen to the carbon structure, while longer treating times lead to higher functionalization of both oxygen and nitrogen groups. Furthermore, the oxidation treatment results on a decrease on the felts conductivity, which worsens when extending the treatment times. However, this procedure is needed to improve the activity towards vanadium reactions. In the case of the sample 12h HT+ST, it presented a drastic conductivity reduction as well as burn off, confirming that those conditions are too destructive for the felts.

Table 4. Physico-chemical properties of carbon felts electrodes measured during the initial investigations. Pristine felt, heat-treated sample for 12 hours (12h HT), heat+salt treated samples for 3, 6 and 12 hours (3h HT+ST, 6h HT+ST, 12h HT+ST, respectively). Treatment temperature: 500 ºC.

Sample	Surface composition			Conductivity	Burn off
	%C	%O	%N	S m^{-1}	%
Pristine	97.9	2.1	0	241	0
12h HT	95.5	4.5	0	150	3
3h HT+ST	90.5	8.0	1.5	148	15
6h HT+ST	88.8	9.3	1.9	104	57
12h HT+ST	83.3	14.3	2.5	35	67

The cyclic voltammograms, presented in **Publication V**, exhibit more reversible reactions for the posolyte redox couple when using shorter treating times, evidenced by sharper current peaks and smaller peak separations. In the case of the negative side reactions, even though there is not a clear trend, the three samples exhibited quite reversible behaviour. Despite the high reversibility demonstrated by the sample 12 HT+ST, it was excluded for the next investigations because of the poor mechanical properties. These results suggest that the most appropriate oxidation consists of the 3-hours heat-salt treatment. In order to validate this assumption, we compared the performance of the 3h HT+ST sample during cyclic voltammetry measurements over 100 scans with the 12h HT and 12h HT+ST samples. While 3h HT+ST demonstrated stable behaviour for the vanadium redox couples of both positive and negative electrodes, the samples treated for 12 hours, with and without salt, exhibited a reduced activity towards the reactions of the V^{+3}/V^{+2} couple after multiple scans. To summarize, the salt treatment at 500 ºC successfully enabled the incorporation of both oxygen and nitrogen to the carbon structure, enhancing activity towards vanadium reactions and stability when not considering too long treatment times. Furthermore, larger improvements are evidenced for the redox couple belonged to the negative electrode.

The discussion of the flow battery experiments was limited to the analysis of the discharge capacity and energy efficiency, measured in the main cell, and the half-cell apparent overpotentials of the positive and negative side, recorded with the experimental set-up. The main cell measurements clearly demonstrated that the inclusion of the salt treatment improved the battery operation when comparing the samples with same treating times (**Figure 36**). The batteries assembled with the heat-treated samples with shorter treating times, 3h HT and 6h HT, demonstrated the worst performance, with the lowest discharged capacity and energy efficiency values for all the current densities studied, which is attributed to the higher potential losses. Indeed, those batteries were not able to cycle at the highest current density (100 mA cm^{-2}) because of the high overpotentials developed, generating a cell voltage that exceeded the cut-off. Considering that the batteries only differed on the electrodes, we can assume that the higher overpotentials arose from the different treatment conditions. Finally, the best performance, with the highest energy efficiency and discharge capacity values, was obtained for the batteries assembled with 3h HT+ST and 12h HT, in agreement with the preliminary results discussed above. In the case of 6h HT+ST, it exhibited high discharge capacity at lower current values, but its performance decayed faster than the other cells at increased current densities. We believe that the salt treatment leads to overoxidation of the felts when the treatment times are extended over 3 hours, as it was clearly evidenced by the 12h HT+ST sample, concluding that the 3h HT+ST sample leads to the best battery performance.

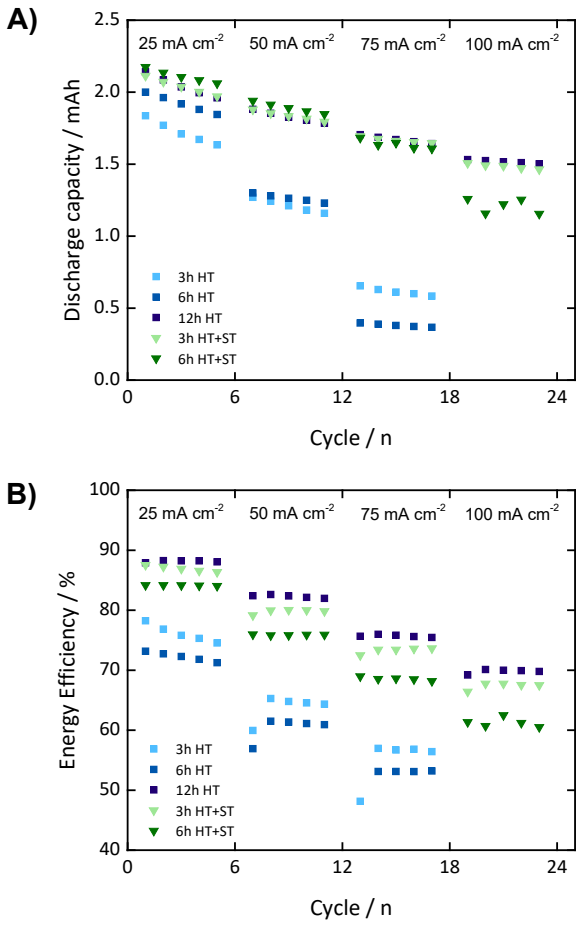

Figure 36. Main cell measurements during flow battery tests at different current densities using carbon felt electrodes with different activation treatments. **A)** Discharge capacity. **B)** Energy efficiency.[v]

The results obtained with the half-cell measurements validated the main cell observations while providing further information about the potential losses distribution. **Figure 37** shows the half-cell apparent overpotentials measured in the steady state at 50% SOC. The highest current densities are not reported because it was challenging to define a clear stable value. The first observation is that most of the potential losses belong to the negative side, in accordance with the sluggish kinetics of the V^{+3}/V^{+2} redox couple, as it has been previously demonstrated and discussed in this dissertation and previous works.[55,183,184] Furthermore, the salt treatment clearly leads to lower apparent overpotentials during battery operation when considering same treating times, in agreement with the main cell measurements. The most interesting remark is that the largest improvement when

including the molten salt is achieved on the apparent overpotentials of the negative side. Considering the 3-hours-treatments, the sample 3h HT+ST exhibited a reduction of about 15-20 % on the positive electrode apparent overpotentials compared with the sample 3h HT, while a much higher reduction of 70% is achieved on the negative side. A similar improvement is obtained when comparing the samples 6h HT+ST and 6h HT. These results indicate that the salt treatment enhances the activity towards vanadium reactions with a higher impact on the negative side, which is the main responsible of the overall electrode potential losses. Finally, the lowest apparent overpotentials were recorded for the samples 3h HT+ST and 12h HT, in agreement with their highest performance measured in the main cell.

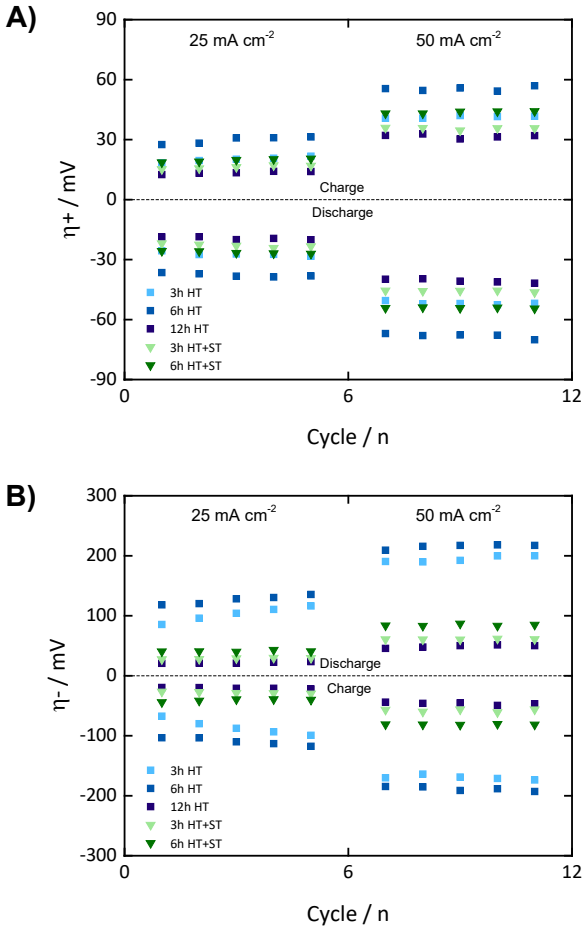

Figure 37. Half-cell apparent overpotentials measured during flow battery tests at different current densities using carbon felt electrodes with different activation treatments. The reported values corresponds to the steady state at 50 %SOC during charge and discharge. **A)** Positive electrode apparent overpotentials. **B)** Negative electrode apparent overpotentials.[v]

Additionally, the results obtained from electrochemical impedance spectroscopy, conducted to measure the ohmic cell resistance, are in agreement with the conductivity of the carbon felts determined during the preliminary investigations. The higher cell resistances were measured for the batteries assembled with the samples treated with salt, which demonstrated lower conductivities. Furthermore, the resistance values increased when considering longer treatment times. These results explain why the sample 6h HT+ST, with the lowest conductivity, operated better at low current densities but its performance strongly decreased at higher current values due to the large ohmic losses.

To summarize, the results obtained from the flow battery studies were in full agreement with the preliminary characterization, confirming the reliability of this approach and providing further information about the electrodes during operation in a flow cell. Despite the limitations to measure the real overpotentials, the experimental measurement set-up demonstrated its capability to provide useful information about the electrode overpotentials distribution and determine the contribution from each side. It is worth to mention that the study can be repeated by blocking the shunt currents to measure the real overpotentials developed on each side of the cell. Finally, the treatment including the nitrate molten salt demonstrated the successfully incorporation of oxygen and nitrogen functional groups to the carbon structure, enabling an increased performance compared with the standard heat-treatment when considering same oxidation times. We attribute this to the presence of nitrogen groups that lead to a reduction of the electrodes overpotentials with a bigger impact on the sluggish negative electrode. The sample treated for 3-hours with the salt demonstrated a similar high performance than the 12-hours heat-treated sample, reducing the oxidation time and the related costs.

7 Conclusions and Outlook

This dissertation focuses on the development of flow batteries for sustainable large-scale energy storage applications. The first part comprises investigations focused on the development of new organic materials intended as negolytes for Aqueous Organic Flow Batteries. By applying different approaches, our investigations demonstrated how the proper molecular design can be applied to tune the desired properties and attain competitive materials.

In the first case, pyridoxals were presented as potential candidates because of their availability from natural sources and reversible electrochemical processes. Unfortunately, our investigations confirmed that the studied pyridoxal derivatives were not suitable for AOFB application because of their low cycling stability in aqueous electrolytes. However, the multidisciplinary research work enabled to rationalize the reaction and decomposition mechanisms, providing useful information for the design of the future organic materials. In the next work, we introduced a new functional group to the structure of a well-established organic negolyte. The resulting bisphosphonate-substituted viologens demonstrated high performance when tested in a flow battery, with one derivative attaining the lowest redox potential reported for viologens. Although the stability of these compounds was not competitive with other previously reported viologens, we understand that the stability was affected by the poor performance of viologens in the studied alkaline media. We still believe that the proposed bisphosphonate group can be considered for incorporation to other organic negolytes to obtain highly soluble materials and low redox potentials, leading to high energy and power densities. Finally, we successfully introduced the azoniafluorenone structure as a new family of organic negolytes. The design involved the incorporation of various functional groups in different positions of the rings. The electrochemical process was fully characterized together with the reduced forms. The best candidate, comprising a quaternary ammonium group in the position 3 of the azoniafluorenone core, demonstrated high performance for two-electron storage in near-neutral pH electrolyte even when tested at high concentrations, achieving outstanding energy capabilities. Although there is room for optimization, these initial results exhibit the high potential of the azoniafluorenone family for the development of neutral pH flow

batteries with large energy capabilities. Further improvements could be realized by considering other functional groups, i.e. to obtain more negative potentials that enhance the cell voltage and battery power. One interesting option would be to replace the ammonium functional group by bisphosphonate, changing from an electron-withdrawing group to a strong electron-donating one, obtaining lower redox potentials while still holding high solubility.

The second part of the thesis presented the experimental set-up developed for monitoring the flow battery operation. The on-line measurements of the half-cell open circuit potentials and apparent overpotentials during battery operation enabled an insight of the battery performance, providing useful information about the studied systems. While the recorded half-cell open circuit potentials allowed a further analysis of the processes that lead to capacity loss and cell imbalance during battery cycling, the half-cell apparent overpotentials measurements provided further information about the distribution of the potential losses and the contribution of each electrode. The experiments performed with this set-up validated previous results obtained for vanadium flow batteries, extending the analysis to an organic system. Furthermore, a simplified configuration allowed the study of carbon felt electrodes treated with a novel chemical approach. The performance of the treated electrodes during actual operation in a vanadium flow cell confirmed the preliminary results, validating the reliability of the measurement set-up. Finally, despite the system limitation to measure the real overpotentials due to shunt currents flowing through the additional cells, we proposed a new configuration based on the use of a Teflon sheet in the additional cell, instead of the ionic membrane, that successfully blocks the shunt currents. Then, the new configuration consists of just one additional cell assembled with the Teflon sheet as separator and including a reference electrode on each side. As a result, the real overpotentials can be measured as well as the half-cell open circuit potentials. Finally, the open circuit voltage can be easily calculated with the half-cell open circuit potentials. This final configuration provides a simple set-up that allows a deep study of FBs operation, which we believe is a useful tool to boost the development of new systems and enable a proper control during operation.

Future research, linked with this dissertation, can be oriented on a fundamental study of azoniafluorenones as negolytes for AOFBs. This new family was just introduced during this research work, exhibiting high solubility and two reversible redox processes in near-neutral pH electrolytes. However, we believe that azoniafluorenones still present extensive room for improvements on the redox potentials and stability. In the case of redox potentials, as mentioned above, one interesting possibility is the inclusion of the bisphosphonate group on the azoniafluorenone core in order to obtain more negative values. Furthermore, computational tools have been extensively developed and allow a fast screening of functional groups that can be incorporated to obtain more suitable redox potentials.

On the other hand, stability issues are still one of the major drawbacks of organic systems, which is aggravated by the challenge of studying them via computational methods. Such analysis requires understanding the mechanisms that lead to capacity losses. We believe that fundamental analytical studies and extensive experimental data are required to access the decomposition mechanisms involved on the organic chemistries. Those studies coupled with computational work can strongly accelerate the discovery of the best candidates for AOFBs anolytes, speeding up the development of these systems to attain the required parameters for actual application. The use of the measurement set-up developed during this work can provide further information about the battery operation and processes related to capacity and voltage losses. It is worth to mention that the future studies should be performed using the simpler set-up suggested in the end, which blocks the shunt currents, in order to measure the real overpotentials and kinetic parameters during actual cell operation.

Acknowledgements

The research work presented in this thesis was conducted in the research group of Battery Materials and Technologies at the Materials Engineering Unit of the University of Turku, Finland. I would like to express my deep gratitude to the University of Turku for the great opportunity to carry out my doctoral studies there, as well as provide all the necessary to get such achievement. I also want to acknowledge the financial support received from the University of Turku Graduate School (UTUGs). I want to extende my gratitude for the funding obtained from European Union's Horizon2020 Research and Innovation programme under grant agreement Nº 875565 (Project CompBat).

I am also greatly thankful to my supervisor, Pekka, who invited me to join his research group on this interesting field of energy storage systems. Besides his expertise and his incredible capacity to find an aswer to every issue, he always shared his knowledge and offered a place where to discuss. Furthermore, during these years, he has been always open to any opportunity that could help to my career, as new topics, conferences, research visits, teaching, etc. What is even more, he did all that with kindness. I also would like to acknowledge my second supervisor, Ulriika, for listening and giving advice every time I knocked at her door.

Then, I want to thank to my colleagues at the battery research group, those who have been for a long time and even for short stays. I am very grateful for all the scientific discussions and the good moments shared in Quantum (and outside too). I want to extend the acknowledgement to all the people in the Materials Engineering Unit for all the help in the labs and the talks in the corridors. I believe I have been very lucky for having the chance of meeting all these people and living that PhD experience within this group. Everything have been much easier and enjoyable that way.

I also would like to say thanks to my collaborators at University of Jyväskylä, who have been an important part of this doctoral research work: special thanks to Anton and Maxime because I enjoyed sharing all those projects with them. Furthermore, I would like to thank Justyna for the opportunity to collaborate on her work, which resulted in my first publication within these doctoral studies. On that sense, I warmly want to acknowledge my collaborators from CompBat project and

all the co-authors of the publications presented in this thesis (and other works too). I have learned a lot from all of them, and the fact that we often belonged to different disciplines has made this PhD experience very fruitful.

As this experience brought me to the other side of the globe, it has been sometimes difficult to be away from my family and friends. However, it gave me the chance to know other incredible people. I will always thank Turku for introducing me Ale, Heidi, Silvia, Leo and Leia, who have been my Argentinian-Finnish family there and helped me feel that Argentina was much closer. The same for all those Spanish friends: Yoli, Fabian, Fran, Bea, Raul, Gaby (Ven), Santiago, Juan and all those (from other countries too) who made Turku to feel like home. I also want to thank to all my friends from Old Irish, Tuto, TUPV and ÅIFK who, during all these years, have shared with me the same passion for football. I don't want to forget Pirkka in this list, because he has shown me so well how that passion speaks all languages. Also, thanks Leo for that incredible gift. All this has helped a lot to keep me grounded during these years far away from home.

Here in the end, I want thank to my dear family in Argentina, who have been an immensurable support during these years regardless the distance. Thanks Viejo, Mami, Javi, Emi, Tota and Ieia for always being there for everything. Thanks Maris for your classes, and Tronko, Samu and Sari for the company when I was there. To my friends in Parana, Santa Fe and Rosario, thanks a lot for always receiving me and helping me to recharge my energies to come back to Finland and continue. Finally, thanks Jenna: for all. I can include her in almost every paragraph of these acknowledgements, as she has been here and there all the time, as a colleague, a friend, and a strong support. And thanks Urho, of course, for always receiving me with all that happiness.

Gabriel Gonzalez
Paraná, 23.04.2025

List of References

1. Hardy, J. T. *Climate change: causes, effects, and solutions* (John Wiley & Sons, Chichester, 2003).
2. Wuebbles, D. J. & Jain, A. K. Concerns about climate change and the role of fossil fuel use. *Fuel Processing* Technology **71**, 99–119 (2001).
3. Zheng, X. *et al.* A review of greenhouse gas emission profiles, dynamics, and climate change mitigation efforts across the key climate change players. *J Clean Prod* **234**, 1113–1133 (2019).
4. Roga, S., Bardhan, S., Kumar, Y. & Dubey, S. K. Recent technology and challenges of wind energy generation: A review. *Sustainable Energy Technologies and Assessments* **52**, 102239 (2022).
5. Maka, A. O. M. & Alabid, J. M. Solar energy technology and its roles in sustainable development. *Clean Energy* **6**, 476–483 (2022).
6. Olabi, A. G. & Abdelkareem, M. A. Renewable energy and climate change. *Renewable and Sustainable Energy Reviews* **158**, 112111 (2022).
7. Yang, Z. *et al.* Electrochemical Energy Storage for Green Grid. *Chem Rev* **111**, 3577–3613 (2011).
8. Barnhart, C. J., Dale, M., Brandt, A. R. & Benson, S. M. The energetic implications of curtailing versus storing solar- and wind-generated electricity. *Energy Environ Sci* **6**, 2804 (2013).
9. Ibrahim, H., Ilinca, A. & Perron, J. Energy storage systems-Characteristics and comparisons. *Renewable and Sustainable Energy Reviews* **12**, 1221–1250 (2008).
10. Koohi-Fayegh, S. & Rosen, M. A. A review of energy storage types, applications and recent developments. *J Energy Storage* **27**, 101047 (2020).
11. Zubi, G., Dufo-López, R., Carvalho, M. & Pasaoglu, G. The lithium-ion battery: State of the art and future perspectives. *Renewable and Sustainable Energy Reviews* **89**, 292–308 (2018).
12. Blakers, A., Stocks, M., Lu, B. & Cheng, C. A review of pumped hydro energy storage. *Progress in Energy* **3**, 022003 (2021).
13. Wang, Q. *et al.* Thermal runaway caused fire and explosion of lithium ion battery. *J Power Sources* **208**, 210–224 (2012).
14. Lisbona, D. & Snee, T. A review of hazards associated with primary lithium and lithium-ion batteries. *Process Safety and Environmental Protection* **89**, 434–442 (2011).
15. Olivetti, E. A., Ceder, G., Gaustad, G. G. & Fu, X. Lithium-Ion Battery Supply Chain Considerations: Analysis of Potential Bottlenecks in Critical Metals. *Joule* **1**, 229–243 (2017).
16. Alotto, P., Guarnieri, M. & Moro, F. Redox flow batteries for the storage of renewable energy: A review. *Renewable and Sustainable Energy Reviews* **29**, 325–335 (2014).
17. Doyle, J. Galvanic-Battery. US-224404 (1880).
18. Shigematsu, T. The development and demonstration status of practical flow battery systems. *Curr Opin Electrochem* **18**, 55–60 (2019).
19. Skyllas-Kazacos, M., Rychcik, M., Robins, R. G., Fane, A. G. & Green, M. A. New All-Vanadium Redox Flow Cell. *J Electrochem Soc* **133**, 1057–1058 (1986).
20. Soloveichik, G. L. Flow Batteries: Current Status and Trends. *Chem Rev* **115**, 11533–11558 (2015).

21. Arevalo-Cid, P., Dias, P., Mendes, A. & Azevedo, J. Redox flow batteries: A new frontier on energy storage. *Sustainable Energy and Fuels* **5**, 5366–5419 (2021).
22. Crawford, A. *et al.* Comparative analysis for various redox flow batteries chemistries using a cost performance model. *J Power Sources* **293**, 388–399 (2015).
23. Pan, F. & Wang, Q. Redox Species of Redox Flow Batteries: A Review. *Molecules* **20**, 20499–20517 (2015).
24. Wang, X., Gautam, R. K. & Jiang, J. Strategies for Improving Solubility of Redox-Active Organic Species in Aqueous Redox Flow Batteries: A Review. *Batter Supercaps* **5**, e202200298 (2022).
25. Zanzola, E. *et al.* Redox Solid Energy Boosters for Flow Batteries: Polyaniline as a Case Study. *Electrochim Acta* **235**, 664–671 (2017).
26. Ma, J. *et al.* Aqueous Organic Redox-Targeting Flow Batteries with Advanced Solid Materials: Current Status and Future Perspective. *Sustainability* **15**, 15635 (2023).
27. Fang, X. *et al.* Multielectron Organic Redoxmers for Energy-Dense Redox Flow Batteries. *ACS Mater Lett* **4**, 277–306 (2022).
28. Park, M., Ryu, J., Wang, W. & Cho, J. Material design and engineering of next-generation flow-battery technologies. *Nat Rev Mater* **2**, 16080 (2016).
29. Arenas, L. F., Ponce de León, C. & Walsh, F. C. Engineering aspects of the design, construction and performance of modular redox flow batteries for energy storage. *J Energy Storage* **11**, 119–153 (2017).
30. Perry, M. L., Rodby, K. E. & Brushett, F. R. Untapped Potential: The Need and Opportunity for High-Voltage Aqueous Redox Flow Batteries. *ACS Energy Lett* **7**, 659–667 (2022).
31. Gong, K., Fang, Q., Gu, S., Li, S. F. Y. & Yan, Y. Nonaqueous redox-flow batteries: organic solvents, supporting electrolytes, and redox pairs. *Energy Environ Sci* **8**, 3515–3530 (2015).
32. Kim, K. J., Kim, Y.-J., Kim, J.-H. & Park, M.-S. The effects of surface modification on carbon felt electrodes for use in vanadium redox flow batteries. *Mater Chem Phys* **131**, 547–553 (2011).
33. da Silva Lima, L. *et al.* Life cycle assessment of lithium-ion batteries and vanadium redox flow batteries-based renewable energy storage systems. *Sustainable Energy Technologies and Assessments* **46**, 101286 (2021).
34. Hu, X., Xu, L., Lin, X. & Pecht, M. Battery Lifetime Prognostics. *Joule* **4**, 310–346 (2020).
35. Wang, Y., Mu, A., Wang, W., Yang, B. & Wang, J. A Review of Capacity Decay Studies of All-vanadium Redox Flow Batteries: Mechanism and State Estimation. *ChemSusChem* **17**, e202301787 (2024).
36. Kwabi, D. G., Ji, Y. & Aziz, M. J. Electrolyte Lifetime in Aqueous Organic Redox Flow Batteries: A Critical Review. *Chemical Reviews* **120**, 6467–6489 (2020).
37. Nolte, O., Volodin, I. A., Stolze, C., Hager, M. D. & Schubert, U. S. Trust is good, control is better: a review on monitoring and characterization techniques for flow battery electrolytes. *Mater Horiz* **8**, 1866–1925 (2021).
38. Aaron, D., Tang, Z., Papandrew, A. B. & Zawodzinski, T. A. Polarization curve analysis of all-vanadium redox flow batteries. *J Appl Electrochem* **41**, 1175–1182 (2011).
39. Sankaralingam, R. K., Seshadri, S., Sunarso, J., Bhatt, A. I. & Kapoor, A. Overview of the factors affecting the performance of vanadium redox flow batteries. *Journal of Energy Storage* **41**, 102857 (2021).
40. Minke, C., Hickmann, T., dos Santos, A. R., Kunz, U. & Turek, T. Cost and performance prospects for composite bipolar plates in fuel cells and redox flow batteries. *J Power Sources* **305**, 182–190 (2016).
41. Gautam, R. K. & Kumar, A. A review of bipolar plate materials and flow field designs in the all-vanadium redox flow battery. *J Energy Storage* **48**, 104003 (2022).
42. Dennison, C. R., Agar, E., Akuzum, B. & Kumbur, E. C. Enhancing Mass Transport in Redox Flow Batteries by Tailoring Flow Field and Electrode Design. *J Electrochem Soc* **163**, A5163–A5169 (2016).

43. Cunha, Á., Martins, J., Rodrigues, N. & Brito, F. P. Vanadium redox flow batteries: a technology review. *Int J Energy Res* **39**, 889–918 (2015).
44. Gencten, M. & Sahin, Y. A critical review on progress of the electrode materials of vanadium redox flow battery. *Int J Energy Res* **44**, 7903–7923 (2020).
45. Pezeshki, A. M., Clement, J. T., Veith, G. M., Zawodzinski, T. A. & Mench, M. M. High performance electrodes in vanadium redox flow batteries through oxygen-enriched thermal activation. *J Power Sources* **294**, 333–338 (2015).
46. Li, W., Liu, J. & Yan, C. Graphite–graphite oxide composite electrode for vanadium redox flow battery. *Electrochim Acta* **56**, 5290–5294 (2011).
47. Xu, J., Zhang, Y., Huang, Z., Jia, C. & Wang, S. Surface Modification of Carbon-Based Electrodes for Vanadium Redox Flow Batteries. *Energy & Fuels* **35**, 8617–8633 (2021).
48. Dixon, D. *et al.* Tuning the performance of vanadium redox flow batteries by modifying the structural defects of the carbon felt electrode. *Beilstein Journal of Nanotechnology* **10**, 1698–1706 (2019).
49. Park, S. & Kim, H. Fabrication of nitrogen-doped graphite felts as positive electrodes using polypyrrole as a coating agent in vanadium redox flow batteries. *J Mater Chem A Mater* **3**, 12276–12283 (2015).
50. Machado, C. A. *et al.* Redox Flow Battery Membranes: Improving Battery Performance by Leveraging Structure–Property Relationships. *ACS Energy Lett* **6**, 158–176 (2021).
51. Prifti, H., Parasuraman, A., Winardi, S., Lim, T. M. & Skyllas-Kazacos, M. Membranes for Redox Flow Battery Applications. *Membranes (Basel)* **2**, 275–306 (2012).
52. Kear, G., Shah, A. A. & Walsh, F. C. Development of the all-vanadium redox flow battery for energy storage: A review of technological, Financial and policy aspects. *Int J Energy Res* **36**, 1105–1120 (2012).
53. Petrov, M. M. *et al.* Redox flow batteries: role in modern electric power industry and comparative characteristics of the main types. *Russian Chemical Reviews* **90**, 677–702 (2021).
54. Rodby, K. E. *et al.* Assessing the levelized cost of vanadium redox flow batteries with capacity fade and rebalancing. *J Power Sources* **460**, 227958 (2020).
55. Kroner, I., Becker, M. & Turek, T. Determination of Rate Constants and Reaction Orders of Vanadium-Ion Kinetics on Carbon Fiber Electrodes. *ChemElectroChem* **7**, 4314–4325 (2020).
56. Barranco, J. E. *et al.* Analysis of the electrochemical performance of carbon felt electrodes for vanadium redox flow batteries. *Electrochim Acta* **470**, 143281 (2023).
57. He, Z. *et al.* Electrode materials for vanadium redox flow batteries: Intrinsic treatment and introducing catalyst. *Chemical Engineering Journal* **427**, 131680 (2022).
58. Eifert, L., Jusys, Z., Behm, R. J. & Zeis, R. Side reactions and stability of pre-treated carbon felt electrodes for vanadium redox flow batteries: A DEMS study. *Carbon N Y* **158**, 580–587 (2020).
59. Huang, Z. *et al.* Experimental Validation of Side Reaction on Capacity Fade of Vanadium Redox Flow Battery. *J Electrochem Soc* **171**, 010521 (2024).
60. Sun, J., Shi, D., Zhong, H., Li, X. & Zhang, H. Investigations on the self-discharge process in vanadium flow battery. *J Power Sources* **294**, 562–568 (2015).
61. Choi, N. H., Kwon, S. & Kim, H. Analysis of the Oxidation of the V(II) by Dissolved Oxygen Using UV-Visible Spectrophotometry in a Vanadium Redox Flow Battery. *J Electrochem Soc* **160**, A973–A979 (2013).
62. Tempelman, C. H. L., Jacobs, J. F., Balzer, R. M. & Degirmenci, V. Membranes for all vanadium redox flow batteries. *J Energy Storage* **32**, 101754 (2020).
63. Shi, Y. *et al.* Recent development of membrane for vanadium redox flow battery applications: A review. *Appl Energy* **238**, 202–224 (2019).
64. Choi, C. *et al.* A review of vanadium electrolytes for vanadium redox flow batteries. *Renewable and Sustainable Energy Reviews* **69**, 263–274 (2017).
65. Wu, X. *et al.* Electrolytes for vanadium redox flow batteries. *Pure and Applied Chemistry* **86**, 661–669 (2014).

66. Zhang, M., Moore, M., Watson, J. S., Zawodzinski, T. A. & Counce, R. M. Capital Cost Sensitivity Analysis of an All-Vanadium Redox-Flow Battery. *J Electrochem Soc* **159**, A1183–A1188 (2012).
67. Milshtein, J. D., Darling, R. M., Drake, J., Perry, M. L. & Brushett, F. R. The Critical Role of Supporting Electrolyte Selection on Flow Battery Cost. *J Electrochem Soc* **164**, A3883–A3895 (2017).
68. Rodby, K. E., Jaffe, R. L., Olivetti, E. A. & Brushett, F. R. Materials availability and supply chain considerations for vanadium in grid-scale redox flow batteries. *J Power Sources* **560**, 232605 (2023).
69. Wedege, K., Konya, D. & Bentien, A. Organic Redox Species in Aqueous Flow Batteries: Redox Potentials, Chemical Stability and Solubility. *Sci Rep* **6**, 39101 (2016).
70. Fischer, P., Mazúr, P. & Krakowiak, J. Family Tree for Aqueous Organic Redox Couples for Redox Flow Battery Electrolytes: A Conceptual Review. *Molecules* **27**(2), 560 (2022).
71. Zhang, L., Feng, R., Wang, W. & Yu, G. Emerging chemistries and molecular designs for flow batteries. *Nature Reviews Chemistry* **6**, 524–543 (2022).
72. Li, T., Zhang, C. & Li, X. Machine learning for flow batteries: opportunities and challenges. *Chem Sci* **13**, 4740–4752 (2022).
73. Asenjo-Pascual, J. *et al.* DFT calculation, a practical tool to predict the electrochemical behaviour of organic electrolytes in aqueous redox flow batteries. *J Power Sources* **564**, 232817 (2023).
74. Cao, J., Tian, J., Xu, J. & Wang, Y. Organic Flow Batteries: Recent Progress and Perspectives. *Energy & Fuels* **34**, 13384–13411 (2020).
75. Sánchez-Díez, E. *et al.* Redox flow batteries: Status and perspective towards sustainable stationary energy storage. *J Power Sources* **481**, 228804 (2021).
76. Liu, B., Li, Y., Jia, G. & Zhao, T. Recent Advances in Redox Flow Batteries Employing Metal Coordination Complexes as Redox-Active Species. *Electrochemical Energy Reviews* **7**, 7 (2024).
77. Koppenol, W. H. & Hider, R. H. Iron and redox cycling. Do's and don'ts. *Free Radical Biology and Medicine* **133**, 3–10 (2019).
78. Hannonen, J., Kiesilä, A., Mattinen, U., Pihko, P. M. & Peljo, P. Electrochemical characterization of redox activity and stability of various tris(2,2'-bipyridine) derived complexes of iron(II) in aqueous solutions. *Journal of Electroanalytical Chemistry* **950**, 117847 (2023).
79. Gao, J., Xia, L., Ou, M. & Tan, Z. Metal Coordination Compounds for Organic Redox Flow Batteries. *Batter Supercaps* **7**, e202400434 (2024).
80. Ding, Y., Zhang, C., Zhang, L., Zhou, Y. & Yu, G. Molecular engineering of organic electroactive materials for redox flow batteries. *Chem Soc Rev* **47**, 69–103 (2018).
81. Mouselly, M., Alawadhi, H. & Senthilkumar, S. T. Current status of ferro-/ferricyanide for redox flow batteries. *Curr Opin Electrochem* **48**, 101581 (2024).
82. Wang, G. *et al.* Unlocking the solubility limit of ferrocyanide for high energy density redox flow batteries. *Mater Today Energy* **28**, 101061 (2022).
83. Luo, J. *et al.* Unprecedented Capacity and Stability of Ammonium Ferrocyanide Catholyte in pH Neutral Aqueous Redox Flow Batteries. *Joule* **3**, 149–163 (2019).
84. Astruc, D. Metallocenes and Sandwich Complexes. *Organometallic Chemistry and Catalysis,* 251–288 (Springer Berlin, Heidelberg, 2007).
85. Fery-Forgues, S. & Delavaux-Nicot, B. Ferrocene and ferrocenyl derivatives in luminescent systems. *J Photochem Photobiol A Chem* **132**, 137–159 (2000).
86. Bao, D. *et al.* Electrochemical Oxidation of Ferrocene: A Strong Dependence on the Concentration of the Supporting Electrolyte for Nonpolar Solvents. *J Phys Chem A* **113**, 1259–1267 (2009).
87. Li, Y. *et al.* Functioning Water-Insoluble Ferrocenes for Aqueous Organic Flow Battery via Host–Guest Inclusion. *ChemSusChem* **14**, 745–752 (2021).

88. Beh, E. S. *et al.* A neutral pH aqueous organic- organometallic redox flow battery with extremely high capacity retention. *ACS Energy Lett* **2**, 639–644 (2017).
89. Breuer, E., Aurich, H. G. & Nielsen, A. Nitroxides. *Nitrones, Nitronates and Nitroxides*, 313–370 (John Wiley & Sons, New York, 1989).
90. Suga, T., Pu, Y.-J., Oyaizu, K. & Nishide, H. Electron-Transfer Kinetics of Nitroxide Radicals as an Electrode-Active Material. *Bull Chem Soc Jpn* **77**, 2203–2204 (2004).
91. Sen, V. D. & Golubev, V. A. Kinetics and mechanism for acid-catalyzed disproportionation of 2,2,6,6-tetramethylpiperidine-1-oxyl. *J Phys Org Chem* **22**, 138–143 (2009).
92. Orita, A., Verde, M. G., Sakai, M. & Meng, Y. S. The impact of pH on side reactions for aqueous redox flow batteries based on nitroxyl radical compounds. *J Power Sources* **321**, 126–134 (2016).
93. Cannon, C. G., Klusener, P. A. A., Brandon, N. P. & Kucernak, A. R. J. Aqueous Redox Flow Batteries: Small Organic Molecules for the Positive Electrolyte Species. *ChemSusChem* **16**, (2023).
94. Luo, J., Hu, B., Hu, M., Zhao, Y. & Liu, T. L. Status and Prospects of Organic Redox Flow Batteries toward Sustainable Energy Storage. *ACS Energy Lett* **4**, 2220–2240 (2019).
95. Zhou, W. *et al.* Fundamental properties of TEMPO-based catholytes for aqueous redox flow batteries: effects of substituent groups and electrolytes on electrochemical properties, solubilities and battery performance. *RSC Adv* **10**, 21839–21844 (2020).
96. Liu, Y. *et al.* Organic electrolytes for aqueous organic flow batteries. *Mater Today Energy* **20**, 100634 (2021).
97. Liu, T., Wei, X., Nie, Z., Sprenkle, V. & Wang, W. A Total Organic Aqueous Redox Flow Battery Employing a Low Cost and Sustainable Methyl Viologen Anolyte and 4-HO-TEMPO Catholyte. *Adv Energy Mater* **6**, 1501449 (2016).
98. Janoschka, T., Martin, N., Hager, M. D. & Schubert, U. S. An Aqueous Redox-Flow Battery with High Capacity and Power: The TEMPTMA/MV System. *Angewandte Chemie International Edition* **55**, 14427–14430 (2016).
99. Kowalski, J. A. *et al.* A stable two-electron-donating phenothiazine for application in nonaqueous redox flow batteries. *J Mater Chem A Mater* **5**, 24371–24379 (2017).
100. Milshtein, J. D. *et al.* High current density, long duration cycling of soluble organic active species for non-aqueous redox flow batteries. *Energy Environ Sci* **9**, 3531–3543 (2016).
101. Zhang, C. *et al.* Phenothiazine-Based Organic Catholyte for High-Capacity and Long-Life Aqueous Redox Flow Batteries. *Advanced Materials* **31**, 1901052 (2019).
102. Hasan, F., Mahanta, V. & Abdelazeez, A. A. Quinones for Aqueous Organic Redox Flow Battery: A Prospective on Redox Potential, Solubility, and Stability. *Advanced Materials Interfaces* **10**, 2300268 (2023).
103. Wu, M., Bahari, M., Fell, E. M., Gordon, R. G. & Aziz, M. J. High-performance anthraquinone with potentially low cost for aqueous redox flow batteries. *J Mater Chem A Mater* **9**, 26709–26716 (2021).
104. Beh, E. S., Bahari, M., Symons, P. & Aziz, M. J. (Invited) Low Cost in Situ Electrosynthesis and Cycling of Quinone Negolytes in a Commercial Flow Battery Stack. *ECS Meeting Abstracts* **MA2024-01**, 1484 (2024).
105. Khetan, A. High-Throughput Virtual Screening of Quinones for Aqueous Redox Flow Batteries: Status and Perspectives. *Batteries* **9**, 24 (2022).
106. Tyburski, R., Liu, T., Glover, S. D. & Hammarström, L. Proton-Coupled Electron Transfer Guidelines, Fair and Square. *J Am Chem Soc* **143**, 560–576 (2021).
107. Huskinson, B. *et al.* A metal-free organic–inorganic aqueous flow battery. *Nature* **505**, 195–198 (2014).
108. Wiberg, C., Carney, T. J., Brushett, F., Ahlberg, E. & Wang, E. Dimerization of 9,10-anthraquinone-2,7-Disulfonic acid (AQDS). *Electrochim Acta* **317**, 478–485 (2019).

109. Forster, R. J. & O'Kelly, J. P. Protonation reactions of anthraquinone-2,7-disulphonic acid in solution and within monolayers. *Journal of Electroanalytical Chemistry* **498**, 127–135 (2001).
110. Yang, G. *et al.* An Aqueous All-Quinone-Based Redox Flow Battery Employing Neutral Electrolyte. *Adv Energy Mater* **14**, 2400022 (2024).
111. Chen, Q., Eisenach, L. & Aziz, M. J. Cycling Analysis of a Quinone-Bromide Redox Flow Battery. *J Electrochem Soc* **163**, A5057–A5063 (2016).
112. Lin, K. *et al.* Alkaline quinone flow battery. *Science (1979)* **349**, 1529–1532 (2015).
113. Kwabi, D. G. *et al.* Alkaline Quinone Flow Battery with Long Lifetime at pH 12. *Joule* **2**, 1894–1906 (2018).
114. Yin, T., Duanmu, J. & Liu, L. Viologen-based aqueous organic redox flow batteries: materials synthesis, properties, and cell performance. *Journal of Materials Chemistry A* **12**, 15519–15540 (2024).
115. Liu, T., Wei, X., Nie, Z., Sprenkle, V. & Wang, W. A Total Organic Aqueous Redox Flow Battery Employing a Low Cost and Sustainable Methyl Viologen Anolyte and 4-HO-TEMPO Catholyte. *Adv Energy Mater* **6**, 1501449 (2016).
116. Yoen Kim, J., Lee, C. & Woo Park, J. The Kinetics of Neutral Methyl Viologen in Acidic H2O+DMF Mixed Solutions Studied by Cyclic Voltammetry. *Journal of Electroanalytical Chemistry* **504**, 104–110 (2001).
117. Park, J. W., Kim, J. H., Hwang, B. K. & Park, K. K. Photosensitized Two-electron Reduction of Viologen and the Reactivity of the Neutral Viologen. *Chem Lett* **23**, 2075–2078 (1994).
118. Zhang, D., Tian, J., Chen, L., Zhang, L. & Li, Z. Dimerization of Conjugated Radical Cations: An Emerging Non-Covalent Interaction for Self-Assembly. *Chem Asian J* **10**, 56–68 (2015).
119. Nikumbe, D. Y. *et al.* Stability of monoradical cation dimer of viologen derivatives in aqueous redox flow battery. *J Appl Electrochem* **54**, 2165–2177 (2024).
120. Rubio-Presa, R., Lubián, L., Borlaf, M., Ventosa, E. & Sanz, R. Addressing Practical Use of Viologen-Derivatives in Redox Flow Batteries through Molecular Engineering. *ACS Mater Lett* **5**, 798–802 (2023).
121. Wang, L. *et al.* Steric hindrance shielding viologen against alkali attack in realizing ultrastable aqueous flow batteries. *Journal of Energy Chemistry* **97**, 529–534 (2024).
122. Venturi, M., Mulazzani, Q. G. & Hoffman, M. Z. Radiolytically induced one-electron reduction of methylviologen in aqueous solution. Platinum-catalyzed formation of dihydrogen. *J Phys Chem* **88**, 912–918 (1984).
123. Liu, Y. *et al.* Degradation of electrochemical active compounds in aqueous organic redox flow batteries. *Curr Opin Electrochem* **32**, 100895 (2022).
124. Jin, S. *et al.* Near Neutral pH Redox Flow Battery with Low Permeability and Long-Lifetime Phosphonated Viologen Active Species. *Adv Energy Mater* **10**, (2020).
125. Luo, J., Hu, B., Debruler, C. & Liu, T. L. A π-Conjugation Extended Viologen as a Two-Electron Storage Anolyte for Total Organic Aqueous Redox Flow Batteries. *Angewandte Chemie International Edition* **57**, 231–235 (2018).
126. Tang, G. *et al.* Designing Robust Two-Electron Storage Extended Bipyridinium Anolytes for pH-Neutral Aqueous Organic Redox Flow Batteries. *JACS Au* **2**, 1214–1222 (2022).
127. Liu, Y. *et al.* Redox-Modulated Host-Guest Complex Realizing Stable Two-Electron Storage Viologen for Flow Battery. *Ind Eng Chem Res* **61**, 14508–14514 (2022).
128. Klatt, L. N. & Rouseff, R. L. Electrochemical reduction of pyrazine in aqueous media. *J Am Chem Soc* **94**, 7295–7304 (1972).
129. Pasadakis-Kavounis, A., Baj, V. & Hjelm, J. Electrochemical Characterization of Aromatic Molecules with 1,4-Diaza Groups for Flow Battery Applications. *Molecules* **26**, 2227 (2021).
130. Winsberg, J. *et al.* TEMPO/Phenazine Combi-Molecule: A Redox-Active Material for Symmetric Aqueous Redox-Flow Batteries. *ACS Energy Lett* **1**, 976–980 (2016).
131. Wang, C. *et al.* Molecular Design of Fused-Ring Phenazine Derivatives for Long-Cycling Alkaline Redox Flow Batteries. *ACS Energy Lett* **5**, 411–417 (2020).

132. Hollas, A. *et al.* A biomimetic high-capacity phenazine-based anolyte for aqueous organic redox flow batteries. *Nat Energy* **3**, 508–514 (2018).
133. Xu, J., Pang, S., Wang, X., Wang, P. & Ji, Y. Ultrastable aqueous phenazine flow batteries with high capacity operated at elevated temperatures. *Joule* **5**, 2437–2449 (2021).
134. de la Cruz, C. *et al.* New insights into phenazine-based organic redox flow batteries by using high-throughput DFT modelling. *Sustain Energy Fuels* **4**, 5513–5521 (2020).
135. Lin, K. *et al.* A redox-flow battery with an alloxazine-based organic electrolyte. *Nat Energy* **1**, 16102 (2016).
136. Feng, R. *et al.* Reversible ketone hydrogenation and dehydrogenation for aqueous organic redox flow batteries. *Science* **372**, 836–840 (2021).
137. Rodriguez, J., Niemet, C. & Pozzo, L. D. Fluorenone Based Anolyte for an Aqueous Organic Redox-Flow Battery. *ECS Trans* **89**, 49–59 (2019).
138. Li, W. *et al.* A novel pyridinium-functionalized fluorenone compound for neutral aqueous organic redox flow batteries. *J Mater Chem A Mater* **11**, 19308–19311 (2023).
139. Gandomi, Y. A. *et al.* Critical Review—Experimental Diagnostics and Material Characterization Techniques Used on Redox Flow Batteries. *J Electrochem Soc* **165**, A970–A1010 (2018).
140. Fell, E. & Aziz, M. High-Throughput Electrochemical Characterization of Aqueous Organic Redox Flow Battery Active Material. *J. Electrochem. Soc* **170**, 100507 (2023).
141. Goulet, M.-A. & Aziz, M. J. Flow Battery Molecular Reactant Stability Determined by Symmetric Cell Cycling Methods. *J Electrochem Soc* **165**, A1466–A1477 (2018).
142. Ghimire, P. C. *et al.* In-situ tools used in vanadium redox flow battery research—review. *Batteries* **7**(3), 53 (2021).
143. khwa Museveni, S., Nakitare Nambafu, G. & Kollongei, N. Understanding degradation of electroactive molecules in organic redox flow batteries: Decomposition analysis methods. *Materials Science for Energy Technologies* **6**, 561–566 (2023).
144. Blomen, L. J. M. J. & Mugerwa, M. N. Electrochemistry of Fuel Cells. *Fuel Cell Systems*, 73–119 (Springer, New York, 1993).
145. Hao, D., Shen, J., Hou, Y., Zhou, Y. & Wang, H. An Improved Empirical Fuel Cell Polarization Curve Model Based on Review Analysis. *International Journal of Chemical Engineering* **2016**, 1–10 (2016).
146. Hung, Y., Bu, Y., Kubin, J. & Weinman, D. Effects of current scan rate on the polarization curve of vanadium redox flow batteries. International Energy and Sustainability Conference (IESC), 1–4 (2017).
147. Langner, J., Melke, J., Ehrenberg, H. & Roth, C. Determination of Overpotentials in All Vanadium Redox Flow Batteries. *ECS Trans* **58**, 1–7 (2014).
148. Houser, J., Clement, J., Pezeshki, A. & Mench, M. M. Influence of architecture and material properties on vanadium redox flow battery performance. *J Power Sources* **302**, 369–377 (2016).
149. Gaberšček, M. Impedance spectroscopy of battery cells: Theory versus experiment. *Curr Opin Electrochem* **32**, 100917 (2022).
150. Hu, W., Peng, Y., Wei, Y. & Yang, Y. Application of Electrochemical Impedance Spectroscopy to Degradation and Aging Research of Lithium-Ion Batteries. *The Journal of Physical Chemistry C* **127**, 4465–4495 (2023).
151. Harrington, D. A. & van den Driessche, P. Mechanism and equivalent circuits in electrochemical impedance spectroscopy. *Electrochim Acta* **56**, 8005–8013 (2011).
152. Tripathi, A. K., Choudhury, D., Joy, M. E. & Neergat, M. Electrochemical Impedance Spectroscopic Investigation of Vanadium Redox Flow Battery. *J Electrochem Soc* **169**, 050513 (2022).
153. Krakowiak, J., Bącalski, W., Lentka, G., Peljo, P. & Ślepski, P. Three modes of electrochemical impedance spectroscopy measurements performed on vanadium redox flow battery. *Sustainable Materials and Technologies* **40**, (2024).

154. Choi, C., Choi, Y., Kim, S., Jung, H. & Kim, H.-T. Resistor Design for the Use of Dynamic Hydrogen Electrode in Vanadium Redox Flow Batteries. *Electrochim Acta* **213**, 490–495 (2016).
155. grosse Austing, J., Nunes Kirchner, C., Hammer, E.-M., Komsiyska, L. & Wittstock, G. Study of an unitised bidirectional vanadium/air redox flow battery comprising a two-layered cathode. *J Power Sources* **273**, 1163–1170 (2015).
156. Cecchetti, M., Casalegno, A. & Zago, M. Local potential measurement through reference electrodes in vanadium redox flow batteries: Evaluation of overpotentials and electrolytes imbalance. *J Power Sources* **400**, 218–224 (2018).
157. Skyllas-Kazacos, M. & Kazacos, M. State of charge monitoring methods for vanadium redox flow battery control. *J Power Sources* **196**, 8822–8827 (2011).
158. Haisch, T., Ji, H. & Weidlich, C. Monitoring the state of charge of all-vanadium redox flow batteries to identify crossover of electrolyte. *Electrochim Acta* **336**, 135573 (2020).
159. Bard, A. J., Faulkner, L. R. & White, H. S. *Electrochemical Methods: Fundamentals and Applications* (John Wiley & Sons, New York, 2022).
160. Nicholson, R. S. Theory and Application of Cyclic Voltammetry for Measurement of Electrode Reaction Kinetics. *Anal Chem* **37**, 1351–1355 (1965).
161. Martínez-González, E. *et al.* Kinetic Properties of Aqueous Organic Redox Flow Battery Anolytes Using the Marcus–Hush Theory. *ACS Appl Energy Mater* **3**, 8833–8841 (2020).
162. Hellmann, H. & Mooney, S. Vitamin B6: A Molecule for Human Health? *Molecules* **15**, 442–459 (2010).
163. Rosenberg, J., Ischebeck, T. & Commichau, F. M. Vitamin B6 metabolism in microbes and approaches for fermentative production. *Biotechnol Adv* **35**, 31–40 (2017).
164. Tian, Z. *et al.* Enhancement of vitamin B6 production driven by omics analysis combined with fermentation optimization. *Microb Cell Fact* **23**, 137 (2024).
165. Shtyrlin, Y. G. *et al.* Chemistry of pyridoxine in drug design. *Russian Chemical Bulletin* **68**, 911–945 (2019).
166. Sevov, C. S., Hendriks, K. H. & Sanford, M. S. Low-potential pyridinium anolyte for aqueous redox flow batteries. *Journal of Physical Chemistry C* **121**, (2017).
167. Hamza, A. *et al.* N-Alkylated Pyridoxal Derivatives as Negative Electrolyte Materials for Aqueous Organic Flow Batteries: Computational Screening. *Chemistry – A European Journal* **29**, (2023).
168. Pelzer, K. M., Cheng, L. & Curtiss, L. A. Effects of Functional Groups in Redox-Active Organic Molecules: A High-Throughput Screening Approach. *The Journal of Physical Chemistry C* **121**, 237–245 (2017).
169. Wang, F. & Stahl, S. S. Electrochemical Oxidation of Organic Molecules at Lower Overpotential: Accessing Broader Functional Group Compatibility with Electron−Proton Transfer Mediators. *Acc Chem Res* **53**, 561–574 (2020).
170. Yin, T., Duanmu, J. & Liu, L. Viologen-based aqueous organic redox flow batteries: materials synthesis, properties, and cell performance. *J Mater Chem A Mater* **12**, 15519–15540 (2024).
171. Bilezikian, J. P., Raisz, L. G. & Martin, T. J. *Principles of Bone Biology* (Academic Press, 2008).
172. Bockman, T. M. & Kochi, J. K. Isolation and oxidation-reduction of methylviologen cation radicals. Novel disproportionation in charge-transfer salts by x-ray crystallography. *J Org Chem* **55**, 4127–4135 (1990).
173. Haratipour, P. *et al.* Completing the β,γ-CXY-dNTP Stereochemical Probe Toolkit: Synthetic Access to the dCTP Diastereomers and ^{31}P and ^{19}F NMR Correlations with Absolute Configurations. *J Org Chem* **85**, 14592–14609 (2020).
174. Li, W. *et al.* A novel pyridinium-functionalized fluorenone compound for neutral aqueous organic redox flow batteries. *J Mater Chem A Mater* **11**, 19308–19311 (2023).
175. Liao, F. *et al.* Are pyridinium ylides radicals? *Chemical Communications* **56**, 11287–11290 (2020).

176. Quan, M., Sanchez, D., Wasylkiw, M. F. & Smith, D. K. Voltammetry of Quinones in Unbuffered Aqueous Solution: Reassessing the Roles of Proton Transfer and Hydrogen Bonding in the Aqueous Electrochemistry of Quinones. *J Am Chem Soc* **129**, 12847–12856 (2007).
177. Ji, Y. *et al.* A Phosphonate-Functionalized Quinone Redox Flow Battery at Near-Neutral pH with Record Capacity Retention Rate. *Adv Energy Mater* **9**, (2019).
178. Li, Z., Jiang, T., Ali, M., Wu, C. & Chen, W. Recent Progress in Organic Species for Redox Flow Batteries. *Energy Storage Mater* **50**, 105–138 (2022).
179. Nicholson, R. S. Theory and Application of Cyclic Voltammetry for Measurement of Electrode Reaction Kinetics. *Anal Chem* **37**, 1351–1355 (1965).
180. Li, Z., Jiang, T., Ali, M., Wu, C. & Chen, W. Recent Progress in Organic Species for Redox Flow Batteries. *Energy Storage Mater* **50**, 105–138 (2022).
181. Singh, V., Kim, S., Kang, J. & Byon, H. R. Aqueous organic redox flow batteries. *Nano Res* **12**, 1988–2001 (2019).
182. Ciobanu, M., Wilburn, J. P., Krim, M. L. & Cliffel, D. E. Fundamentals. *Handbook of Electrochemistry,* 3–29 (2007).
183. Aaron, D. *et al.* In Situ Kinetics Studies in All-Vanadium Redox Flow Batteries. *ECS Electrochemistry Letters* **2**, A29–A31 (2013).
184. Sun, C.-N. *et al.* Probing Electrode Losses in All-Vanadium Redox Flow Batteries with Impedance Spectroscopy. *ECS Electrochemistry Letters* **2**, A43–A45 (2013).
185. Xu, Q., Zhao, T. S. & Zhang, C. Effects of SOC-dependent electrolyte viscosity on performance of vanadium redox flow batteries. *Appl Energy* **130**, 139–147 (2014).
186. Fang, Y.-H. & Liu, Z.-P. Tafel Kinetics of Electrocatalytic Reactions: From Experiment to First-Principles. *ACS Catal* **4**, 4364–4376 (2014).
187. Roznyatovskaya, N., Noack, J., Fühl, M., Pinkwart, K. & Tübke, J. Towards an all-vanadium redox-flow battery electrolyte: electrooxidation of V(III) in V(IV)/V(III) redox couple. *Electrochim Acta* **211**, 926–932 (2016).

TURUN
YLIOPISTO
UNIVERSITY
OF TURKU

Painosalama, Turku, Finland 2025

ISBN 978-952-02-0175-3 (Print)
ISBN 978-952-02-0176-0 (PDF)
ISSN 2736-9390 (Print)
ISSN 2736-9684 (Online)